UCGE Reports

Number 20339

Department of Geomatics Engineering

Investigation of GPS Observations for Indoor GPS/INS Integration

(URL: http://www.geomatics.ucalgary.ca/graduatetheses)

by

Behnam Aminian

October 2011

UNIVERSITY OF CALGARY

Investigation of GPS Observations for Indoor GPS/INS Integration

by

Behnam Aminian

A THESIS

SUBMITTED TO THE FACULTY OF GRADUATE STUDIES

IN PARTIAL FULFILMENT OF THE REQUIREMENTS FOR THE

DEGREE OF MASTER OF SCIENCE

DEPARTMENT OF GEOMATICS ENGINEERING

CALGARY, ALBERTA

October, 2011

Abstract

Global Positioning System (GPS) receivers suffer significant degradation in indoor environments due to the effects of multipath fading. In addition, signal attenuation of up to 30 dB caused by loss of signal strength through a medium (e.g., building materials) makes signal detection more difficult. Special algorithms and techniques such as Assisted GPS (A-GPS), block processing and High Sensitivity (HS) GPS are utilized in receivers for enhancing the accuracy and availability of signal parameters. Even with these enhanced receivers, sometimes it is not possible to provide an indoor navigation solution. In order to overcome the difficulties of positioning in indoor environments, satellite systems are often integrated with Inertial Navigation Systems (INS). In a GPS/INS integrated system, GPS observations can improve the position solution only if their accuracy is well known.

In this study, the accuracy of indoor GPS observations, including pseudorange and Doppler measurements, is studied and their different characteristics in indoor environments are discussed. Then, a reference-rover receiver that utilizes A-GPS and block processing techniques is introduced. This software is used for Doppler analysis and characterization in various indoor environments where the receiver experiences different dynamics. It is shown that the accuracy of Doppler measurements in indoor environments follows the theoretical model introduced in the thesis for velocities lower than 20 cm/s.

Finally, three practical variance models are provided for weighting indoor observations in a GPS/INS integrated system. To examine the effects of the weighting methods on a GPS/INS integrated system, different data sets in a residential house are collected and the position accuracy of navigation solutions related to different methods

are analyzed and compared. It is shown that the use of a power dependent weighting model provides the best accuracy. This model improves indoor position accuracy by 50% as compared to an elevation dependent model.

Acknowledgements

I am honoured to have had my work supervised by Professor Gérard Lachapelle. I would like to express my deepest gratitude and sincere appreciation for his continuous encouragement, guidance, patience and immense knowledge.

Thanks to my co-supervisor, Professor Mark Petovello, for his kind support, for sharing his insights and assisting me in this work. This research would have been much more challenging without his support. In addition, I would like to thank Dr. Daniele Borio, Dr. Valérie Renaudin, Dr. Cillian O'Driscoll, Dr. Vahid Dehghanian and Dr. Ali Broumandan for their friendship and valuable advice during my studies.

I owe special thanks to Nasim, my lovely wife, for her support and constant love during my education. I am grateful to my parents without whose support I would never have gotten this far. Also, I would like to thank my sister for her encouragement throughout my education.

My thanks go to all of my colleagues and friends in the PLAN Group who helped me to acquire this professional experience. Specifically, I would like to thank Nima Sadrieh, Pejman Kazemi, Mohammadreza Zaheri, Hatef Keshvadi, Billy Chan, Pratibha Anantharamu and Shashank Satyanarayana for their invaluable assistance.

This work was sponsored by a Research In Motion grant, matched by a Natural Sciences and Engineering Research Council of Canada Collaborative Research and Development grant, and an Industry Sponsored Collaborative grant from Alberta Advanced Education and Technology.

Dedication

To my beloved wife Nasim, my parents Behnaz and Amir and my sister Banafsheh.

Table of Contents

List of Tables

List of Figures and Illustrations

List of Symbols and Abbreviations

Symbol	Definition
$(\bullet)(t)$	… Quantity $(\bullet)$ as a function of time
$(\bullet)^a$	… Quantity $(\bullet)$ in frame a
$(\bullet)_k$	… Quantity $(\bullet)$ at the k^{th} epoch
$(\bullet)_{a,b}$	… element of the a^{th} row and the b^{th} column of the matrix $(\bullet)$
A	… signal amplitude
B_d	… Doppler bandwidth
$(C/N_0)_i$	… carrier to noise ratio of the ith satellite
C/N_0	… Carrier-to-Noise density power ratio
$C/N_0(zenith)$	… C/N_0 of the signal at the zenith in the open sky
E	… elevation angle of the satellite
F	… skew-symmetric matrix of specific force measurements
G	… design matrix when clock drift is included
H	… design matrix
$H_{nf}(z)$	… noise frequency transfer function in the z domain
I	… Identity matrix
N	… matrix representing the non-orthogonality of sensor triads
Q	… cofactor matrix
R_x^y	… rotation matrix from the frame ‘x’ to frame ‘y’
R_E	… Earth radius (spherical model)
S	… skew-symmetric matrix of the angular increment $\Delta\theta$
	… matrix of linear scale factor error
T_C	… integration time
U	… satellite-receiver unit vector in ENU coordinate frame
Vr	… velocity of the rover antenna

Vs	… satellite velocity
a	… acceleration vector
b	… sensor bias vector
cd	… clock drift of the receiver
$diag(\alpha_i)$	… diagonal matrix of time constants for the accelerometer bias models
$diag(\beta_i)$	… Diagonal matrix of time constants for the gyro bias models
f	… specific force vector
f_{ref}	… Doppler from the outdoor (reference) antenna
f_{rov}	… Doppler from the indoor (rover) antenna
f_{rr}	… Doppler measured by the reference-rover receiver
f_{True}	… true Doppler
g	… gravity vector
$\tilde{g}$	… gravitational acceleration vector
h	… Height
r	… position vector
t	… Time
t_0	… initial time
v	… velocity vector
α	… angle between Vr and the satellite-receiver unit vector
β	… angle between Vs and the satellite-receiver unit vector
$\Delta(\bullet)$	… Change in quantity $(\bullet)$
Δt	… time interval ($t_{k+1} - t_k$)
Δv	… velocity increments
$\Delta\theta_{bc}^{a}$	… Vector of angular increments of frame c, relative to frame b, expressed in frame a
Ω	… skew-symmetric form of the rotation rate vector ω
$\delta(\bullet)$	… Perturbation of quantity $(\bullet)$
δf^b	… vector of accelerometer sensor errors
$\delta\omega_{ib}^{b}$	… vector of gyro sensor errors

ε	… vector of misalignment angles along each axis
	… Doppler error
ξ	… roll of the vehicle
η	… pitch of the vehicle
	… sensor random noise
λ	… longitude
	… wavelength
σ_0^2	… apriori variance
$\sigma_{(\bullet)}$	… standard deviation of quantity $(\bullet)$
ϕ	… phase of the signal
φ	… Latitude
ψ	… azimuth or yaw of the vehicle
ω	… Doppler frequency of the signal
	… angular velocity of the turntable
ω_{yz}^{x}	… represents the angular velocity of frame 'z' with respect to frame 'y', expressed in the frame 'x'
ω^{e}	… earth's rotation rate (15 degree/hr)

Abbreviation Definition

A-GPS	… Assisted Global Positioning System
ADC	… Analog to Digital Converter
C/A	… Coarse/Acquisition
C/N_0	… Carrier-to-Noise density power ratio
CCIT	… Calgary Center of Innovative Technology
CDMA	… Code Division Multiple Access
DOD	… Department of Defense
DOP	… Dilution of precision

DR	… Dead Reckoning
EKF	… Extended Kalman Filter
FLI	… Frequency Lock Indicator
FLL	… Frequency Lock Loop
FOG	… Fiber Optic Gyros
GM	… Gauss Markov
GNSS	… Global Navigation Satellite Systems
GPS	… Global Positioning System
HS	… High Sensitivity
HSGPS	… High Sensitivity Global Positioning System
IF	… Intermediate Frequency
IMU	… Inertial Measurement Unit
INS	… Inertial Navigation System
LOS	… Line of Sight
LBS	… Location Based Services
MEMS	… Micro Electro Mechanical Systems
ML	… Maximum Likelihood
NavLab	… Navigation Laboratory
NI	… National Instruments
NLOS	… Non Line of Sight
PDR	… Pedestrian Dead Reckoning
PLL	… Phase Lock Loop
PNS	… Pedestrian Navigation System
PPM	… Parts Per Million
PRN	… Pseudo Random Noise
PSD	… Power Spectral Density
PVT	… Position, Velocity and Time
RF	… Radio Frequency
RMS	… Root Mean Square

RSS	… Received Signal Strength
TDOA	… Time Difference of Arrival
TOA	… Time of Arrival
UHF	… Ultra High Frequency
WPS	… Wi-Fi Positioning System
ZUPT	… Zero Velocity Update

Chapter One: Introduction

Positioning and navigation play an ever increasing role in human life. Their importance is becoming more significant with an increasing number of users and a variety of applications. Recently, indoor pedestrian navigation has experienced some of the fastest advancements because of a fast growing number of Location Based Services (LBS). A cell phone that provides its location in a building is just one example of a device that can estimate and transmit its location during an emergency call to save life (Reed et al 1998).

Satellite-based positioning is the most common navigation technology these days. Unfortunately, conventional receivers cannot easily detect satellite signals propagated through buildings since the signal suffers from attenuation and fading. On the Line of Sight (LOS) between the satellite and the receiver, this attenuation can exceed tens of dB. In order to compensate for these shortcomings, advanced methods of weak signal detection and combination with inertial sensors can be introduced as appropriate tools for indoor pedestrian navigation. This dissertation exploits advanced detection methods to provide signal parameters such as pseudorange and Doppler in a degraded signal environment and focuses on Doppler measurements in terms of accuracy and characterization. These measurements are then integrated with inertial sensors and performance is evaluated for diverse indoor environments, different methods of extracting satellite based signal parameters, and different techniques of weighting these parameters in the integrated system.

1.1 Background

The solutions that have been introduced for indoor navigation can be divided into two major groups. The first group consists of those that require infrastructure equipment to be installed in buildings. Pseudolites are an example of such equipment and interested readers are referred to Kao & Tsai (2003). Another example of this group is Wi-Fi Positioning Systems (WPS), which calculates the position of the user through nearby Wi-Fi access points. WPS estimate the distance between the user and Wi-Fi access points based on the Received Signal Strength (RSS) (Zhao et al 2010). There are three other methods of using Wi-Fi as a navigation solution. Fingerprinting uses RSS measurements from multiple access points and compares these measurements with a previously compiled database (Pahlavan et al 2010, Xiang et al 2004). Time of Arrival (TOA) and Time Difference of Arrival (TDOA) are two methods based on measuring the time it takes for the signal to propagate between the access points and the device. These methods are explained by Bensky (2008). It is laborious to implement this category because of hardware requirements and limitations of the solution to infrastructure availability. In the second group of indoor navigation solutions, the navigation system is carried by the user and the solution availability is dependent on the limitations of this equipment. Global Positioning Systems (GPS) and Inertial Navigation Systems (INS) are two examples of these systems with a wide range of applications.

The concepts of GPS are well known and well documented in the literature (e.g. Kaplan 1996). A GPS receiver carried by the user detects GPS signals and provides three-dimensional position and velocity components. The accuracy of the positioning

solution is from metres to centimetres given the conditions, measurements, and adopted methods (e.g. Lachapelle 2009).

Unfortunately, this accuracy is not achievable indoors because the signals are attenuated significantly. However, attenuated indoor signals still carry information that can be extracted by using receivers other than conventional standard GPS receivers. As an example, high sensitivity receivers can use block processing techniques with long integration times to estimate GPS signal parameters without the use of tracking loops (Feng & van Graas 1999, Satyanarayana et al 2009, Yang & Han 2007, Anyaegbu 2006). Assisted GPS (A-GPS) is another approach to improve the performance of standard GPS for indoor environments (Brown & Oslon 2005). Assistance data reduces the frequency and the code-delay search space. The clock offset, a priori position, a priori time and satellite orbits are necessary for reducing the frequency search space. Moreover, a priori time and position are necessary for reducing the code delay (van Diggelen 2009). In a degraded signal environment, it is necessary to integrate received signals in time and extract the weak signals from noise. The assistance information (data bit) is crucial for integration times longer than 20 ms (Borio & O'Driscoll 2009). These methods enhance the sensitivity of signal processing, providing more accurate Doppler and code-delay measurements indoors (Hu et al 2009).

The Doppler effect is one of the signal parameters measured by a GPS receiver. Doppler measurements combined with satellite trajectory and user position can be used to derive 3D user velocities with mm/s accuracy outdoors (van Graas & Soloviev 2004). Szarmes et al (1997) demonstrated that, for an aircraft under low acceleration (<0.5 m/s^2), the accuracy of estimated velocity is at the level of 3.8 mm/s. In Szarmes et al (1997),

Doppler measurements are derived from carrier phase measurements to reduce the noise level. This high accuracy, obtained under LOS conditions, is impressive and results in a significant interest in using Doppler measurements for indoor navigation as well. Although Doppler measurements are affected by noise and multipath indoors, they still carry valuable information. Aminian et al (2010) demonstrated that the standard deviation of velocity errors in a residential house is about 10 cm/s. Doppler multipath is a function of many parameters including the receiver velocity, which is quite limited in the case of indoor applications such as pedestrian navigation. In contrast, pseudorange multipath under NLOS conditions is unlimited (Lachapelle 2009), making pseudorange measurements inadequate for indoor navigation.

INSs are self-contained and provide the position, velocity and attitude of the user. They provide a complete, three-dimensional dead-reckoning solution (Groves 2008). An INS includes inertial sensors collectively known as the Inertial Measurement Unit (IMU), a navigation algorithm and a processor. The IMU is a triad of gyros and accelerometers. These sensors measure angular rate and acceleration in an inertial frame, respectively. As a result, the accelerometers and gyros are not only affected by user motion, but also by the Earth's rotation and gravity. To this end, the IMU outputs cannot be used for navigation solutions directly. To provide a navigation solution, the equations of motion are used. These equations describe the change in the position, velocity and attitude of the vehicle based on the IMU outputs. A navigation algorithm solves the equations of motion. For this purpose, mechanization equations numerically integrate the equations of motion (El-Sheimy 2007, Jekeli, 2000). Mechanization is an integration process that first obtains the position, velocity and attitude increments and then, combined with the initial

conditions of the system, provides the navigation solution (Petovello 2003). The navigation solution is based on the integration of inertial sensor outputs and, since errors exist in their outputs, the solution drifts with time.

GPS is based on radio signal propagation and these signals may be blocked or attenuated before arriving at the receiver. In contrast, an INS is an autonomous system whose standalone performance is unaffected in indoor environments. This feature makes the INS a subject of interest to be utilized for indoor navigation.

INS operates continuously in degraded signal environments, provides high rate outputs (a few hundreds of Hz) and contains low short-term noise in measurements. But the accuracy of the INS degrades with time as the errors are integrated in the navigation algorithm. Thus, errors are time dependent and drift (Groves 2008).

GPS provides high long-term position accuracy. The accuracy of GPS measurements is time-independent with bounded errors but GPS signals are subject to obstruction and interference. Moreover, compared to INS, the output rate is low (typically around 10 Hz or less) and does not measure the attitude, unless equipped with multiple antennas.

GPS and INS as stand-alone systems have limitations. However, the benefits and drawbacks of GPS and INS are complementary. Their advantages and disadvantages are shown in Table 1.1. By integrating INS and GPS, the advantages of both systems are combined to give a continuous, high bandwidth, complete navigation solution with high, long and short term accuracy. An integrated GPS/INS system provides an enhanced navigation system where GPS measurements prevent the inertial solution from drifting and INS smooth the GPS solution and bridges the GPS signal outages (Groves 2008). For

indoor environments where GPS signal outages are common, this hybridization is particularly effective.

Table 1.1: GPS and INS characteristic comparison (from El-Sheimy 2007)

System	INS	GPS
Advantages	Not dependent on RF signals	Errors time independent (bounded)
	High data rate	
	Position, velocity and attitude information	No pre information needed
		Standard time, GPS time
	High accuracy in short term	
	No indoor limitation	
Disadvantages	Errors time dependent	Sensitive to RF interference
	Need initial alignment	Low data rate
	No standard time	No attitude information
		Indoor limitation

Most of the solutions introduced above use radio signals to measure ranges from known transmitters to a user based on TOA, TDOA or RSS. The problem of range-based positioning has been studied for many years and it is known that appropriately weighting these measurements based on their accuracy improves the positioning performance (Cheung et al 2004). Tarrio et al (1999) show that in a Wi-Fi network, the position results are more accurate and robust when appropriate weighted techniques are used for RSS-based positioning. Lau & Mok (1999) also show that accuracy of relative GPS positioning is improved in an outdoor multipath environment when observations are weighted according to their carrier-to-noise density ratios. Wieser et al (2005) argue that an appropriate weighting model based on the variances of GPS observations significantly improves the positioning accuracy.

1.2 Limitation of Previous Work

Pedestrian Navigation Systems (PNS) constitute a subject of great interest for numerous applications such as E911 and activity monitoring. Because of these important applications, much research concentrating on pedestrian navigation systems has been conducted. Some of this research is introduced below and the limitations are explained.

A close look at GPS from a pedestrian navigation point of view reveals its limitations. In addition to open sky areas, PNS typically operates in environments where GPS signals are either obstructed or attenuated. As an example, in urban areas, GPS signals may be blocked or attenuated by buildings or the received signal may be degraded when the system enters a building.

As mentioned in Section 1.1, some technological advancements like High Sensitivity GPS (HSGPS) and A-GPS receivers make it feasible to detect signals indoors. HSGPS receivers use a longer integration time to estimate GPS signal parameters and A-GPS receivers are assisted by external sources to extract GPS signal parameters. Karunanayake et al (2004) demonstrated that an A-GPS receiver provides a 13 dB improvement in acquisition sensitivity over an HSGPS receiver. However, the reliability and accuracy of such techniques still needs improvement (Mezentsev 2005).

As a result, to provide an improved navigation solution when the user moves in indoor environments, GPS is integrated with other complementary self-contained sensors such as IMUs. The integration of GPS and INS is well known (e.g. Jekeli 2000, Groves 2008, El-Sheimy 2007, Petovello 2003). However, much of the work done so far has focused on positioning in urban areas or environments where GPS outages occur for

small periods of time. Over periods of several seconds without GPS updates, positioning accuracies of centimetres to decimetres are achievable (Petovello 2003). GPS and INS integration for indoor applications, where GPS signals are degraded, requires further investigation in view of the complexity of the problem.

In contrast to traditional INS mechanizations, Pedestrian Dead Reckoning (PDR) exploits the kinematics of human walking. PDR uses accelerometer signals to detect steps, estimate step length and propagate position using a measured heading. As such, the position error tends to increase with distance. Heading is calculated, for example, by a levelled compass which is difficult in indoor environments due to strong magnetic disturbances. Magnetic field perturbation is characterized for pedestrian navigation environments (Afzal 2011). The magnetic disturbance can be detected and corrected by coupling a compass with a gyro triad but the tuning of such a filter is not easy (Mezentsev et al 2005). Gyros can also be used, but this requires an initial heading be available and errors from the gyro accumulate with time.

In inertial systems the positioning accuracy is limited by the gyro accuracy since it introduces a third order position error that grows with time. In Godha et al (2006) the IMU is mounted on the foot of the user. This has the advantage that it exploits the small period during which the foot comes to rest at each step and uses Zero Velocity Update (ZUPT) to keep the INS errors bounded in the absence of GPS. However, this approach has three drawbacks. First, for most applications it is inconvenient to place an IMU on the foot. Second, the sensors do not provide ZUPT when the pedestrian travels in a vehicle. Third, since the GPS antenna is not mounted next to the INS, the lever arm between the GPS and INS is variable and should be modeled (Bancroft 2010).

One objective of this research is to provide accurate measurements from GPS signals in a degraded signal environment. These measurements update the INS and, therefore, there is no need to mount the INS on a foot for zero velocity updates. The GPS and INS are mounted on the same platform with a known lever arm. In this work a reference-rover receiver is introduced for increasing the accuracy and availability of the Doppler and pseudorange measurements. This information aids the INS to obtain better indoor accuracy for pedestrian navigation.

As stated in Section 1.1, GPS Doppler measurements are carrying information on the user's dynamics. GPS receivers produce more accurate Doppler and velocity measurements than ranges and positions. This accuracy can be useful in signal degraded environments. A GPS/INS integrated system can exploit accurate velocity and Doppler measurements to correct INS sensor errors. Although pseudorange multipath errors are unlimited, they are still necessary for updating the INS since the navigation solution without these measurements drifts in time. This type of hybridization can only work if the quality of Doppler and pseudorange measurements in terms of variance is correctly characterized. Due to unlimited pseudorange multipath errors, it is not possible to provide a theoretical model for pseudorange accuracy and only the quality of indoor Doppler is investigated in this work.

Previous works focused on the Doppler quality of outdoor applications (Borio et at 2009). For indoor pedestrian navigation, Doppler has not been fully characterized. Moreover, Doppler measurements are always available outdoors, but their availability in signal degraded environments should be better investigated for different indoor environments. The quality of outdoor Doppler measurements has been investigated and a

preliminary analysis has been provided by Borio et al (2009) and Sokolova (2009). Additional work is required to characterize the Doppler variance induced by the surroundings (impact of multipath and fading).

Petovello et al (2003) encountered some problems in terms of Doppler measurements indoors. These included the long integration time used by the receiver and the large clock drift of the receiver oscillator. In order to overcome the clock drift problem, an A-GPS with a common clock for the reference and rover is used. Later, the clock drift will be estimated as an unknown to investigate its effect on Doppler measurements and navigation solution.

1.3 Objectives

The limitations of the previous work described in Section 1.2 are the basis for the research toward the use of the GPS Doppler and pseudorange measurements to update the INS for indoor applications. The overall objective of this work is to enhance the accuracy of integrated navigation solutions in indoor environments where GPS signals are corrupted. In order to achieve this goal, the sub-objectives are identified as:

1. Investigate ways of improving Doppler and pseudorange measurements in indoor environments.

2. Discuss and compare indoor channel effects such as multipath and attenuation errors on Doppler and pseudorange measurements.

3. Characterize indoor Doppler measurements in terms of variance based on signal strength and receiver motion using a reference-rover receiver.

4. Analyze and compare the quality of indoor Doppler measurements provided by different types of receivers including commercial HS, standard and reference-rover receivers in various indoor environments.

5. Analyze and compare the performance of different indoor GPS measurement weightings on the accuracy of an integrated navigation solution.

1.4 Thesis Outline

This dissertation consists of six chapters and the subsequent chapters are outlined below.

Chapter Two describes an overview of positioning systems. This chapter summarizes GPS characteristics and related errors. INS is introduced. Coordinate frames, mechanization equations and the error model of inertial systems are elaborated and, finally, methods of GPS/INS integration are discussed.

Chapter Three discusses indoor GPS signal behavior and presents methods of providing signal parameters in degraded signal environments. The A-GPS and the block processing method are described. These methods are used later for Doppler characterization.

In Chapter Four, a practical method for indoor Doppler characterization is introduced. Doppler reference and its accuracy are discussed. Real measurements for Doppler characterization are described and analysed.

Chapter Five provides descriptions of the field tests, analysis and performance evaluation. It presents the performance results of GPS/INS integration and compares different variance models used for weighting Doppler and pseudorange measurements.

Chapter Six summarizes the works presented in the thesis and draws conclusions based on the test results. Finally, recommendations for future work are suggested.

Chapter Two: Navigation System Overview

This chapter gives a brief review of GPS and INS. The basic concepts of GPS, including signals, observations and related error sources, are introduced in Section 2.1. In Section 2.2 the fundamentals of INS are presented explaining coordinate frames, mechanization equations and error sources. Finally, diverse methods of GPS/INS integration are described at the end of the chapter.

2.1 Global Positioning System

GPS is a satellite-based navigation system that provides accurate three-dimensional Position and Velocity as well as Time (PVT) worldwide, at any time and in all-weather conditions. The nominal GPS constellation consists of 24 satellites, divided into six orbital planes with four satellites per orbit. The planes are inclined at angles of 55 degrees with respect to the equatorial plane. Currently, 32 active satellites are in orbit. Satellites broadcast Radio Frequency (RF) signals that enable receivers to compute the ranges to the satellites based on the Time of Arrival (TOA) ranging principle in the passive, listen only mode (Misra & Enge 2006). A receiver observes RF signal parameters to estimate PVT. In order to introduce these observations, the structure of the signal is described briefly in Section 2.1.1.

2.1.1 Signal Structure

GPS is a navigation system with spread spectrum Code Division Multiple Access (CDMA) signals. Each GPS RF signal consists of the following three parts (Misra & Enge 2006):

- Carrier: The signals are transmitted on three carrier frequencies, namely L1 (1575.42 MHz), L2 (1227.60 MHz) and L5 (1176.45). These carrier frequencies belong to the Ultra High Frequency (UHF) band. All the satellites broadcast L1 and L2. L5 is only available on block IIF satellites and, till now, only one satellite from this block has been launched with the operational L5 signal.
- Ranging code: Pseudo Random Noise (PRN) codes are modulated on the carrier frequencies. Each satellite has its own unique PRN code that allows satellites to transmit their signals on the same carrier frequency. Coarse/Acquisition codes (C/A-codes) are transmitted on L1 for civil users, and precision or P(Y)-codes are transmitted on both L1 and L2. The P-code is encrypted by the Y-code to limit access to authorized users.
- Navigation data: Satellite health status, ephemeris (satellite position and velocity), time, clock bias parameters and an almanac giving reduced-precision ephemeris data on all satellites, are encoded in a binary message called navigation data. In addition to ranging code, the navigation data is modulated on the carrier frequencies.

In this research only the L1 signals are used and, in the following sections, receiver observations for this single frequency are introduced.

2.1.2 GPS Observations

In general, a GPS receiver can obtain pseudorange, carrier phase and Doppler measurements from L1 signals. Although all these measurements are utilized for position and velocity estimation, Doppler measurements and pseudoranges are adequate for this estimation and carrier phase, whenever available, can improve the estimation accuracy. The carrier phase is available if the receiver works in Phase Lock Loop (PLL) mode. A standard receiver starts with acquisition and, after acquiring the signal, continues with signal tracking in Frequency Lock Loop (FLL) and PLL modes. In a degraded signal environment, the receiver cannot remain in PLL mode since it may lose lock or switch between the FLL and PLL modes. Hence, in an indoor environment the carrier phase is observable discontinuously with cycle slips and is not useful for navigation solutions. Since Indoor navigation is the aim of this work, only pseudorange and Doppler measurements are described in the following sections.

2.1.2.1 Pseudorange Measurements

Pseudoranges or code phase observations are provided by measuring the transit time of the signal from the satellite to the receiver. The transit time is measured by the correlation between the C/A-code, received from a GPS satellite, and its replica generated at the receiver. Since the clocks, installed on the satellite and the receiver, are not synchronized, the measured range is biased and called a pseudorange. To this end, the receiver's clock bias with respect to the satellite's GPS time has to be taken into account and leads to four unknowns (three-dimensional position and clock bias) in the positioning

equations. Therefore, at least four pseudorange observations are required to estimate the receiver's three-dimensional position and clock offset.

2.1.2.2 Doppler Measurements

A receiver can observe the carrier frequency of the received signal by generating a replica carrier wave. Based on the Doppler effect, the observed frequency differs from the L1 signal or any other carrier frequency emitted from the satellites once the receiver frequency drift is corrected. This frequency shift is due to the relative motion of the receiver and the satellite and is called Doppler measurement. By providing Doppler measurements and knowing the satellite velocity and the satellite-receiver unit vector, one can determine the receiver velocity. The carrier wave replica generated in the receiver is related to the receiver internal clock and its drift. As a result, a common frequency offset, called clock drift, is observed in Doppler measurements from all satellites. Three velocity components and the clock drift are the four unknowns in the Doppler measurement equations and at least four Doppler measurements are necessary to estimate them.

2.1.3 Errors

The quality of the PVT estimates obtained by a GPS unit depends upon the geometry of the satellites and the quality of the pseudorange and Doppler measurements. Error sources can be categorized into the following three basic groups (Lachapelle 2009): satellite-based errors, receiver-based errors and propagation errors. The satellite-based errors include orbital errors, satellite clocks and group delays. The receiver-based errors

consist of the receiver clock, multipath and receiver thermal noise. The propagation errors are due to ionospheric and tropospheric errors. In an indoor environment, two of the effects buildings have on signals are signal attenuation and multipath. Signal attenuation boosts the effect of noise and, when combined with multipath, increases the receiver-based errors. Multipath and attenuation errors in weak signal environments are discussed in Chapter Three. The details of other errors and their mitigation techniques are not discussed here, but can be found in a number of references (e.g. Lachapelle 2009, Misra & Enge 2006, Leva et al 1996).

2.2 Inertial Navigation Systems

Inertial navigation is an autonomous or self-contained process of computing position by doubly integrating the acceleration of a point, whose position is to be determined (Jekeli 2001). As a result, INS works based on the relative positioning principle and has to be initialized with an initial velocity, position and attitude. Such a navigation system, where the current position is evaluated by the relative increment from the previous known position, is called a Dead Reckoning (DR) system. INS as a DR system is comprised of the following parts (Jekeli 2001):

- IMU: INS exploits sensors that follow Newton's law to measure the motion parameters of the vehicle (Section 2.2.2).
- Platform: All the inertial sensors (i.e., the IMU) are mounted on a rigid platform. The methods of installing or mechanizing this platform on the vehicle, whose navigation states are desired, are discussed in Section 2.2.3.

- Computer: The calculations that transform sensed IMU measurements to navigation state changes and update the navigation states are performed in a computer. The calculations are based on mechanization equations (Section 2.2.4) and the navigation states are position, velocity and attitude.

2.2.1 Coordinate Frames

An INS uses sensors that provide measurements relative to the inertial frame and, depending on the user's application, computes navigation states in another or the same coordinate frame. The five coordinate frames that are generally used by an INS are introduced here. The superscript denotes the frame in which a measurement is obtained. The details of these coordinate frames follow from El-Sheimy (2007), Godha (2006), Petovello (2003) and Jekeli (2001).

The Inertial frame (i-frame) is considered to be non-rotating and non-accelerating frame relative to far-off galaxies (Petovello 2003) with the following conventions:

- Origin: Earth's centre of mass
- Z-axis: Parallel to the spin axis of the Earth
- X-axis: Pointing towards the mean vernal equinox
- Y-axis: Orthogonal to the X and Z axes to complete a right-handed frame

The Earth Centered Earth Fixed frame (ECEF or e-frame) is fixed to the earth and is defined as follows:

- Origin: Earth's centre of mass
- Z-axis: Parallel to the mean spin axis of the Earth
- X-axis: Pointing towards the zero meridian
- Y-axis: Orthogonal to the X and Z axes to complete the right-handed frame

The Local Level Frame (LLF or l-frame) is defined as follows:

- Origin: Coinciding with the centre of the navigation system
- Z-axis: Orthogonal to the reference ellipsoid pointing up
- X-axis: Pointing towards geodetic east
- Y-axis: Pointing towards geodetic north

The Body frame (b-frame) represents the orientation of the IMU axes (Petovello 2003). Depending on the mechanization method (Section 2.2.3), different conventions are adopted for the body frame. Since this work uses a strapdown configuration, the body frame is aligned with the vehicle frame and is defined as follows:

- Origin: Centre of the IMU
- X-axis: Pointing towards the right of the vehicle
- Y-axis: Pointing towards the front of the vehicle
- Z-axis: Orthogonal to the X and Y axes to complete a right-handed frame

The Navigation frame is the frame used for the implementation of the mechanization equations.

2.2.2 Inertial Measurement Unit

The motion sensors of an INS are called the IMU. There are two types of motion, namely translational and rotational. Consequently, the following two types of sensors exist in an IMU:

- Accelerometer that senses linear acceleration along its sensitive axis.
- Gyroscope (or gyro) that senses the angular rate around its sensitive axis.

In order to measure the three components of the acceleration and angular velocity vectors, a triad of gyros and accelerometers are arranged orthogonally in the IMU. As stated in Section 2.2.1, the IMU axes identify the b-frame coordinate axes, thus the IMU measurements are represented by the superscript 'b'.

An accelerometer output is a specific force vector, f^b, which is related to the body acceleration vector, a^b, via the gravitational acceleration vector, $\tilde{g}^b$, as follows:

$$f^b = a^b - \tilde{g}^b . \qquad 2\text{-}1$$

Gyros sense the angular rate due to the Earth rotation, the orientation changes of the l-frame, and the rotation of the body relative to the l-frame. Consequently, the body angular velocity is determined by the gyros after compensating for the earth's rotation rate and the l-frame change of orientation (ω_{il}^b). This can be written as

$$\omega_{lb}^b = \omega_{ib}^b - \omega_{il}^b , \qquad 2\text{-}2$$

where the angular velocity vector, ω_{yz}^{x}, represents the angular velocity of frame 'z' with respect to frame 'y', expressed in the frame 'x', and

ω_{lb}^{b} is the body angular velocity vector relative to the l-frame and

ω_{ib}^{b} is the body angular velocity vector measured by the gyros.

2.2.3 Mechanization

The mechanization of an INS describes the physical arrangement of inertial sensors on the vehicle. There are two general types of mechanization (Jekeli 2001), namely the stabilized platform and the strapdown configuration. The stabilized platform isolates the angular motion of the platform from the vehicle by using torques derived from the measured angular rates. In this type of mechanization the IMU is kept aligned to a particular navigation frame (e.g. e-frame). As a result, the navigation frame coincides with the body frame and this makes mechanization equations as simple as doubly integrating the accelerometer outputs to provide velocity and position. In a strapdown system, the platform holding the IMUs is attached firmly to the vehicle and the body frame has an arbitrary orientation. In a strapdown system, the processing load increases since the accelerometer outputs should be rotated from the body frame to the navigation frame using the measured rotation rates from the gyros.

For general navigation applications, there is a rapid advance of strapdown systems at this time because of their advantages in reliability, power consumption, weight and cost (El-Sheimy 2007). Also, the development of strapdown systems is totally dependent on the advancement of processor technology that is necessary for strapdown

mechanization equations. In this work only strapdown systems are discussed and their mechanization equations are explained in Section 2.2.4.

2.2.4 Mechanization Equations

Mechanization equations are the set of equations used to convert the specific force, f^b, and angular velocity, ω_{ib}^b, measurements obtained from an IMU into useful position, velocity and attitude information (Godha 2006). In this work, strapdown mechanization is implemented in the l-frame as the navigation frame. The position of a moving platform in the l-frame is expressed in terms of the curvilinear coordinates (latitude, longitude and height) and the velocity is expressed by three components along the east, north and vertical directions as follows:

$$r^l = \begin{bmatrix} \varphi \\ \lambda \\ h \end{bmatrix} \tag{2-3}$$

$$v^l = \begin{bmatrix} v^e \\ v^n \\ v^u \end{bmatrix}, \tag{2-4}$$

where

r is the position vector and

v is the velocity vector.

In the strapdown system, the body sensed acceleration, a^b, from Equation 2-1 cannot be integrated directly to obtain velocity and position as in the case of the

stabilized platform. Instead, the measured acceleration in the b-frame must be transformed to the l-frame, a^l, by using the transformation (rotation) matrix, R_b^l, according to

$$a^l = R_b^l a^b, \tag{2-5}$$

where R_x^y is the rotation matrix from the frame 'x' to frame 'y'.

In order to compute the rotation matrix, the body sensed angular rates are integrated using the approach described in Section 2.2.4.2.

INS mechanization equations are provided in a few steps to solve the equations of motion, which describe the vehicle's motion based on the physics of motion and sensor measurements. To this end, the equations of motion are described in the following section.

2.2.4.1 Equations of Motion

The motion of the vehicle can be described mathematically by the equations of motion. These equations are given by (El-Sheimy 2007)

$$D^{-1} = \begin{bmatrix} 0 & 1/(R_E + h) & 0 \\ 1/(R_E + h)\cos\varphi & 0 & 0 \\ 0 & 0 & 1 \end{bmatrix} \tag{2-6}$$

$$\begin{bmatrix} \dot{r}^l \\ \dot{v}^l \\ \dot{R}_b^l \end{bmatrix} = \begin{bmatrix} D^{-1}v^l \\ R_b^l f^b - (2\Omega_{ie}^l + \Omega_{el}^l)v^l + g^l \\ R_b^l(\Omega_{ib}^b - \Omega_{il}^b) \end{bmatrix}, \tag{2-7}$$

where the dots denote the time derivative and

R_E is the Earth radius (spherical model),

Ω is the skew-symmetric form of the rotation rate vector ω and

g is the gravity vector.

Equation 2-7 shows that the specific force, f^b, and the angular rate, ω_{ib}^b, measurements from the inertial sensors are input into the equations. These equations that express the relationship between the derivatives of a function and the function itself consists of differential equations. In order to solve these equations, numerical methods (e.g. Jekeli 2001) are normally used and initial conditions are needed. Here, the initial position and velocity are input by GPS while the user is static in an open sky area and the initial orientation of the system is provided by an initial alignment. Afterwards, mechanization equations are used to solve the equations of motion to provide the information needed for navigation solution. The mechanization equations can be divided into the following basic steps:

- Attitude update
- Transformation of the specific force to navigation frame (here l-frame)
- Velocity and position calculation.

The block diagram of these steps is shown in Figure 2-1 and each of these steps is explained in the following sections.

Instead of specific forces and angular rates, the outputs of many inertial sensors are velocity increments, Δv^b, for accelerometers and angular increments, $\Delta\theta_{ib}^b$, for gyros

over the interval t_k to t_{k+1}. It is assumed in the following sections that these measurements are provided by the IMUs.

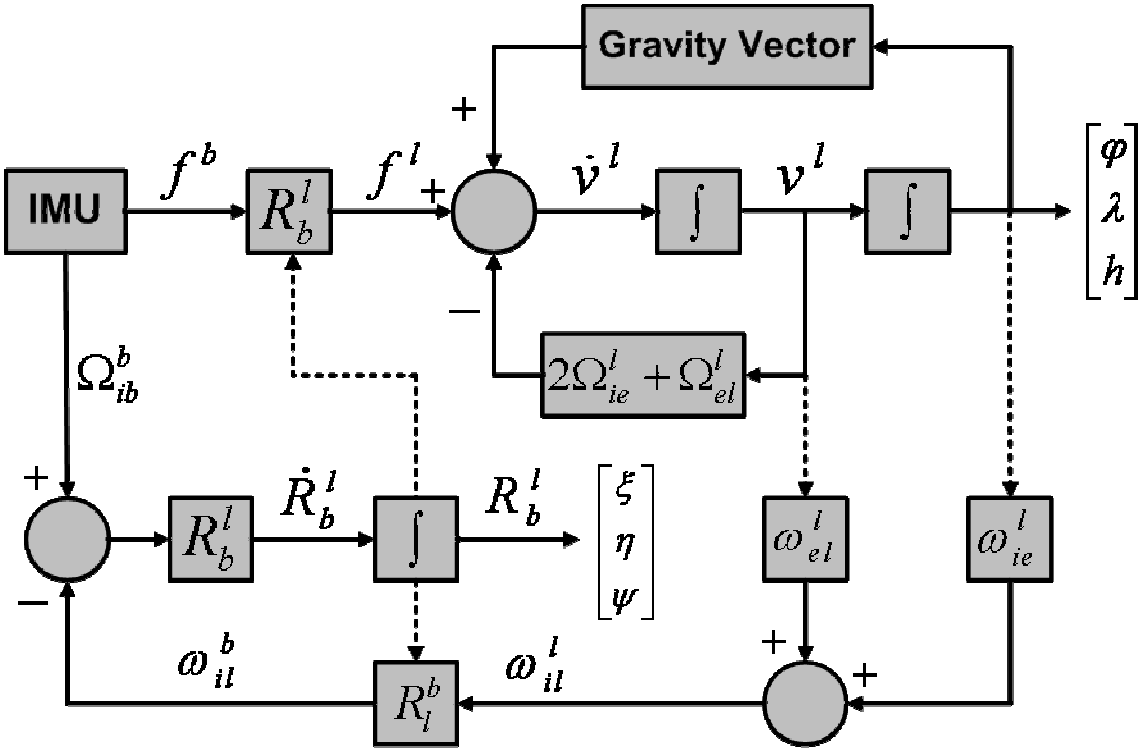

Figure 2-1: INS Mechanization in l-frame

2.2.4.2 Attitude Update

Equation 2-2 shows that the body angular increments with respect to the l-frame are given by

$$\Delta\theta_{lb}^b = \omega_{ib}^b \Delta t - \omega_{il}^b \Delta t = \Delta\theta_{ib}^b - R_l^b \omega_{il}^l \Delta t \,, \qquad 2\text{-}8$$

where

R_l^b is the rotation matrix from the l-frame to the body frame and

Δt is the time interval ($t_{k+1} - t_k$).

The first term, $\Delta\theta_{ib}^{b}$, is obtained directly from the gyros and ω_{il}^{l} in the second term includes the earth's rotation rate, ω_{ie}^{l}, and the orientation changes of the l-frame, ω_{el}^{l}. This part can be computed if the velocity and position are known from the previous epoch and is given by

$$\omega_{il}^{l} = \omega_{ie}^{l} + \omega_{ei}^{l} = \begin{bmatrix} 0 \\ \omega^{e}\cos\varphi \\ \omega^{e}\sin\varphi \end{bmatrix} + \begin{bmatrix} -v^{n}/(R_{E}+h) \\ v^{e}/(R_{E}+h) \\ v^{e}\tan\varphi/(R_{E}+h) \end{bmatrix}, \qquad 2\text{-}9$$

where

ω^{e} is the earth's rotation rate (15 degree/hr).

As a result, by knowing the rotation matrix, R_{l}^{b}, from the previous epoch, the angular increment vector of the body relative to the l-frame can be obtained in Equation 2-8. This angular increment then can be used to update the rotation matrix in Equation 2-7 using a first order approximation as follows:

$$R_{b}^{l}(t_{k+1}) = R_{b}^{l}(t_{k})(I + S_{lb}^{b}), \qquad 2\text{-}10$$

where

S_{lb}^{b} is the skew-symmetric matrix of the angular increment $\Delta\theta_{lb}^{b}$.

The computed rotation matrix, R_{b}^{l}, is used in the next step of the mechanization equations. The transformation between b-frame and l-frame can be performed by three consecutive rotations around Z^{b}, X^{b} and Y^{b}, and is assumed to be defined as follows:

$$R_{b}^{l} = R_{3}(\psi)\,R_{1}(-\eta)\,R_{2}(-\xi), \qquad 2\text{-}11$$

where

ξ is the roll of the vehicle,

η is the pitch of the vehicle,

ψ is the azimuth or yaw of the vehicle, and

R_i is the rotation matrix around the i^{th} axis.

The rotation matrix is then used in the following equations to estimate the attitude of the b-frame or the vehicle:

$$\xi = -\tan^{-1}\left(\frac{\left(R_b^l\right)_{3,1}}{\left(R_b^l\right)_{3,3}}\right) \quad \text{2-12}$$

$$\eta = -\sin^{-1}\left(\left(R_b^l\right)_{3,2}\right) \quad \text{2-13}$$

$$\psi = \tan^{-1}\left(\frac{\left(R_b^l\right)_{1,2}}{\left(R_b^l\right)_{2,2}}\right), \quad \text{2-14}$$

where

$\left(R_b^l\right)_{a,b}$ is the element of the a^{th} row and the b^{th} column of the R_b^l matrix.

2.2.4.3 Transformation of the Specific Force to the Navigation Frame

In this step, the specific force measurements are rotated from the b-frame to the l-frame (navigation frame) as follows:

$$f^l = R_b^l f^b . \quad \text{2-15}$$

Integrating Equation 2-15, the velocity increment can be obtained based on specific force measurements and the rotation matrix from Section 2.2.4.2 and is given by

$$\Delta v_f^l = \int_{t_k}^{t_{k+1}} R_b^l(t) f^b(t) dt , \qquad 2\text{-}16$$

where the f subscript in the velocity increment notes that it is measured based on the specific force.

In Equation 2-16, the rotation matrix is a function of time and the average orientation of the vehicle during the integration interval is used to calculate the velocity increment (Godha 2006, Petovello 2003). One of the two following equations can be used to compute the velocity increment in the navigation frame:

$$\Delta v_f^l = R_b^l(t_k)\left(I + \frac{1}{2} S_{lb}^b\right)\Delta v_f^b \qquad 2\text{-}17$$

$$\Delta v_f^l = R_b^l(t_{k+1})\left(I - \frac{1}{2} S_{lb}^b\right)\Delta v_f^b . \qquad 2\text{-}18$$

2.2.4.4 Velocity and Position Calculation

The velocity increments due to the specific force represented in Equations 2-17 and 2-18 require some corrections based on the motion equations provided in Equation 2-7. The corrected velocity increment in the l-frame is given by

$$\Delta v^l = \Delta v_f^l - (2\Omega_{ie}^l + 2\Omega_{el}^l) v^l \Delta t + g^l \Delta t , \qquad 2\text{-}19$$

where the second term on the right-hand side is the Coriolis correction and the third term is the gravity correction. These two terms are computed using the navigation states from

the previous epoch. After computing the velocity increment relative to the previous epoch, the velocity at the current epoch is computed by using the modified Euler formula as

$$v_{k+1}^{l} = v_{k}^{l} + 0.5\left(\Delta v_{k}^{l} + \Delta v_{k+1}^{l}\right), \tag{2-20}$$

and finally, using the modified Euler formula again, the l-frame coordinates can be obtained from the velocity provided in Equation 2-20 as

$$r_{k+1}^{l} = r_{k}^{l} + 0.5D^{-1}\left(v_{k}^{l} + v_{k+1}^{l}\right)\Delta t\,. \tag{2-21}$$

2.2.5 INS Errors

In Section 2.2.4, the INS mechanization was discussed without accounting for the inertial sensor errors. To correct for these errors, GPS measurement updates are used (Section 2.3). This is commonly done by using a Kalman filter that estimates the INS errors. In the following sections, the effect of inertial sensor errors on navigation states is shown and various sensor errors are described.

2.2.5.1 INS Error Equations

Since INS is an integration system, the navigation state errors at a previous epoch influence the current epoch. In addition, INS sensor errors at each epoch increase with time. This can be shown by the INS error equations, which are represented by a series of differential equations and are given by (El-Sheimy 2007)

$$M = \begin{bmatrix} 0 & 1/(R_E + h) & 0 \\ -1/(R_E + h) & 0 & 0 \\ -\tan\varphi/(R_E + h) & 0 & 0 \end{bmatrix} \quad 2\text{-}22$$

$$\begin{bmatrix} \delta\dot{r}^l \\ \delta\dot{v}^l \\ \dot{\varepsilon}^l \end{bmatrix} = \begin{bmatrix} D^{-1}\delta v^l \\ -F^l\varepsilon^l \\ M\,\delta v^l \end{bmatrix} + \begin{bmatrix} 0 \\ R_b^l \delta f^b \\ R_b^l \delta\omega_{ib}^b \end{bmatrix}, \quad 2\text{-}23$$

where a δ in front of a parameter means an error of that parameter and

F is the skew-symmetric matrix of specific force measurements,

ε is a vector of misalignment angles along each axis,

δf^b is the vector of accelerometer sensor errors, and

$\delta\omega_{ib}^b$ is the vector of gyro sensor errors.

In Equation 2-23, the first term on the right-hand side represents the effect of the previous epoch's state errors and the second term is the effect of current sensor errors.

2.2.5.2 Inertial Sensor Error Model

In this section, the various errors present in the inertial sensors and the methods of estimating them are described. The errors in accelerometers and gyros include sensor noise, bias, scale factor error and non-orthogonality errors. These errors for accelerometer and gyros are given by (El-Sheimy 2007)

$$\delta f^b = b_f + S_f f^b + N f^b + \eta_f \quad 2\text{-}24$$

$$\delta\omega_{ib}^b = b_\omega + S_\omega \omega_{ib}^b + N\omega_{ib}^b + \eta_\omega, \quad 2\text{-}25$$

where the subscript f denotes accelerometer specific errors, the subscript ω denotes gyro specific errors and

b is the sensor bias vector,

S is the matrix of linear scale factor error,

N is a matrix representing the non-orthogonality of sensor triads, and

η is the sensor random noise.

The inertial sensor errors are described below.

- Noise: Noise is inherent to any measurement and is an additional signal resulting from the sensor itself or any other electronic equipment that interferes with the output signals being measured. It is generally stochastic and thus cannot be removed from the data using deterministic models. Instead, it is modeled as a zero-mean white Gaussian noise and its power is estimated. Petovello (2003) estimated the Power Spectral Density (PSD) of the noise present in accelerometer and gyro measurements by taking the standard deviation of a few seconds of static data. This was repeated at several points of a long static data sequence and the mean was used for estimation of the noise power.
- Sensor Bias: The inertial sensor bias is defined as an offset in the sensor output, measured at specific operating conditions, and has no correlation with input acceleration or rotation (Kwakkel 2008, Godha 2006). The bias consists of two components, namely a deterministic part and a stochastic part. The deterministic part can be obtained by lab calibration procedures and the stochastic part is called a bias drift, which refers to the rate at which the error in an inertial sensor

accumulates with time (El-Sheimy 2007). The bias drift is generally modeled as a Gauss Markov (GM) process (Godha 2006, Petovello 2003). The details of the GM model are described in a number of references (e.g. Jekeli 2001, Petovello 2009). Petovello (2003) showed that the autocorrelation function of raw data collected under static conditions for a long time can be used to determine the parameters of the GM model. In this work, static raw data was collected for about forty hours in the same environmental circumstances that the IMU is expected to operate in.

- Scale Factor Error: The scale factor is the ratio of a change in the output to a change in the input intended to be measured (El-Sheimy 2007). The scale factor error is expressed in Parts Per Million (PPM) and is measured by the slope of the line that can be fitted to the input-output data by the method of least-squares (ibid).
- Non-Orthogonality Error: The accelerometers and gyros in an IMU are to be mounted in an orthogonal triad. The misalignment in their axes causes an error called a non-orthogonality error. As a result, each axis is affected by the measurements of the other two axes in the b-frame. Axis misalignments can be calibrated using lab calibration techniques.

Attempting to model all the error parameters for using them in a Kalman filter is not practical in this work. The accurate estimation of more states (INS error parameters) needs more observations and this is not the case for indoor applications where there are generally a lower number of GPS observations. In addition, under operational conditions,

more error states increase the computational burden. Thus, it is assumed in this work that only bias and noise are present in the inertial sensor errors and can be written as:

$$\delta f^b = b_f + \eta_f \tag{2-26}$$

$$\delta\omega_{ib}^b = b_\omega + \eta_\omega . \tag{2-27}$$

Error models in Equations 2-26 and 2-27 are used in the INS error equations to obtain the final system model. Also, it is assumed that bias states are modeled as first-order GM processes as follows:

$$\begin{bmatrix} \delta\dot{r}^l \\ \delta\dot{v}^l \\ \dot{\varepsilon}^l \\ \delta\dot{b}_f^b \\ \delta\dot{b}_\omega^b \end{bmatrix} = \begin{bmatrix} 0 & D^{-1} & 0 & 0 & 0 \\ 0 & 0 & -F^l & R_b^l & 0 \\ 0 & M & 0 & 0 & R_b^l \\ 0 & 0 & 0 & -diag(\alpha_i) & 0 \\ 0 & 0 & 0 & 0 & -diag(\beta_i) \end{bmatrix} \begin{bmatrix} \delta r^l \\ \delta v^l \\ \varepsilon^l \\ \delta b_f^b \\ \delta b_\omega^b \end{bmatrix} + \begin{bmatrix} 0 & 0 & 0 & 0 \\ R_b^l & 0 & 0 & 0 \\ 0 & R_b^l & 0 & 0 \\ 0 & 0 & I & 0 \\ 0 & 0 & 0 & I \end{bmatrix} \begin{bmatrix} \eta_f \\ \eta_\omega \\ \eta_{bf} \\ \eta_{b\omega} \end{bmatrix}, \tag{2-28}$$

where a δ in front of a parameter means the error of that parameter and

$diag(\alpha_i)$ is a diagonal matrix of time constants for the accelerometer bias models,

$diag(\beta_i)$ is a diagonal matrix of time constants for the gyro bias models,

η_{bf} is the driving noise for the accelerometer biases, and

$\eta_{b\omega}$ is the driving noise for the gyro biases.

The noise and bias parameters for the sensors used in this work are measured using the above methods. For the noise, PSD measurements are summarized in Table 2.1 and for the bias, first-order GM parameters, including the time constant and the temporal variance, are summarized in Table 2.2, for two tactical grade IMUs.

Table 2.1: Sensor Noise Spectral Densities for HG1700 and SPAN-CPT

Sensor	Noise Spectral Density		
	SPAN-CPT	HG1700	Unit
Accel X	7.6e-3	7.9e-2	$m/s/\sqrt{Hz}$
Accel Y	7.2e-3	7.8e-2	
Accel Z	8.9e-3	7.8e-2	
Gyro X	35.6	175	deg/ $hr/\sqrt{Hz}$
Gyro Y	27.5	176	
Gyro Z	26.5	332	

Table 2.2: Gauss-Markov Parameters for HG1700 and SPAN-CPT

Sensor	First-Order Gause-Markov Parameters					
	Time Constant			Temporal Variance		
	SPAN-CPT	HG1700	Unit	SPAN-CPT	HG1700	Unit
Accel X	124	185	minute	7.2e-5	8.2e-7	m^2/s^4
Accel Y	136	84		5.8e-5	8.5e-8	
Accel Z	132	110		6.4e-5	5.8e-7	
Gyro X	32	85		16.6	0.16	deg^2/hr^2
Gyro Y	47	67		2.03	0.31	
Gyro Z	50	83		3.41	0.29	

2.3 GPS/INS Integration

Since GPS and INS are complementary navigation systems, it is very common to integrate them to overcome each of their limitations, providing a continuous and reliable solution. Typically, there are four strategies for the integration of GPS and INS, which are classified as follows (Petovello 2003, Jekeli 2001):

- Uncoupled Integration: This method switches between GPS only or INS only solutions. Since GPS solutions are typically considered high-accuracy solutions, whenever GPS data is available, they are used to provide navigation solutions. Also, GPS solutions are used to correct INS solution errors. In the absence of

GPS, INS data is used to provide navigation solutions. In the case of an INS only solution, the accuracy of the navigation solution decreases until the next high-accuracy GPS data is available.

- Loose Integration: GPS and INS generate independent navigation solutions and the information from them is blended using an estimator to form a third navigation solution (El-Sheimy 2007). Typically, an Extended Kalman Filter (EKF) is used to accomplish the blending of GPS and INS information and the states of the EKF are used to correct INS errors. Loose integration is shown in Figure 2-2.

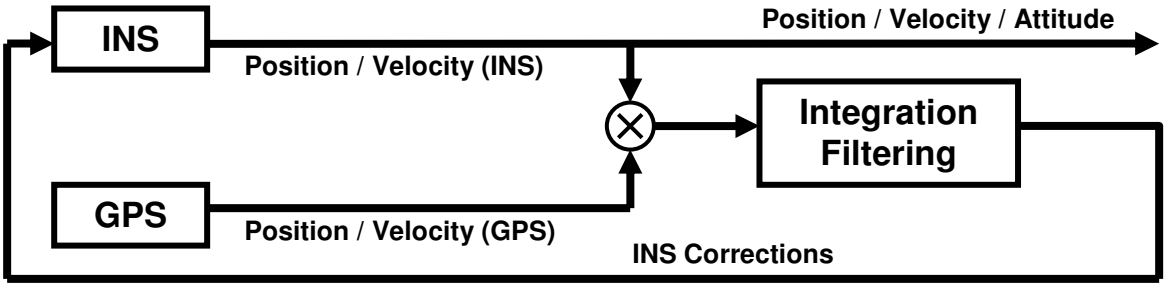

Figure 2-2: Loose Integration Strategy

- Tight Integration: Compared to loose integration, there is no separate GPS navigation solution in this scheme. Instead of blending navigation solutions from GPS and INS, the raw pseudorange and Doppler measurements from the GPS tracking loops and those from the INS prediction are combined to form the input to the EKF. The output of the EKF is the estimated INS errors that are used to correct the INS navigation solution. A tight integration block diagram is shown in Figure 2-3.

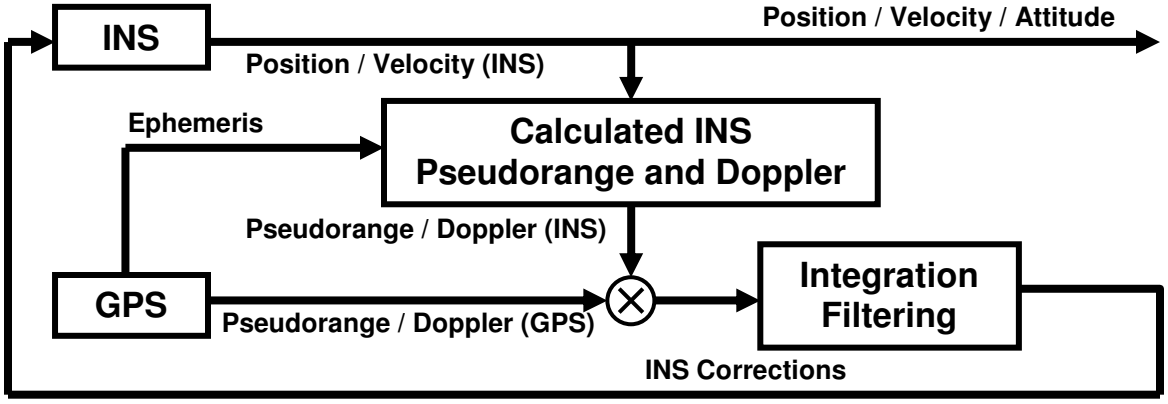

Figure 2-3: Tight Integration Strategy

- Deep / Ultra-Tight Integration: In this strategy the GPS and INS no longer work independently. Instead, GPS updates are used to correct INS errors and INS aids GPS receiver tracking loops when GPS signals are degraded. Since the INS can measure a user's dynamics and it is applied in the GPS signal replica generated in a tracking loop, a lower tracking loop bandwidth is needed compared to absolute dynamic tracking. Thus, using ultra-tight integration increases noise resistance in the tracking loop (Groves 2008).

In this work, the tight GPS/INS integration is implemented. It has two advantages over the loose integration method. First, there is no requirement of a minimum number of GPS satellites since Doppler and pseudorange measurements are used rather than the final calculated navigation solution that needs at least four satellites. Second, because process noise is added to a single filter in the tight integration approach, the filtering of the GPS measurements is improved (Petovello 2003). The main advantage of loose

integration over tight integration is its lower number of states that decreases the processing load.

Chapter Three: Indoor GPS Observations and Block Processing

It was shown in Chapter Two that GPS observations (pseudorange and Doppler measurements) can be exploited in a Kalman filter to estimate the INS errors. For a precise estimation of INS errors, the Kalman filter needs to know the accuracy of GPS observations. In this chapter the accuracy of GPS observations for indoor applications is investigated. The challenges associated with the processing and analysis of indoor signals are discussed in Section 3.1. In Section 3.2, the block processing technique is discussed as an alternative to the standard sequential tracking for indoor signal parameter estimation. Finally, a few theoretical models for predicting Doppler and pseudorange measurement errors are discussed in Sections 3.3 and 3.4.

3.1 Indoor Signal Challenges

In an indoor environment, multipath fading, signal attenuation and secondary paths are the main channel effects on the signals. These effects increase the receiver errors in GPS signal parameter estimation. Consequently, the major challenges for a GPS receiver in indoor environments are (Watson et al 2006):

- Overcoming multipath fading and signal attenuation
- Measuring the pseudorange and Doppler of the LOS signals affected by secondary paths.

These two challenges are described in the following sections. In Section 3.1.1 the definitions of multipath fading and signal attenuation are presented and their impact on

GPS receiver performance is discussed. Then, in Section 3.1.2, the secondary path and its effects on Doppler and pseudorange measurements are discussed.

3.1.1 Multipath Fading and Signal Attenuation

Multipath fading in the form of signal power fluctuation in time and space arises from the superposition of multiple replicas of a transmitted signal at the receiver antenna (Rappaport 2002). Replicas are reflections of the transmitted signal from the surfaces of scatterers surrounding the receiver and the transmitter. Each signal replica experiences different attenuations, delays and phase shifts while traveling from the transmitter to the receiver. The superposition of the signal replicas can result in either constructive or destructive interference, amplifying or attenuating the signal power seen at the receiver. Strong destructive interference is referred to as a deep fade. In addition to multipath fading, another common channel effect on the signal strength is signal attenuation. The gradual loss of signal strength through a medium is referred to as signal attenuation.

In an indoor environment, multipath fading and signal attenuation change the strength of the signal based on the following (Watson et al 2006):

- Nature of LOS obstacles: Signal attenuation is a function of the building material and structure. As an example, received signals in a concrete building are more attenuated as compared to those in a typical North American residential house consisting of a wooden frame and light construction materials.
- Multipath geometry: In a multipath environment, the geometry of obstacles, scatterers, satellites and the receiver unit is an important factor affecting the signal strength. For indoor applications where nearby scatterers, the user and the

satellites are in motion, the received signal envelope and its strength is a time-dependent variable (Lee 1977).

Figure 3-1 shows the carrier to noise density power ratio of a GPS signal collected by a dynamic user in a residential house. Since the user and the satellites are in motion, multipath geometry is changing and signal strength is a time-dependent variable. As shown in this figure, the received signal power in a fading channel undergoes fast variations. These variations pose a formidable challenge to signal tracking algorithms through increasing the measurement errors and possible loss of lock. Moreover, in the case of signal acquisition it is impossible to detect the signal from noise when it is in a deep fade.

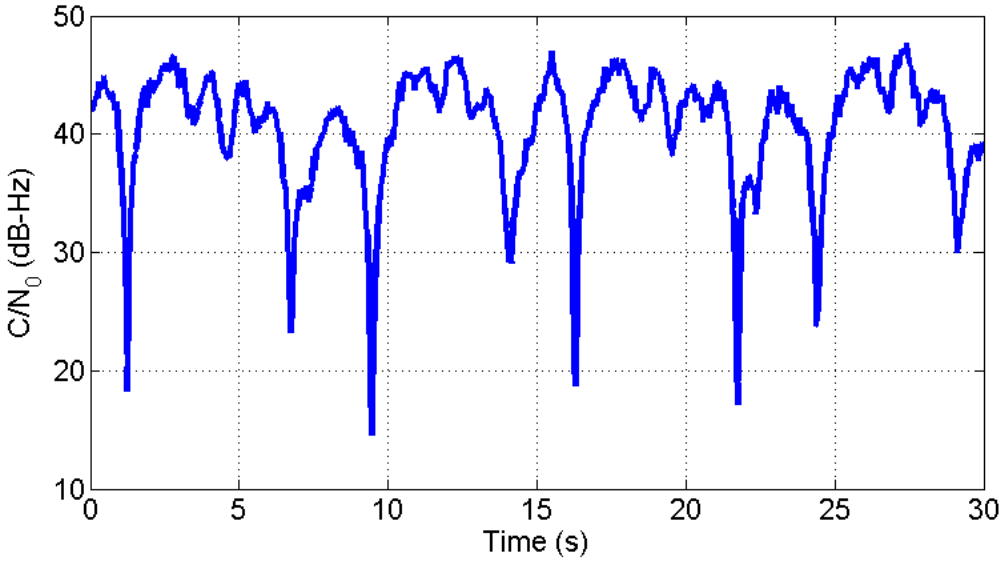

Figure 3-1: Fading in a multipath environment

3.1.2 Secondary Paths

Secondary path signals are the group of NLOS signals that arrive at the receiver antenna from secondary paths through reflection from large structures such as buildings, walls, metallic doors, etc. The parameters of reflected signals are dependent on the multipath geometry and are different from those of the direct signal. This difference causes an error in signal parameter estimation known as multipath error. A typical multipath geometry for a secondary path signal is shown in Figure 3-2. The direct (D) and reflected (R) signals can be presented by

$$S_D(t) = A_D \cdot \cos(\omega_D \cdot t + \phi_D) \quad 3\text{-}1$$

$$S_R(t) = A_R \cdot \cos(\omega_R \cdot t + \phi_R), \quad 3\text{-}2$$

where

ω is the Doppler frequency of the signal,

A is the signal amplitude and

ϕ is the phase of the signal.

The following sections show that multipath errors are a function of the receiver velocity and the reflected signal parameters such as power, A, phase, ϕ, and angle of arrival. In these sections, Doppler and pseudorange multipath errors are described separately and their effects on Doppler and pseudorange measurements are discussed.

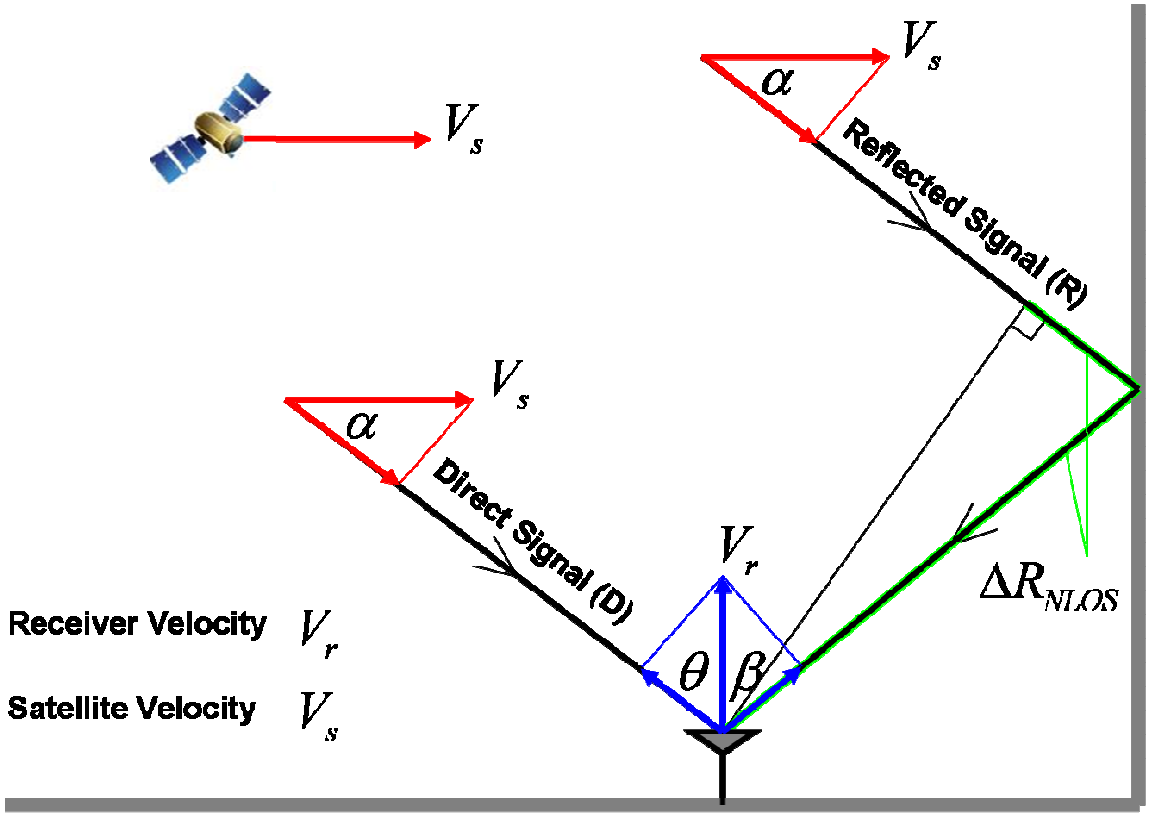

Figure 3-2: Multipath geometry for a secondary path

3.1.2.1 Pseudorange Multipath Errors

A reflected signal is a delayed and usually weaker version of the direct signal. Thus, the C/A-code correlator output consists of a superposition of delayed, scaled replicas of the triangular autocorrelation function. This summation does not necessarily provide a sharp undistorted peak resulting in erroneous pseudorange estimation.

Figure 3-2 shows that the path difference, ΔR_{NLOS}, is dependent on the multipath geometry. When there is no LOS between the receiver and the satellite, the pseudorange is derived only from the reflected signal. In this case, the pseudorange multipath error is equal to the path difference and is theoretically unlimited (Lachapelle 2009).

GPS errors (e.g. due to the orbits, clocks and the ionosphere) can cause temporal variations in pseudorange measurements (Olynik et al 2009). In an indoor environment, these variations are increased by pseudorange multipath errors when multipath geometry changes. This presents a problem in applications that a stable indoor position is required.

3.1.2.2 Doppler Multipath Errors

From Figure 3-2, the Doppler frequencies of the direct and reflected signals are given by

$$\omega_D = \left(V_s \cdot \cos\alpha + V_r \cdot \cos\theta\right)/\lambda \qquad 3\text{-}3$$

$$\omega_R = \left(V_s \cdot \cos\alpha + V_r \cdot \cos\beta\right)/\lambda\,, \qquad 3\text{-}4$$

where

λ is the wavelength.

It is the summation of the direct and reflected signals that is tracked by a GPS receiver. According to Equations 3-3 and 3-4, for a static receiver the Doppler frequency of the direct and reflected signals are equal and the receiver can measure the Doppler frequency of the composite signal with no Doppler errors. In contrast, for dynamic conditions, the Doppler frequencies of the two signals arriving from different angles are different. Under these conditions, the Doppler frequency estimated by the receiver is not equal to the direct signal Doppler frequency. The difference between the estimated and the direct signal Doppler frequencies is called the Doppler multipath error and is a function of the receiver's velocity and the angle of arrival. Note that the Doppler

multipath error is expected to be minimal for pedestrian applications due to limited velocity.

In order to compare limited Doppler multipath errors with unlimited pseudorange multipath errors, indoor Doppler and pseudorange measurements are used separately in Chapter Five to update the INS. In doing so, their effect on the navigation solution provided by the updated INS is analyzed.

Since changes in multipath geometry affect the Doppler frequency of the reflected signal, the Doppler multipath is not smooth. For this reason, Doppler measurements are noisy at the receiver. However, for low dynamics, Doppler measurements are expected to be less noisy as compared to pseudorange measurements.

3.2 GPS Receivers in Indoor Environments

The challenging nature of signal parameter estimation in indoor environments affects the performance of a standard GPS receiver designed for open sky areas. In the following sections the drawbacks of a sequential tracking method used in standard receivers are discussed. Then, a block processing technique is proposed as a solution and, finally, a reference-rover receiver is introduced as the block processing receiver used in this work.

3.2.1 Drawbacks of Standard Receivers in Indoor Multipath Environments

The main disadvantages associated with the use of a standard receiver in indoor environments are described below.

- Multipath fading and signal attenuation cause the standard tracking loop to lose lock. When the signal strength returns to the nominal value after the loss of lock, it may take several seconds until the receiver re-establishes a track on the signal (Feng & van Graas 1999). This means the receiver loses some measurements after each deep fade. For an indoor environment with a high fading rate, a standard receiver cannot provide continuous measurements.
- As mentioned in Section 3.1.2, multipath errors are not constant and change based on multipath geometry. These changes make the tracking loops unstable. By increasing the loop filter bandwidth in the tracking loop, the receiver becomes more robust to multipath geometry changes but the measurements become noisier. However, this cannot compensate for unlimited pseudorange multipath errors. For example, assume that the direct signal is blocked and the receiver is tracking the reflected signal. Because of geometry changes, the direct signal may become available to the receiver but will not be tracked since the receiver is tracking the reflected signal. This wrong measurement is due to the low observability of the sequential tracking loop that tries to estimate new signal parameters around the previous signal parameters estimated in the last epoch. After a while, the reflected signal may disappear. Under such a circumstance, the receiver loses lock, regardless of the loop filter bandwidth.

In Section 3.2.2, block processing is proposed as an alternative method to the sequential tracking and as a solution to the problems faced by standard receivers in indoor environments such as loss of lock and low observability.

3.2.2 Block Processing

Any digital signal processing technique that operates on a block of samples is called block processing (Uijt de Haag 1999). This definition emphasizes operation on each block of data without considering the rest of the data as opposed to operation on sequential data.

In general, the performance of sequential and block processing techniques differs in two main aspects (van Graas et al 2005), namely computational expenses and signal observability. Sequential processing requires less memory and fewer operations to process the data while block processing has the advantage of better observability over the block of data.

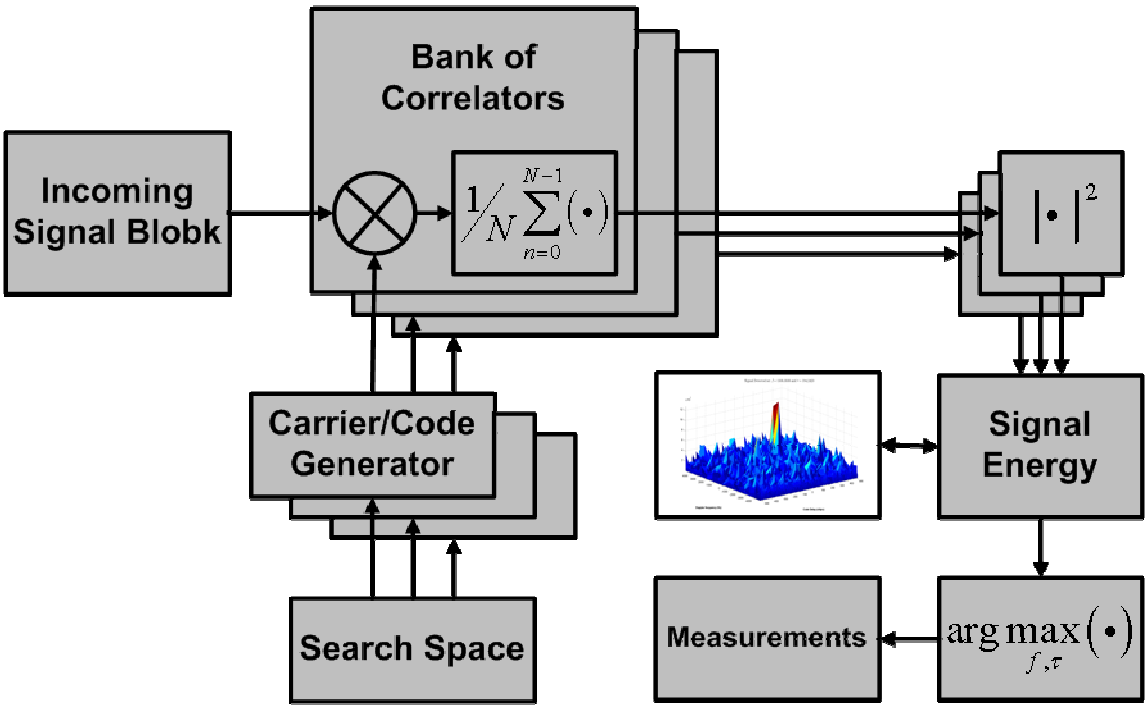

Figure 3-3: Architecture of block processing

In a GPS receiver, blocks of data can be generated by the front-end and the Analog to Digital Converter (ADC). Figure 3-3 shows the generalized architecture of a block processing receiver. Note that the acquisition and tracking stages are not separated. This means that, in contrast to the fact that sequential tracking loses some measurements after each loss of lock, the block processing approach does not need to re-establish track on the signal since the latter is seen immediately when it reappears after a temporary signal fading.

A block processor obtains signal parameters by acquiring the signal for every block of the data. To do so, a search space is formed based on a grid of code and frequency bins containing the incoming signal parameters. Afterwards, a bank of correlators is constructed based on the replica signals corresponding to the search space. The incoming block is correlated by the bank of correlators. The magnitude square of correlator outputs, known as signal energy, is then used to determine the Maximum Likelihood (ML) estimate of the signal carrier frequency and code phase.

Block processing provides an estimate of signal parameters without utilizing a closed tracking loop. Instead, an open tracking loop architecture is exploited. This architecture is not dependent on the signal parameter estimations from the previous epochs of the sequential data. Therefore, in the presence of reflected signals with unlimited pseudorange multipath errors, the observability of a block processing technique is higher than that of sequential tracking.

The advantages of block processing can be summarized as follows:

- Improved tracking robustness.

- Improved signal observability.

According to these advantages, the block processing technique is a substitute for sequential tracking that can be utilized for indoor channels. However, because of the computational burden of this technique, additional computational resources are required. The development of fast processors with low cost may overcome this problem in the future.

In order to exploit the advantages of the block processing technique in this work, a reference-rover receiver with a lower computational burden and some application limitations are discussed in Section 3.2.3.

3.2.3 Reference-Rover Receiver

In this section, the methodology for determining signal measurements in a reference-rover receiver that uses a block processing method is described.

3.2.3.1 Assisted GPS

A reference-rover receiver extracts navigation data, code phase, and carrier frequency from a reference signal and utilizes this information to acquire and track the rover signal. The rover and reference signals are (Satyanarayana et al 2010):

- **Rover signals** that are coming from a rover antenna carried by the user in an indoor environment.
- **Reference signals** from which aiding information is extracted are coming from a static (reference) antenna that is located outdoors, in a LOS environment.

Rover and reference signals are collected simultaneously using two front-ends that are driven by the same clock. Thus, clock errors, including clock drift and clock bias, are common to the reference and rover signals.

The standard sequential tracking loops are used for processing the reference signals to extract carrier frequency and code delay measurements. The navigation bits of the reference signal are also estimated from the correlator outputs of the sequential tracking receiver. These pieces of information are then used for the block processing of the rover signals.

The navigation bits of the rover signals are the same as the extracted navigation bits of the reference signals. In order to enable a long coherent integration of the rover signals, the estimated navigation message is used for wiping-off the data bits from the rover signals. Long coherent integration is discussed in Section 3.2.3.2.

As mentioned earlier, the computational burden is the main disadvantage of block processing methods. To this end, in the reference-rover receiver a very small search space that is expected to contain the signal parameters is determined for creating a smaller bank of correlators with fewer computational resources. The search space is a grid of frequency and code delay centred at the Doppler frequency and code delay of the reference signals. Since the two front-ends used for the reference and rover signals are driven by the same clock, the rover signal parameters are expected to be close to the centre of the search space. The size of the search space is a function of the user dynamics for the frequency dimension and a function of the distance between the reference and rover antennas for the code dimension. The code and frequency steps are chosen based on the application and computational resources available for the block processing.

3.2.3.2 Long Coherent Integration

Since C/A code length is 1 ms, every 1 ms of incoming data is correlated with its locally generated replica in the receiver. Therefore, the correlator outputs are based on 1 ms of data. Because of multipath fading and signal attenuation, 1 ms of coherent integration is not enough to extract the attenuated signal from noise. Consequently, a long coherent integration based on accumulating many 1 ms correlator outputs is utilized. For a long coherent integration (>20 ms), it is necessary to wipe-off data bits before accumulating the correlator outputs.

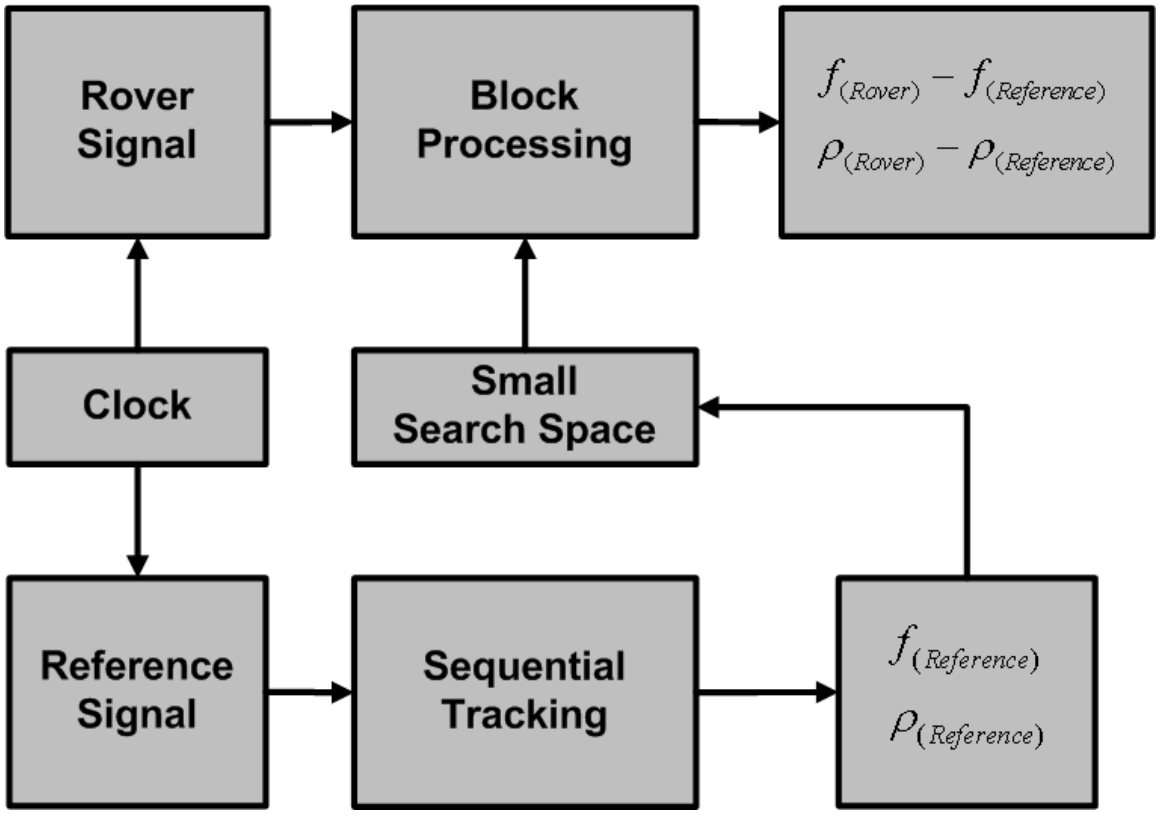

Figure 3-4: Architecture of reference-rover receiver

The architecture of a reference-rover receiver is shown in Figure 3-4. In this receiver, Doppler frequency and code delay measurements for the rover signals are differential values computed with respect to the parameters of the reference signals. It is obvious that exact values for the rover signal parameters can be provided by adding the reference signal parameters to the reference-rover receiver outputs.

3.2.3.3 Limitations

Although a reference-rover receiver overcomes hardware processing limitations, this receiver can be used only in a test environment as a cable is required between the reference and rover antennas since the two front-ends used for reference and rover signals are driven by the same clock. This means that the indoor rover antenna is always connected to the static antenna in an open area. This limits the mobility of the user. As a result, the reference-rover receiver only shows the capability of the block processing technique.

3.3 Observation Accuracy

The methods described in Section 3.2 are used herein for providing GPS observations in indoor environments. It is essential to assess the accuracy of GPS observations before utilizing them in a GPS/INS integrated system. Although both pseudorange and Doppler measurements are used for updating the INS, only Doppler measurements are characterized here. The reason that pseudorange measurements are not investigated is discussed in Section 3.3.1.

3.3.1 Pseudorange Measurement Accuracy

Multipath errors are the main factor affecting the accuracy of the pseudorange measurements in an indoor environment. As mentioned in Section 3.1.2, pseudorange multipath is unlimited for NLOS signals which vary based on multipath geometry. Since multipath geometry is unique to a given environment, and due to the difficulties of considering all channel effects in pseudorange measurements, it is not practical to assume a theoretical model for assessing the accuracy of these measurements in an indoor channel.

3.3.2 Doppler Measurement Accuracy

It is feasible to investigate the accuracy of Doppler observations because of their robustness against communication channel impairments and the reduced impact of multipath errors as compared to pseudorange measurements (Borio et al 2010).

In spite of unlimited pseudorange multipath errors, Doppler multipath errors are insignificant or zero for a static receiver and only multipath fading and signal attenuation are the channel effects. Also, for indoor pedestrian applications with low dynamics, multipath fading and signal attenuation are the dominant Doppler error sources, while Doppler multipath errors arising from pedestrian motion are negligible, as will be discussed in Chapter Four. Multipath fading and signal attenuation can be evaluated by measuring the C/N_0 at the receiver. Thus, C/N_0 is an appropriate criterion for determining the impact of the channel on Doppler measurement accuracy. In this section, a theoretical approach for evaluating Doppler measurement accuracy is discussed in which the variance of the Doppler estimate is shown to be a function of the type of

receiver, its parameters and the C/N_0 of the received signal. In Chapter Four, real data is collected in different indoor environments and the agreement between the theoretical and empirical results is tested.

Using the framework described in Borio et al (2009) and Sokolova (2009), the standard deviation of Doppler measurements is inversely proportional to the square root of the C/N_0. In the following two sections, Doppler measurement accuracy is expressed for both standard sequential receivers and reference-rover receivers adopting block processing techniques. Note that only fading and attenuation effects are considered in these expressions and the multipath error effect is neglected.

3.3.2.1 Standard Sequential

In a standard Phase Lock Loop (PLL) receiver, the Doppler tracking jitter is given by (Sokolova 2009 and Borio et al 2009)

$$\sigma_f = \frac{1}{T_C}\sqrt{\frac{B_d}{C/N_0}\left(1+\frac{1}{2TcC/N_0}\right)} \qquad \left[\frac{rad}{s}\right], \tag{3-5}$$

where

σ_f is the standard deviation of Doppler measurement,

T_C is the integration time, and

B_d is the Doppler bandwidth.

As shown in Equation 3-5, the accuracy of Doppler measurements depends on the input C/N_0, coherent integration time and Doppler bandwidth. Doppler bandwidth is a parameter of the receiver that quantifies the amount of noise transferred from the input noise to the frequency estimates and is given by (Borio et al 2009)

$$B_d = \frac{1}{2}\int_{-0.5/Tc}^{0.5/Tc} \left| H_{nf}\left(e^{j2\pi fTc}\right)\right|^2 df \,, \qquad 3\text{-}6$$

where $H_{nf}(z)$ is the noise frequency transfer function in the z domain and is derived from the linear equivalent model of the loop.

A Frequency Lock Loop (FLL) receiver differs from a PLL receiver in that it utilizes a frequency discriminator and an integrator after the loop filter (Ward et al 1996). Borio et al (2010) demonstrated that PLL and FLL receivers with the same loop and Doppler bandwidths produce frequency estimates with the same standard deviation. Thus, Equation 3-5 also applies to FLL receivers with Doppler bandwidth being computed in a similar fashion to Equation 3-6.

3.3.2.2 Block Processing

The following equation shows the standard deviation of Doppler measurements in receivers that utilize block processing (Borio et al 2010):

$$\sigma_f = \frac{1}{T_C}\sqrt{\frac{B_d}{C/N_0}} \qquad \left[\frac{rad}{s}\right], \qquad 3\text{-}7$$

where

σ_f is the standard deviation of the Doppler measurement,

T_C is the integration time, and

B_d is the Doppler bandwidth and is given by

$$B_d = \frac{6}{T_C} \quad [Hz]. \tag{3-8}$$

In block processing techniques, Doppler bandwidth determines the ability of a receiver to smooth Doppler measurements. The Doppler bandwidth is one of the receiver parameters that can be measured from Equation 3-8.

3.4 Weighting Observations

As shown in Chapter Two, GPS position and velocity estimation requires a minimum of four observations from different satellites. When a GPS receiver is able to track more than the minimum observations required for three-dimensional position and velocity, observation redundancy increases. Redundant observations are inconsistent. By using statistical methods such as least-squares estimation or Kalman filtering, the inconsistencies of observations are exploited for increasing the position and velocity precision. To exploit inconsistencies, observations need to be weighted based on their accuracies such that an imprecise observation is assigned a lower weight.

An INS provides a complete navigation solution and in an integrated GPS/INS integrated system, GPS observations provide redundant information for reducing the INS

errors in a Kalman filter. Therefore, assessing the quality of GPS observations is essential in improving the performance of an integrated system.

In order to weight the observations based on their quality, their variance should be known. This variance must incorporate the effects of all the errors listed in Section 2.1.3. It is not practical to model all the errors theoretically in the variance of observations. More specifically, in indoor channels where pseudorange multipath errors are not known, it is not possible to model the variance of observations theoretically. Instead, a practical model for weighting the observations is used. This practical model has to provide nearly optimum position and velocity measurements.

Three different weighting models are introduced in this section. These practical models are easy to implement and are given below (Wieser 2007).

3.4.1 Identical variance

This is the simplest variance model and here it is assumed that all observations of the same type have an equal variance. This model is shown as follows:

$$\mathrm{var}_{(ID)} = \sigma^2, \qquad 3\text{-}9$$

where

σ is the standard deviation of the observations.

This is not a suitable model and is valid only in an open sky area for high elevation satellites.

3.4.2 Elevation dependent variance

In this model, the variance of the GPS observations is a function of the satellite elevation angle. Satellite and receiver positions are known and elevation angles are calculated from the satellite-receiver unit vector. The calculated angles are then used in the following equation to measure the variance:

$$\mathrm{var}_{(ELV)} = \sigma^2 \frac{1}{\sin^2(E)}, \qquad 3\text{-}10$$

where

σ is the standard deviation of the observations at the zenith, and

E is the elevation angle of the satellite.

This model is a suitable model for an open sky area where multipath and fading do not exist.

3.4.3 Power dependent variance

In this model the variance of the observations is a function of the Carrier-to-Noise density power ratio (C/N_0). Receivers used in this work are able to determine the C/N_0 of GPS signals. The following model shows the power dependent variance model:

$$\mathrm{var}_{(C/N_0)} = \sigma^2 \frac{C/N_0(zenith)}{C/N_0}, \qquad 3\text{-}11$$

where

σ is the standard deviation of the observations at the zenith, and

$C/N_0(zenith)$ is the C/N_0 of the signal at the zenith in the open sky.

This model is very similar to the Doppler accuracy presented in Equation 3-7 since both Equations 3-7 and 3-11 show that the variance of the observations is inversely proportional to the C/N_0. The rest of the parameters in these two equations are parameters of the receiver and are constant. Because of this similarity the power dependent variance model is more suitable for indoor channels than the previous two models.

In this work all the practical weighting models presented here are used for indoor GPS/INS integration and the accuracy of their positioning results is compared in Chapter Five.

Chapter Four: Indoor Doppler Measurement and Velocity Characterization

This chapter focuses on Doppler characterization in indoor environments where signals are affected by multipath fading, signal attenuation (insertion loss) and secondary paths. Doppler information in various signal degraded environments is extracted using a reference-rover receiver. The accuracy of these measurements is assessed based on a comparison of the measured Doppler with an accurate reference Doppler provided by a GNSS/INS integrated system and, alternatively, a turntable.

An introduction to Doppler characterization in indoor environments is presented in Section 4.1 and methodologies adopted for indoor Doppler extraction and characterization are described in Section 4.2. Section 4.3 analyzes experimental results. For this purpose, real GPS data was collected and Doppler measurements are evaluated in two different indoor environments, a concrete building and a residential house, which differ in terms of signal attenuation (a concrete building structure results in a significantly larger insertion loss as compared to a residential house). When possible, velocity estimation is provided from the Doppler measurements. Finally, a summary of the chapter is provided in Section 4.4.

4.1 Doppler Characterization in an Indoor Environment

Indoor channel effects on Doppler and pseudorange measurements were discussed in Chapter Three. It was shown that the Doppler multipath error is a function of receiver velocity which is limited, relative to the pseudorange multipath error, for pedestrian applications. Therefore, Doppler measurement errors were assumed to be negligible and a

theoretical model for Doppler measurement accuracy was presented in Section 3.3.2. In order to support this assumption, the quality of Doppler should be characterized based on measurements in an indoor environment. In this work, evaluating Doppler quality in terms of variance is called Doppler characterization. Velocity estimation based on Doppler measurements can be improved if the quality of the Doppler measurements is known by the estimation algorithm (least squares or Kalman filter).

Borio et al (2009) studied the quality of Doppler measurements in outdoor environments. Nevertheless, additional work is required to measure Doppler variance induced by the surroundings (impact of multipath and fading).

4.2 Doppler Characterization Methodology

In this section a practical method for characterizing indoor Doppler measurements is introduced. For this purpose a GPS receiver is used to extract Doppler measurements. These measurements are then compared to reference Doppler values. The difference between a measurement and the reference Doppler value is called a Doppler error and is used for Doppler characterization.

Different receivers can be used for indoor measurements resulting in different characterizations. Here, Doppler measurements are provided by the reference-rover receiver described in Section 3.2.3. This receiver employs a maximum likelihood estimator and establishes bounds on the performance of other available GPS receivers.

Where possible, a commercial High Sensitivity (HS) receiver is also used for indoor Doppler measurements. This receiver is not utilized for Doppler characterization but its performance is compared to that of the reference-rover receiver. In this work, the

u-blox Antaris® 4 GPS was chosen for its HS capabilities and is used to assess the ability of commercial receivers to acquire and track GPS signals under degraded signal conditions.

As mentioned in Chapter Three, for a reference-rover receiver, reference signals are provided by a static reference antenna. Moreover, a reference Doppler, as the true expected Doppler, is required for assessing the accuracy of indoor Doppler measurements. The phrase 'reference' refers to two concepts and may cause confusion. In this work, 'reference signal' refers to the signal captured by the static antenna located in an open sky area and 'reference Doppler', estimated by a GNSS/INS integrated system, is referred to as the 'true Doppler' at the rover location.

4.2.1 Doppler Measurements

A Doppler measurement is referred to as the difference between the carrier frequency estimated by the receiver and the known frequency transmitted by GPS satellites (here L1). A Doppler measurement is a combination of clock drift and motion effects, illustrated in Figure 4-1(a) for a reference-rover receiver. Motion effects include the two portions caused by satellite motion and receiver motion. The satellite motion effect is a function of satellite velocity projected on the line of sight between satellite and receiver and as such does not provide any information about receiver velocity. In contrast, the second portion carries information about the receiver velocity because it is a function of the receiver velocity projected on the same line of sight. Most GNSS receivers do not separate the effects of satellite and user motion in their Doppler measurements. These receivers can separate these effects once the navigation solution is

computed or the satellite motion effect is calculated from ephemeris data and the receiver position. The reference-rover receiver separates the motion effects of the satellite and the receiver while it is providing Doppler measurements without any additional velocity estimation or satellite motion effect calculation.

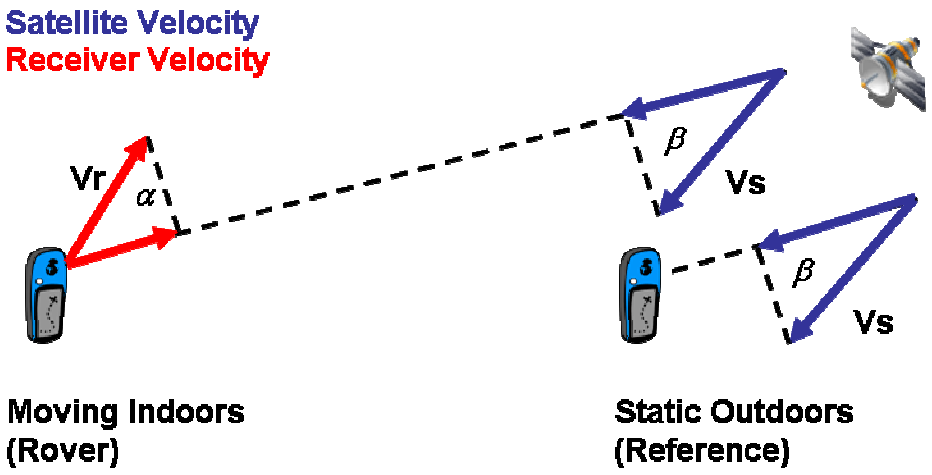

(a)

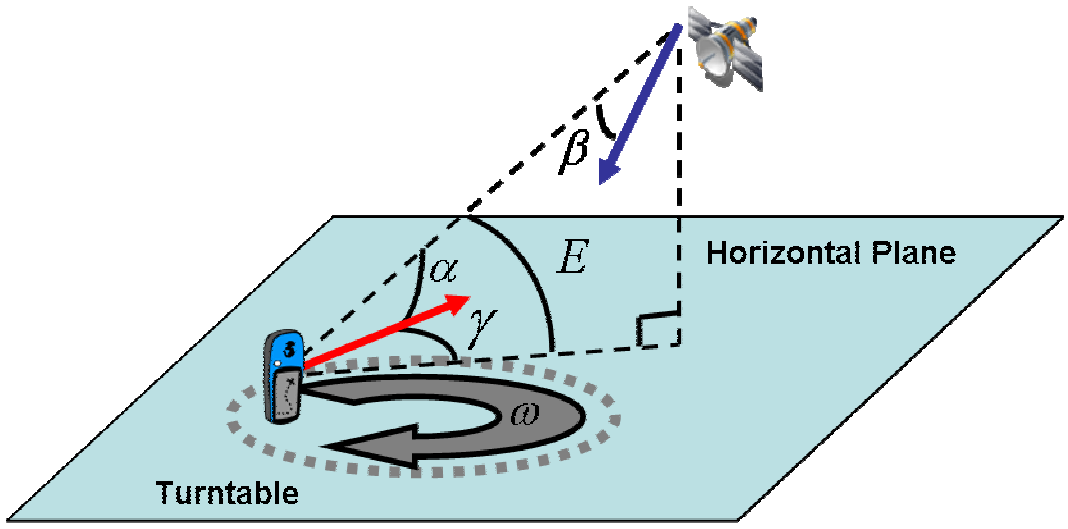

(b)

Figure 4-1: Doppler trajectory for a reference-rover receiver (a) and a turntable (b).

The GSNRx™ software receiver (O'Driscoll et al 2009 and Petovello & O'Driscoll 2007), developed at the University of Calgary, is a standard receiver. A modified version of this receiver jointly processes the reference and rover signals together in a reference-rover configuration. For this reason the modified version is named the GSNRx-rr™. A description of the software structure can be found in Satyanarayana et al (2010). In this work, this software is used for extracting and characterizing Doppler in several indoor environments.

The front-ends used for reference and rover signals are driven by a common clock. Doppler measurements extracted by the GSNRx-rr™ for the rover signal are differential values computed with respect to the Doppler of the reference signal. Therefore, Doppler measurements from the GSNRx-rr™ have the following features:

- They include only a receiver motion effect.
- They do not contain clock drift and are given by

$$f_{rr} = f_{rov} - f_{ref} + \varepsilon , \qquad 4\text{-}1$$

where

f_{rr} is the Doppler measured by the reference-rover receiver,

f_{rov} is the Doppler from the indoor (rover) antenna,

f_{ref} is the Doppler from the outdoor (reference) antenna, and

ε is the Doppler error, which will be discussed in Section 4.2.3.

Reference and rover antennas are close to each other relative to the distance between the satellite and receiver and, therefore, it can be assumed that the lines of sight

between a satellite and the two antennas are parallel. Based on this assumption and from Equation 4-1, f_{rr} can be rewritten as:

$$f_{rr} = \left(\frac{1}{\lambda} Vs \cdot \cos\beta + \frac{1}{\lambda} Vr \cdot \cos\alpha\right) - \left(\frac{1}{\lambda} Vs \cdot \cos\beta\right) + \varepsilon \qquad 4\text{-}2$$

$$f_{rr} = \frac{1}{\lambda} Vr \cdot \cos\alpha + \varepsilon\,, \qquad 4\text{-}3$$

where

Vs is the satellite velocity,

β is the angle between Vs and the satellite-receiver unit vector,

Vr is the velocity of the rover antenna, and

α is the angle between Vr and the satellite-receiver unit vector.

4.2.2 True (Reference) Velocity and Doppler

To study the indoor Doppler and velocity measurements of the reference-rover receiver, the true velocity of the rover antenna is needed. True Doppler is then obtained by projecting the receiver velocity along the satellite-receiver unit vector.

In this work, the true velocity is estimated in two different ways. First, the receiver's motion is known, e.g. the rover is static or mounted on a linear/turntable with known dynamics. Second, the receiver dynamics are estimated using an accurate commercial GNSS/INS integrated system such as the NovAtel SPAN system equipped with a Honeywell HG1700 inertial measurement unit. The accuracy of this system as a

velocity reference for pedestrian navigation applications in indoor environments is investigated in Appendix A and is shown to be 1.7 cm/s.

From Figure 4-1, the theoretical expression of true Doppler is

$$f_{True} = \frac{1}{\lambda} Vr \cdot \cos\alpha \,. \tag{4-4}$$

Figure 4-1(b) shows that the receiver is installed on a turntable which is horizontally aligned. Vr is known and the angle between Vr and the satellite-receiver unit vector, α, is given by

$$\cos\alpha = \cos E \cdot \cos\gamma \tag{4-5}$$

$$\gamma = \omega \cdot (t + t_0)\,, \tag{4-6}$$

where

E is the elevation angle of the satellite,

t is time,

t_0 is initial time, and

ω is the angular velocity of the turntable.

Correspondingly, from Equations 4-4 to 4-6, true Doppler can be determined as follows:

$$f_{True} = \frac{1}{\lambda} Vr \cdot \cos E \cdot \cos\left(\omega \cdot (t + t_0)\right). \tag{4-7}$$

As a result, in this case, the true Doppler has a sinusoidal pattern when the rover is mounted on a turntable.

4.2.3 Doppler Errors

By comparing Equations 4-3 and 4-4, the following equation is obtained:

$$f_{rr} = f_{True} + \varepsilon \,. \qquad 4\text{-}8$$

Equation 4-8 shows that Doppler measurements from a reference-rover receiver are directly comparable with the true Doppler. The error in Doppler measurements is characterized by evaluating the difference between the measured Doppler and the true Doppler.

Doppler errors in indoor environments were discussed in Chapter Three. It was shown that the standard deviation of Doppler measurements for a reference-rover receiver is a function of the C/N_0 as in Equation 3-7 which is repeated here for convenience:

$$\sigma_f = \frac{1}{T_C}\sqrt{\frac{B_d}{C/N_0}} \qquad \left[\frac{rad}{s}\right], \qquad 4\text{-}9$$

where

σ_f is the standard deviation of the Doppler error (ε),

T_C is the integration time, and

B_d is the Doppler bandwidth and is given by

$$B_d = \frac{6}{T_C} \qquad [Hz]. \qquad 4\text{-}10$$

Standard deviations are computed over a sliding window of the Doppler errors provided by Equation 4-8. The width of the window is from 0.5 to 1 second depending on the coherent integration time needed to have enough samples for calculating the standard deviation of the errors. In Section 4.3, the data collections are performed in two different indoor environments and the calculated standard deviation of Doppler error is compared to that obtained using Equation 4-9.

4.3 Experimental Assessment

In order to conduct data collections for indoor Doppler characterization, the equipment was configured based on the methodology described in Section 4.2. A National Instruments (NI) PXI-5661 signal analyzer was used to provide the front-ends for collecting signals from the reference and rover antennas. This signal analyzer is able to drive its front-ends with a common clock and provides synchronized signals from the reference and rover antennas to be processed by the GSNRx-rr™ software receiver. A u-blox Antaris® 4 HSGPS receiver was used for assessing the performance of commercial high sensitivity receivers. In addition, the accuracy of the measurements provided by the GSNRx-rr™ and the u-blox Antaris® 4 is assessed based on comparing the measured Doppler to an accurate true Doppler provided by a GNSS/INS integrated system or, alternatively, a turntable.

Two different indoor locations were chosen to collect data. The first environment is a concrete building with metal-coated windows representing a harsh multipath environment. The second indoor environment is a typical North American private

residence. Where possible, some or all of the following parameters were extracted, namely the satellite availability with associated Dilution of Precision (DOP), the Carrier-to-Noise power density ratio (C/N_0), the variance of Doppler errors and the velocity solution.

4.3.1 Navigation Laboratory Test

The first test was performed in the Navigation Laboratory (NavLab) on the third floor of the Calgary Center of Innovative Technology (CCIT) building on the University of Calgary campus. The CCIT building is a modern building with concrete walls and metal-coated windows. Under such conditions, a GPS signal is highly attenuated and successful signal acquisition requires a long coherent integration.

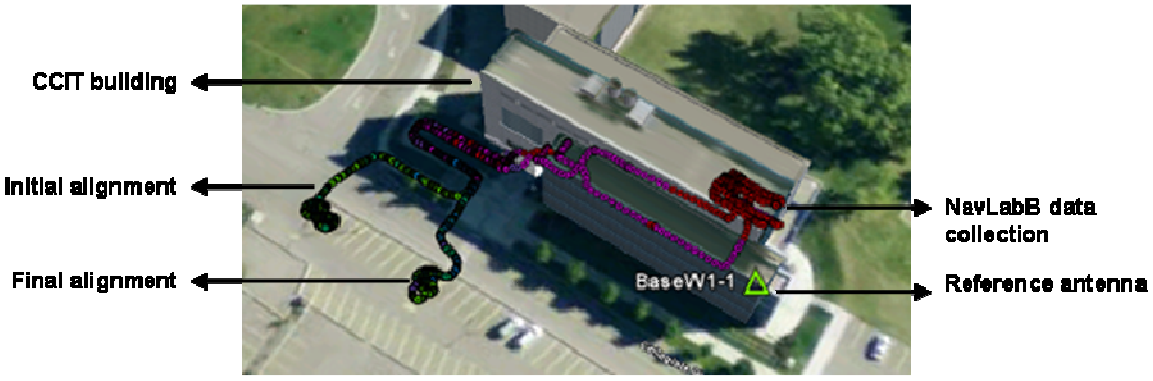

Figure 4-2: Post-processed trajectory in CCIT building provided by SPAN system. Initial and final alignments were done outdoors.

During the data collection in the CCIT building, four different datasets were collected in the NavLab with the reference antenna located on the roof of the CCIT building. The GPS/INS SPAN system was used to provide true velocity. Initial and final

alignments of the SPAN are necessary to achieve high accuracy for true velocity. These alignments are only possible if appropriate GNSS data becomes accessible to the SPAN. As a result, before and after the four datasets were collected in the building, the IMU was aligned in an open sky area, as shown in Figure 4-2. During the data collection, zero velocity updates (ZUPT) were performed every 30 seconds in different locations to improve the accuracy of true velocity. The true trajectory and true velocity were post-processed in a tightly coupled mode using the software Inertial Explorer from NovAtel.

Figure 4-3(a), shows the location of four data collections. In the first test, the user was moving inside the laboratory without following a pre-defined trajectory. During other tests, the user was moving backwards and forwards following the straight trajectories indicated in Figure 4-3(a). The true velocity extracted by a post-processing solution is shown in Figure 4-3(b). Since the position of the rover and satellites are known during the data collection, the true velocity is projected on the satellite-receiver unit vector for determining the true Doppler. This is done for Satellite 18 in Test One and is shown in Figure 4-4(a).

It is important to know the accuracy of true Doppler provided by the SPAN system. The accuracy of this GNSS/INS integrated system has been investigated and the velocity accuracy is 1.7 cm/s for pedestrian navigation with ZUPT of every 30 seconds (Appendix A). By using ZUPT, it is possible to reset the error of the velocity solution to zero. Therefore, ZUPT has been frequently used during the experiment assuring that the error does not drift. In a worst case scenario, the error of the true Doppler is maximized when the direction of the true velocity error becomes parallel to the satellite-receiver unit vector. Under this condition, the true Doppler error, which is the projection of the true

velocity error on the unit vector, is maximized and the accuracy of true Doppler is equal to the accuracy of true velocity (1.7 cm/s) divided by the wavelength (19 cm for L1). Therefore, the accuracy of true Doppler is better than 0.1 Hz for L1.

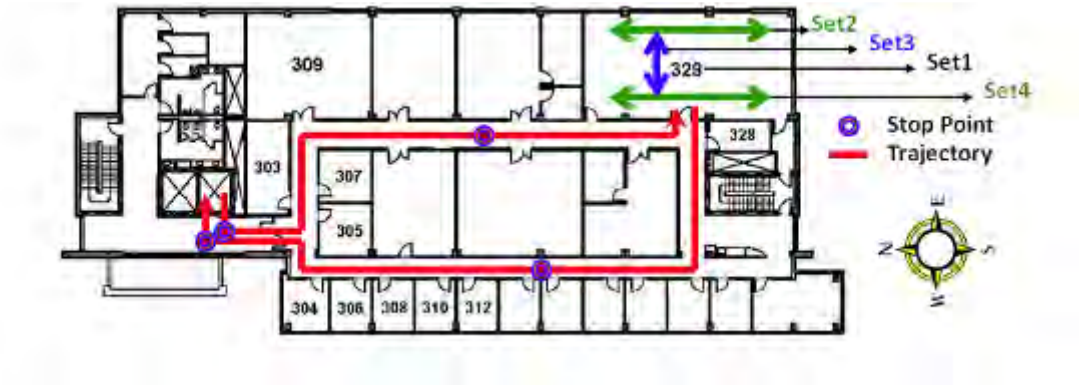

(a)

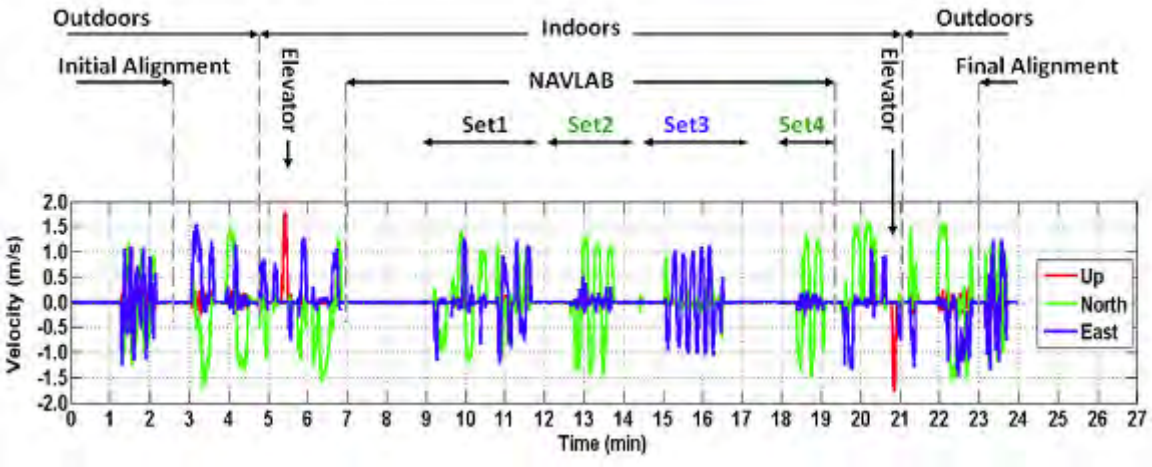

(b)

Figure 4-3: Map of the third floor of the Calgary Centre of Innovative Technology (CCIT) building (a) and true velocities (East, North, Up) obtained using the SPAN HG1700 system. (b) Four different tests are shown.

During each test, reference and rover signals are collected using the NI PXI-5661 signal analyzer. These signals are processed by the GSNRx-rr™ to extract the Doppler measurements. Due to the concrete walls and metal-coated windows in the NavLab, a long integration time of 200 ms is required. The u-blox Antaris® 4 HSGPS was not able to track GPS signals in such environments.

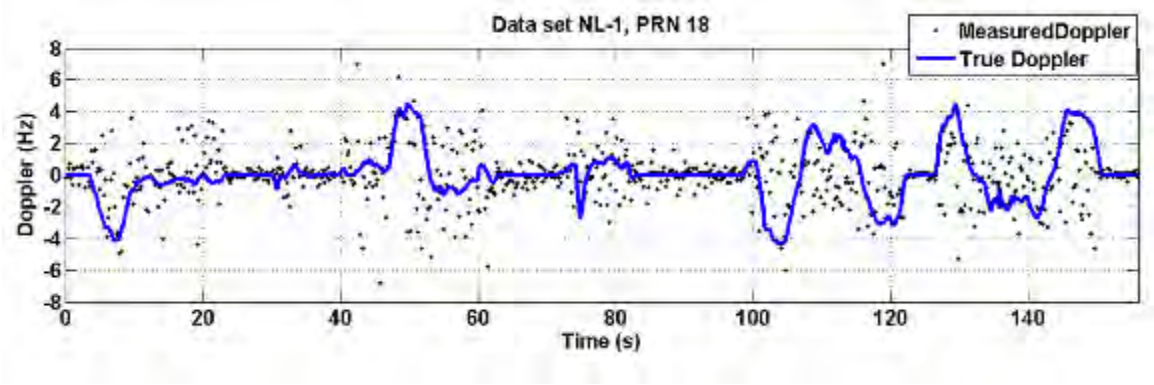

(a)

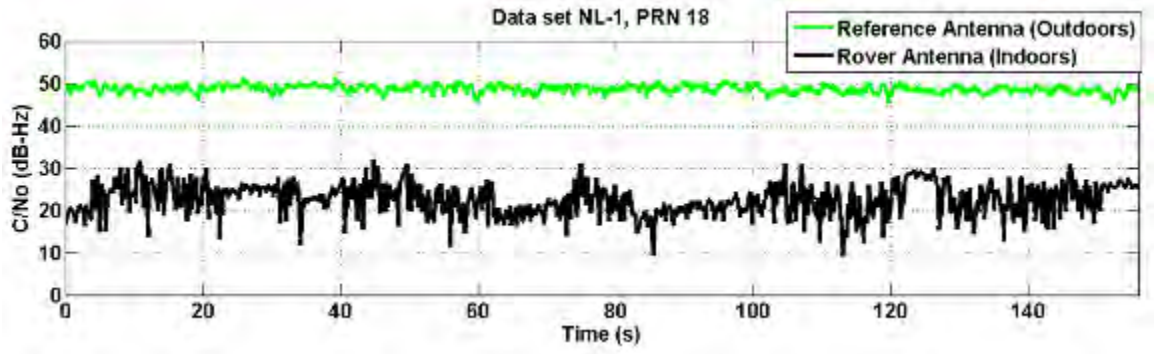

(b)

Figure 4-4: Doppler measurements (a) and C/N_0 levels (b) obtained for PRN 18 using GSNRx-rr™ in the NavLab, Test One.

Doppler measurements produced by GSNRx-rr™ are compared with the true Doppler provided by the SPAN system. Doppler measurements for Satellite 18 of Test One are depicted in Figure 4-4(a). Figure 4-4(b) compares the C/N_0 of the outdoor reference antenna with that of the rover antenna in the NavLab. As can be seen, the average insertion loss is about 25 dB-Hz, which is due to the presence of concrete walls and ceiling, and metal-coated windows. The attenuation in the NavLab is the major reason why Doppler measurements do not follow the true Doppler. Note that higher user dynamics disable the effectiveness of a long integration time and increase multipath errors. For these reasons, the quality of Doppler measurements is lower when the receiver is in motion. This is illustrated in Figure 4-4(a), where the measured Doppler follows the true Doppler only for the static rover, corresponding to zero Doppler values. Therefore, in such environments, Doppler multipath errors are not negligible and the model provided in Equation 4-9 is not valid for Doppler measurement errors.

In order to compare the accuracy of Doppler measurements when the rover antenna is static to the same measurements when the rover is in motion, a static data collection was conducted in the NavLab. Since the rover antenna is static in this test, there is no need to utilize the SPAN system for providing the true Doppler. In the static test, the true Doppler is equal to zero and Doppler measurements from the GSNRx-rr™ receiver are therefore considered as Doppler errors. These measurements in the NavLab are shown in Figure 4-5(a) for Satellite 26, which was chosen since it has an average C/N_0 close to that of Satellite 18 in Test One. The C/N_0 of the reference and rover antennas in the static test are shown in Figure 4-5(b). It is observed that during the static

periods, the C/N_0 changes slowly. Rapid changes in the C/N_0 during the periods of high dynamics are due to fast Doppler geometry changes and consequent multipath fading. A comparison of Figure 4-4(a) and Figure 4-5(a) shows that, for signals with equal C/N_0, Doppler errors increase while the rover antenna is in motion and the Root Mean Square (RMS) of Doppler errors increases from 0.3 Hz for Satellite 26 in the static test to 2.2 Hz for Satellite 18 in Test One.

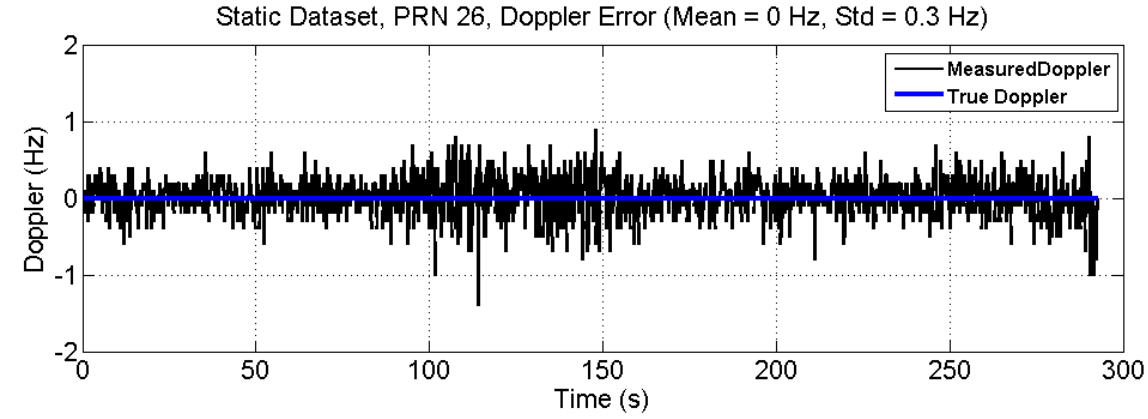

(a)

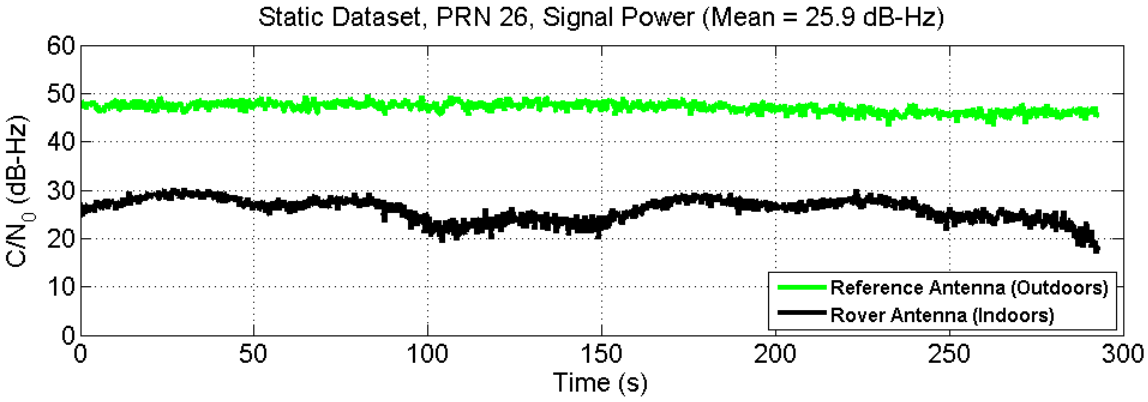

(b)

Figure 4-5: Doppler measurements (a) and C/N_0 levels (b) obtained for PRN 26 using the GSNRx-rr™ in the NavLab while the rover antenna is static.

Similar results are obtained for other satellites and other tests conducted in the NavLab. The Doppler error RMS values for each satellite are shown in Figure 4-6 as a function of the average C/N_0 of the satellite. The RMSE of the Doppler measurements for the static rover while the C/N_0 is 20 dB-Hz is 0.4 Hz, but for the same value of C/N_0 for other dynamic tests, the RMSE of the Doppler measurements exceeds 2 Hz.

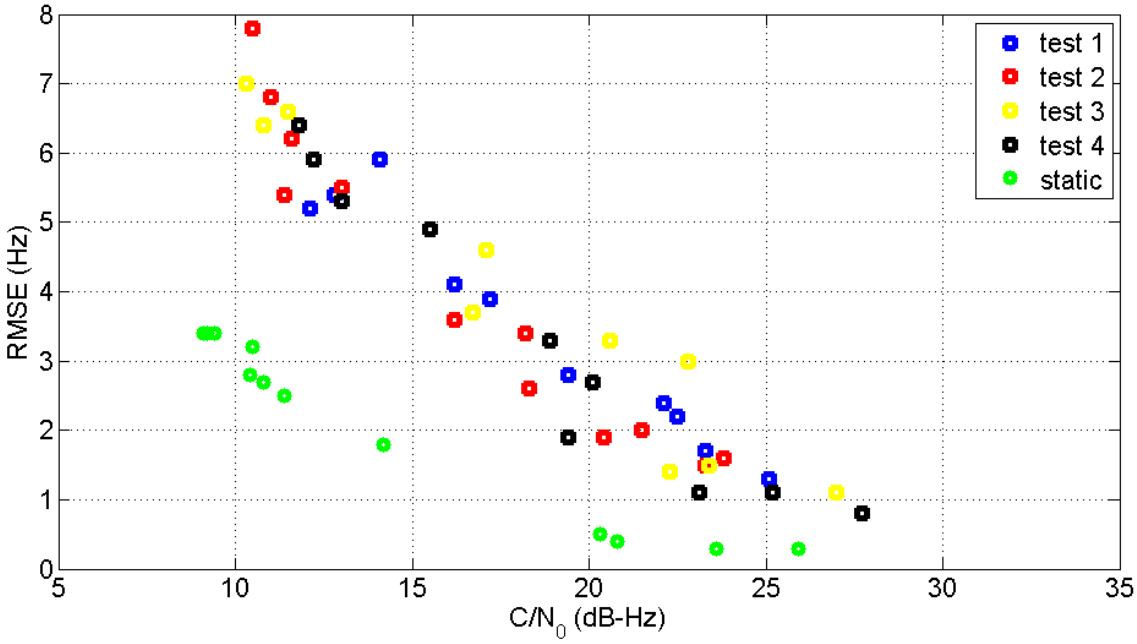

Figure 4-6: Accuracy of Doppler measurements for each of the satellites available in four dynamic tests and one static test collected in the NavLab as a function of average C/N_0 during the test.

Figure 4-6 shows that in environments such as the NavlLab, where GPS signals are highly attenuated, Doppler measurements are more reliable for velocity measurements when the rover is static.

4.3.2 Residential House Test

The second test was performed in a typical North American residence (Figure 4-7). In this house, several datasets were collected on the main floor and in the basement with different types of motion. A turntable was used to provide various velocities. The known trajectory of the turntable was used for extracting the true velocity and Doppler.

The characteristics of different tests are summarized in Table 4.1 where each test is labelled with an ID. This table shows different dynamics considered during the data collection (from very low velocity up to pedestrian velocity). These datasets were again collected using the NI PXI-5661 signal analyzer. The reference and rover antennas were connected to the NI system. The rover antenna was also connected to the u-blox Antaris® 4 HSGPS, in order to conduct additional Doppler analysis.

Since the turntable was used, the antenna displacement is known in terms of angular speed and the radius of the turntable. Thus, there is no need to use the SPAN system. It was shown in Equation 4-7 that the true Doppler is sinusoidal when a turntable is used. In addition, since the turntable is horizontally aligned, the true velocity has a sinusoidal waveform in the North and East directions and it is equal to zero in the vertical direction.

(a)

(b)

(c)

Figure 4-7: Typical North American residence (a), main floor data collection using a turntable (b) and basement data collection (c).

Similar to the NavLab experiment, the GSNRx-rr^{TM} is used as a receiver for extracting Doppler measurements. As expected, C/N_0 values are higher than in the NavLab. Thus, a shorter coherent integration time (50 ms) is utilized to extract Doppler

measurements. Furthermore, it was observed that the u-blox Antaris® 4 HSGPS was also able to measure Doppler in this environment. An analysis of the recorded data follows.

Table 4.1: Summary of the data collections performed in the residential house. Each data collection is identified by an ID code.

Test ID	Location	TurnTable		
		Radius (cm)	Rotation Rate (turn/min)	Linear Speed (cm/s)
WH-1	Main floor	36	1	3.8
WH-2	Main floor	36	2	7.5
WH-3	Main floor	36	3	11.3
WH-4	Main floor	36	4	15.1
WH-5	Main floor	51	4	21.4
WH-6	Main floor	51	8	42.7
WH-7	Main floor	51	15	80.1
WH-8	Basement	36	4	15.1

In this section, results for the test WH-2 experiment are described. The antenna rotates at a constant rate of two cycles per minute, meaning the Doppler measurements are expected to change with a frequency of 0.0334 Hz. This frequency is used in Equation 4-7 to compute the true Doppler. In order to measure the initial phase of the sinusoid in Equation 4-7, a replica of the true Doppler with the frequency described above, the elevation angle of the satellite, and an initial phase equal to zero is correlated with Doppler measurements from the same satellite. The correlation function is maximized at the initial phase. This is repeated for all satellites and the average of the initial phases obtained from the different satellites is used in Equation 4-7. The true

Doppler for Satellite 29 of Test WH-2 is shown in Figure 4-8 and Figure 4-9(a) for the u-blox and GNSRx-rr™ receivers, respectively.

Since sinusoidal Doppler variations are expected, a Fourier analysis will be used to better analyze the quality of the measurements. When valid measurements are extracted, a clear peak emerges from the spectrum of the Doppler observations corresponding to the angular velocity of the turntable (0.0334 Hz).

Figure 4-8 illustrates the Doppler measurements obtained with the u-blox Antaris® 4 GPS receiver for Satellite 29 in the dataset WH-2. These measurements are corrected for the receiver clock drift and satellite motion. To do this, the measurements for the static antenna, located outdoors, were produced using the standard GSNRx™ and they were subtracted from the u-blox HSGPS measurements. Moreover, clock drifts for the standard GSNRx™ and u-blox HSGPS were computed and compensated for. The clock drift of these receivers is estimated by the velocity solution from their Doppler measurements.

Figure 4-8 shows that Doppler measurements provided by the u-blox HSGPS do not follow the true Doppler very well. For this receiver, the Doppler error RMS for Satellite 29 with an average C/N_0 of 41.3 dB-Hz is equal to 1.5 Hz. The Doppler error RMS for the rest of the satellites in Test WH-2 will be summarized in this section for the u-blox HSGPS and will be compared to the GSNRx-rr™ receiver results.

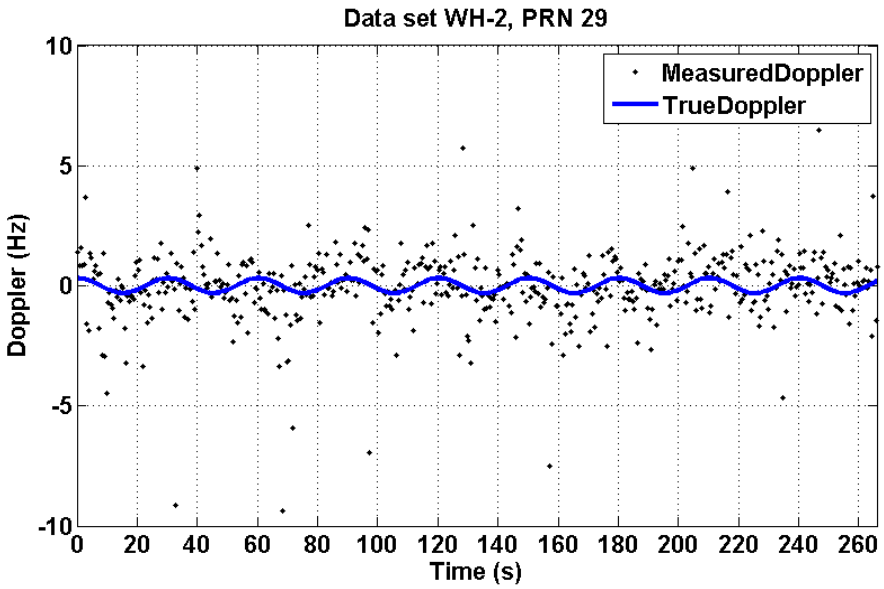

Figure 4-8: Doppler measurements provided by a u-blox Antaris® 4 high sensitivity receiver for Satellite 29, Test WH-2. The measurements are corrected for the clock drift and the satellite motion.

The GSNRx-rr™ is used to extract Doppler measurements for all tests collected in the residence. This receiver has an advantage with respect to the u-blox Antaris® 4 in that the Doppler errors are smaller and the measurements follow the expected Doppler pattern. In Figure 4-9, the obtained Doppler measurements and the corresponding C/N_0 levels are depicted. The estimated Doppler follows the true Doppler shown in blue in Figure 4-9(a). Note that the measurement variance increases as the C/N_0 drops. This is consistent with the theoretical analysis provided in Equation 4-9.

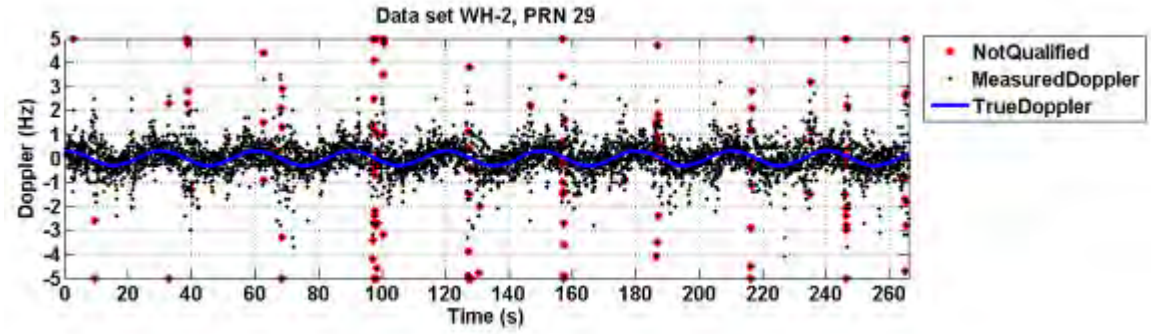

(a)

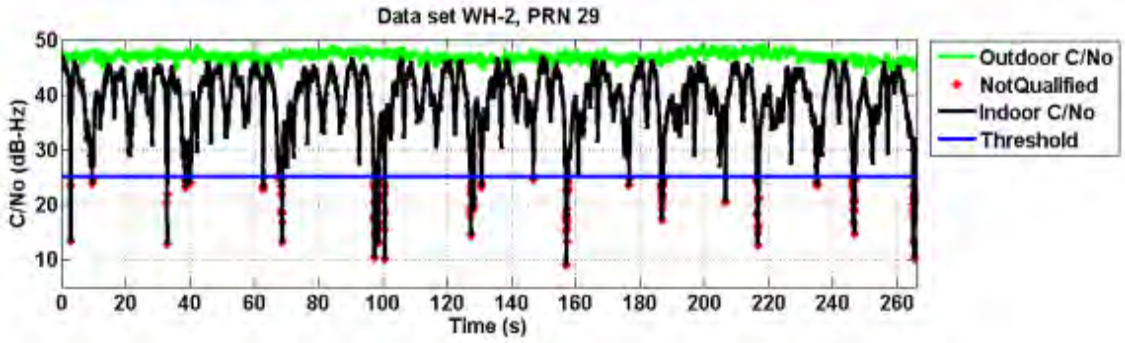

(b)

Figure 4-9: Doppler measurements (a) and C/N_0 levels (b) obtained for PRN 29 using the GSNRx-rr™ in the WH-2 test. Below a specific C/N_0 threshold (25 dB-Hz), Doppler measurements become unreliable and are discarded. Red dots indicate unreliable Doppler measurements.

When the C/N_0 drops below a specific threshold, Doppler measurements become unreliable and should be discarded. When the C/N_0 is very low, no signal is detectable in the search space and the peak corresponds only to the noise. In this case, Doppler measurements are not following the true Doppler pattern and are distributed over the search space. The threshold for C/N_0 is chosen empirically. For this purpose all the data

collections in the residence are investigated and it was observed that Doppler measurements are distributed over the search space when the C/N_0 is lower than 25 dB-Hz. Discarding the measurements with a C/N_0 lower than this threshold is herein called pre-filtering. The red dots in Figure 4-9 are related to the measurements with C/N_0 lower than 25 dB-Hz and are distributed over the search space and increase the standard deviation of the Doppler error in the test. To avoid this, pre-filtering is used to reduce the standard deviation from 0.8 Hz to 0.6 Hz. Pre-filtering is useful for velocity estimation since large errors in Doppler measurements result in an increase in velocity error.

As expected, the pattern of the C/N_0 for the rover signal in Figure 4-9(b) is periodic due to the periodic motion of the turntable. The observed attenuations are caused by multipath fading effects.

Since the true Doppler is sinusoidal, the magnitude of its Fast Fourier Transform (FFT) has a peak at the frequency corresponding to the angular speed of the turntable. With this in mind, the Fourier transform can be used to analyze the quality of Doppler measurements. In Figure 4-10, the magnitude of the FFT of Doppler measurements is compared with that of the FFT of true Doppler measurements. They both have a peak at the same frequency showing that Doppler measurements are following the expected Doppler pattern.

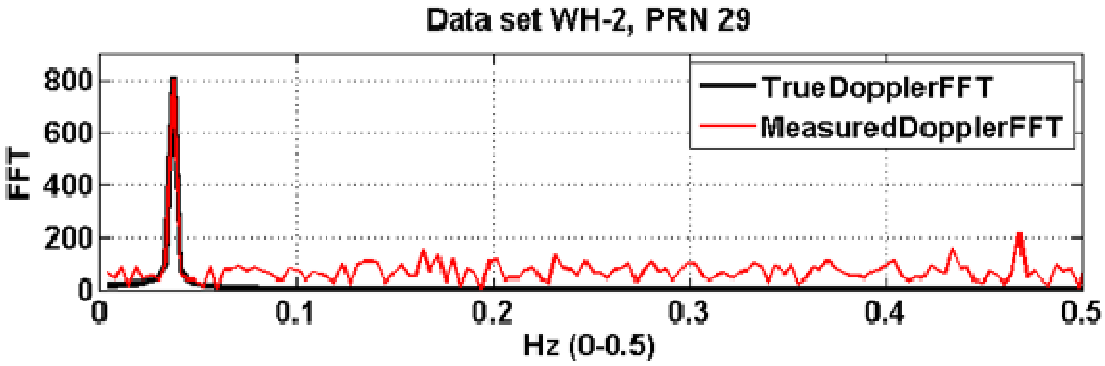

Figure 4-10: Magnitude of the Fourier Transform of Doppler measurements provided by the GSNRx-rr™ for PRN 29, WH-2 experiment. A clear peak is present at a frequency corresponding to the angular velocity of the turntable.

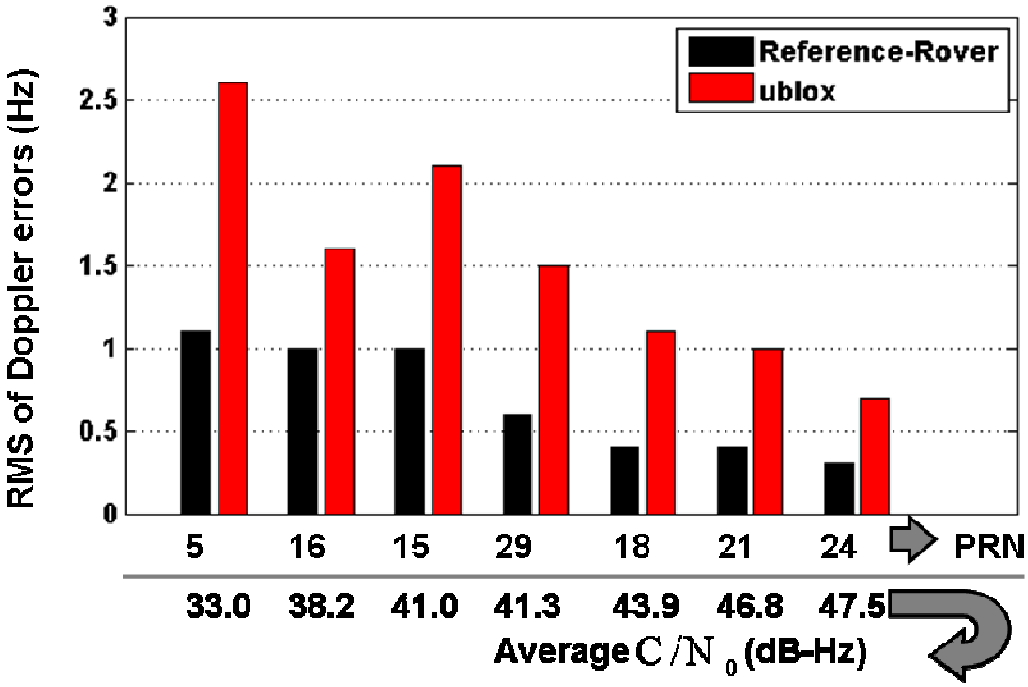

Figure 4-11: Comparison of the accuracy of Doppler measurements provided by the u-blox HSGPS and the GSNRx-rr™ for all the available satellites in test WH-2 and the average C/N_0 of each satellite.

The Doppler measurements provided by the u-blox HSGPS and GSNRx-rr™ are compared with the true Doppler and the RMS of Doppler errors is measured for all satellites available in Test WH-2. The RMS of Doppler errors for these two receivers is shown in Figure 4-11. This figure shows that the GSNRx-rr™ receiver provides more accurate Doppler measurements. This accuracy is because of the advantages of the reference-rover receiver described in Section 3.2.3. In addition, the GSNRx-rr™ receiver does not need to estimate clock drift to correct the Doppler measurements. Doppler measurements provided by the u-blox HSGPS are corrected for the clock drift of the receiver and the error in clock drift estimation increases the error in the corrected Doppler measurements.

4.3.2.1 Covariance of Doppler Measurements

It was theoretically shown that the standard deviation of Doppler measurements is a function of integration time, C/N_0 and Doppler bandwidth (Section 3.3.2). The related formula is shown in Equation 4-9. For Satellite 29 of dataset WH-3, the standard deviations of Doppler measurements are calculated using a sliding window over the Doppler errors. The width of the moving window is 0.5 second equal to 10 samples. In Figure 4-12, these standard deviations are depicted based on the mean C/N_0 of the samples in the moving window.

Using Equation 4-10 and knowing the coherent integration time, Doppler bandwidth is computed and is equal to 120 Hz. Figure 4-12 shows that the theoretical model based on Equation 4-9 matches the measured standard deviations.

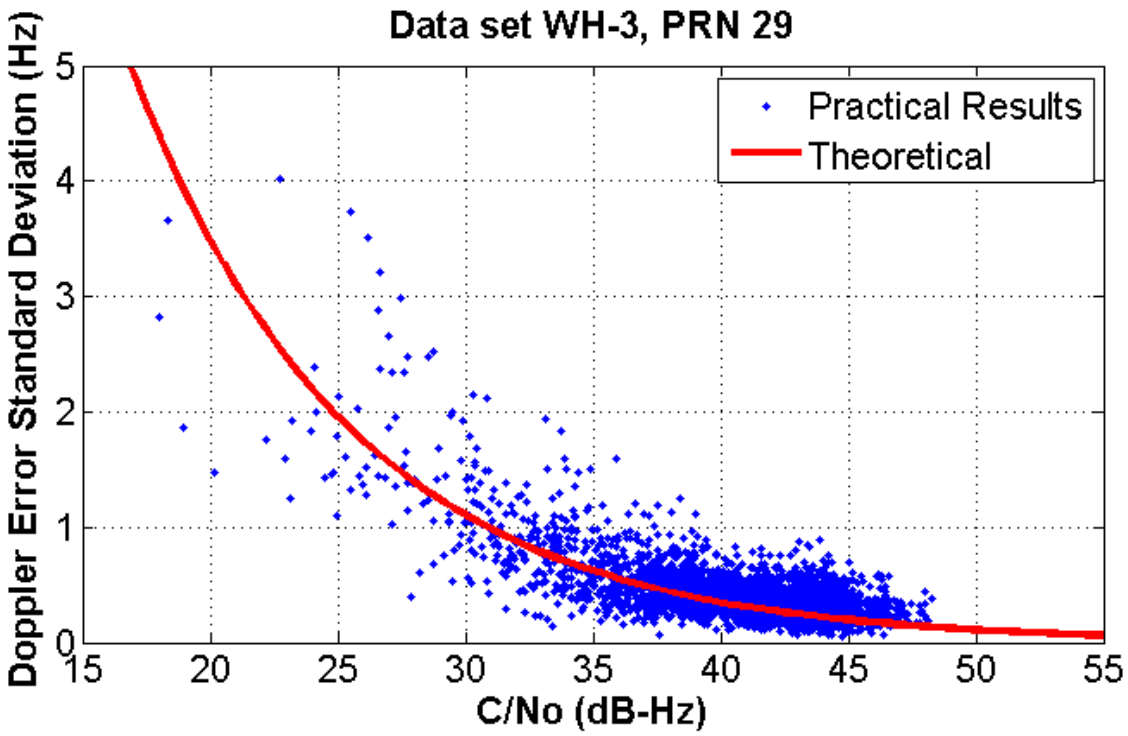

Figure 4-12: Standard deviation of Doppler measurements as a function of the C/N_0 for PRN 29, Test WH-3. Practical results match the theoretical model.

The Doppler bandwidth is one of the receiver parameters and is constant for all the measurements from the other satellites. Therefore, a unique theoretical model for the standard deviation of Doppler measurements shown in Figure 4-12 must be valid for the rest of the satellites in dataset WH-3. This is tested for all available satellites and Figure 4-13 shows that the Doppler measurement standard deviations for six available satellites match the same theoretical model.

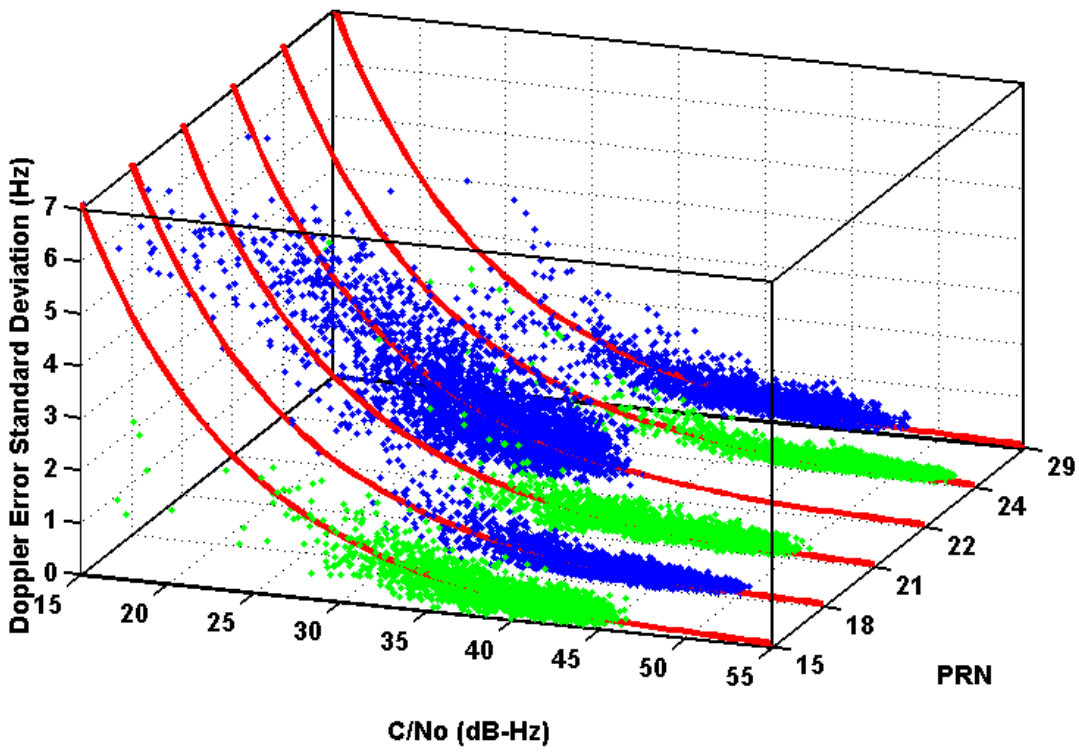

Figure 4-13: Standard deviation of Doppler measurements as a function of C/N_0 for all satellites, dataset WH-3. Doppler bandwidth is equal to 120 Hz for all satellites.

Doppler bandwidth and integration time are common for all satellites and the variance of measurements are provided by Equation 4-9. If all measurements are assumed to be uncorrelated for k available satellites, the covariance matrix of the Doppler measurements is given by

$$C_z = \sigma_0^2 Q_Z = \frac{B_d}{T_C^2}\begin{bmatrix} (C/N_0)_1^{-1} & 0 & \cdots & 0 \\ 0 & (C/N_0)_2^{-1} & \cdots & 0 \\ \vdots & \vdots & \ddots & \vdots \\ 0 & 0 & \cdots & (C/N_0)_k^{-1} \end{bmatrix}, \qquad 4\text{-}11$$

where

σ_0^2 is the apriori variance,

Q_Z is the cofactor matrix of the measurements, and

$(C/N_0)_i$ is the carrier to noise ratio of the ith satellite.

The standard deviation of Doppler measurements for different tests is summarized in Table 4.2 to Table 4.9. In these tables, each row is related to one satellite and each column is related to measurements with a C/N_0 within an interval of 5 dB-Hz. The centre of each C/N_0 interval is shown in the tables.

Table 4.2: Average Doppler measurement Standard deviations in C/N_0 intervals of 5 dB-Hz for satellites available during Test WH-1.

Test WH-1, Linear Speed 3.8 cm/s Standard deviation (Hz)											
C/N$_0$		10	15	20	25	30	35	40	45	50	55
PRN	5	4.6	4.2	2.8	1.8	1.1	0.7	0.6	-	-	-
	15	-	-	-	1.4	1.0	0.6	0.4	0.3	0.2	-
	16	-	3.9	3.1	2.0	1.2	0.8	0.6	0.5	-	-
	18	-	-	-	1.9	1.0	0.5	0.4	0.3	0.2	-
	21	-	-	-	1.1	0.9	0.5	0.3	0.3	0.2	0.2
	24	-	-	3.1	1.7	1.0	0.6	0.4	0.2	0.2	0.2
	29	-	-	-	-	1.0	0.7	0.4	0.3	0.2	-
Average Std of all PRNs		4.6	4.1	3.0	1.7	1.1	0.6	0.4	0.3	0.2	0.2

Table 4.3: Average Doppler measurement Standard deviations in C/N_0 intervals of 5 dB-Hz for satellites available during Test WH-2.

Test WH-2, Linear Speed 7.5 cm/s Standard deviation (Hz)											
C/N_0		10	15	20	25	30	35	40	45	50	55
PRN	5	4.1	3.8	3.0	1.8	1.1	0.8	0.7	-	-	-
	15	-	3.8	3.3	2.6	1.7	1.0	0.6	0.4	0.3	-
	16	-	-	3.0	2.1	1.1	0.8	0.6	0.5	-	-
	18	-	-	3.1	2.1	1.2	0.6	0.4	0.3	0.3	-
	21	-	-	-	2.8	1.6	0.8	0.5	0.3	0.3	-
	24	-	-	-	-	1.2	0.6	0.4	0.2	0.2	0.2
	29	-	3.5	3.1	1.9	1.2	0.6	0.4	0.3	-	-
Average Std of all PRNs		4.1	3.7	3.1	2.2	1.3	0.7	0.5	0.4	0.3	0.2

Table 4.4: Average Doppler measurement Standard deviations in C/N_0 intervals of 5 dB-Hz for satellites available during Test WH-3.

Test WH-3, Linear Speed 11.3 cm/s Standard deviation (Hz)											
C/N_0		10	15	20	25	30	35	40	45	50	55
PRN	15	-	-	-	1.8	1.1	0.7	0.4	0.3	-	-
	18	-	-	-	-	1.4	0.7	0.4	0.3	0.2	-
	21	-	-	-	-	1.0	0.6	0.4	0.3	0.2	-
	22	3.9	3.8	3.1	1.9	1.3	0.9	0.7	-	-	-
	24	-	-	-	-	1.6	0.7	0.4	0.2	0.2	0.2
	29	-	-	-	2.0	1.1	0.6	0.4	0.3	0.3	-
Average Std of all PRNs		3.9	3.8	3.1	1.9	1.2	0.7	0.5	0.3	0.2	0.2

Table 4.5: Average Doppler measurement Standard deviations in C/N_0 intervals of 5 dB-Hz for satellites available during Test WH-4.

Test WH-4, Linear Speed 15.1 cm/s Standard deviation (Hz)											
C/N_0		10	15	20	25	30	35	40	45	50	55
PRN	15	-	-	3.0	2.7	1.5	0.8	0.4	0.3	0.4	-
	18	-	-	-	1.8	1.9	0.8	0.5	0.3	0.3	-
	21	-	-	3.1	2.0	1.1	0.8	0.4	0.3	0.3	-
	24	-	-	-	-	-	0.9	0.5	0.3	0.2	0.2
	29	-	-	-	-	1.2	0.7	0.5	0.4	0.4	-
Average Std of all PRNs		-	-	3.1	2.1	1.4	0.8	0.5	0.3	0.3	0.2

Table 4.6: Average Doppler measurement Standard deviations in C/N_0 intervals of 5 dB-Hz for satellites available during Test WH-5.

Test WH-5, Linear Speed 21.4 cm/s Standard deviation (Hz)											
C/N_0		10	15	20	25	30	35	40	45	50	55
PRN	15	-	-	-	2.4	1.5	0.8	0.5	0.4	0.3	-
	18	-	-	-	2.5	1.9	1.2	0.6	0.3	0.3	-
	21	-	-	-	-	-	1.2	0.6	0.3	0.3	-
	24	-	-	-	2.3	1.9	1.3	0.6	0.3	0.2	0.2
	29	-	-	3.0	2.3	1.5	0.8	0.5	0.4	0.3	-
Average Std of all PRNs		-	-	3.0	2.4	1.7	1.1	0.6	0.3	0.3	0.2

Table 4.7: Average Doppler measurement Standard deviations in C/N_0 intervals of 5 dB-Hz for satellites available during Test WH-6.

Test WH-6, Linear Speed 42.7 cm/s Standard deviation (Hz)											
C/N_0		10	15	20	25	30	35	40	45	50	55
PRN	18	-	-	4.5	3.4	3.0	2.2	1.1	0.6	0.4	-
	21	-	-	-	-	1.3	1.2	0.8	0.5	0.5	-
	24	-	-	-	3.5	2.2	2.0	1.0	0.6	0.4	0.3
	29	-	-	5.0	3.3	2.5	1.6	0.9	0.8	-	-
Average Std of all PRNs		-	-	4.7	3.4	2.2	1.8	1.0	0.6	0.4	0.3

Table 4.8: Average Doppler measurement Standard deviations in C/N_0 intervals of 5 dB-Hz for satellites available during Test WH-7.

Test WH-7, Linear Speed 80.1 cm/s Standard deviation (Hz)											
C/N_0		10	15	20	25	30	35	40	45	50	55
PRN	6	-	-	5.1	4.3	3.1	2.2	1.4	0.9	-	-
	15	-	-	-	3.7	2.8	2.0	1.5	1.0	1.0	-
	18	-	-	-	-	-	-	0.8	0.8	0.5	-
	21	-	-	-	-	-	1.5	1.3	0.9	0.8	-
	22	-	6.5	5.3	4.3	3.8	3.5	2.2	-	-	-
	24	-	-	-	4.0	3.4	3.0	1.7	1.4	0.8	-
	29	-	-	5.0	4.0	3.3	2.9	1.9	1.7	-	-
Average Std of all PRNs		-	6.5	5.1	4.1	3.3	2.5	1.5	1.1	0.8	-

Table 4.9: Average Doppler measurement Standard deviations in C/N_0 intervals of 5 dB-Hz for satellites available during Test WH-8.

Test WH-8, Linear Speed 15.1 cm/s Standard deviation (Hz)											
C/N_0		10	15	20	25	30	35	40	45	50	55
PRN	3	4.4	3.8	2.9	2.2	1.2	0.8	0.6	-	-	-
	6	4.4	3.7	3.0	2.1	1.3	0.7	0.4	0.3	-	-
	18	4.1	4.3	2.9	2.1	1.2	0.7	0.4	0.4	-	-
	19	4.5	3.8	3.0	2.0	1.2	0.9	-	-	-	-
	21	4.2	3.9	3.1	2.3	1.4	0.7	0.4	0.4	-	-
	22	4.2	4.3	2.9	1.9	1.3	0.7	0.5	0.4	-	-
	24	4.2	4.0	3.1	2.0	1.2	0.9	-	-	-	-
	26	4.1	4.1	2.9	1.9	1.3	0.8	0.6	-	-	-
Average Std of all PRNs		4.3	4.0	3.0	2.1	1.3	0.8	0.5	0.4	-	-

Figure 4-14 summarizes the tables above and compares them to the theoretical standard deviations obtained with Equation 4-9. In this figure, the last row of each table, which is an average among all the satellites, is plotted for each test.

It was mentioned that a C/N_0 threshold of 25 dB-Hz was chosen for pre-filtering. This threshold is used in Figure 4-14 to divide it into two portions. The right side of the threshold is related to the measurements that are qualified and the left side is related to the measurements that are not qualified after pre-filtering. For the qualified measurements, the standard deviation in the tests with a linear speed of less than 20 cm/s matches the theoretical Doppler standard deviation. For the same measurements, when the linear speed of the turntable is higher than 20 cm/s, the standard deviation is above the theoretical model. As an example, for a speed of 80 cm/s, a signal with the power of 35 dB-Hz has a standard deviation of 2.5 Hz, which is 2 Hz higher than the value of 0.5

Hz obtained from the theoretical model. This is because the Doppler multipath error is a function of user velocity. Figure 4-14 shows that the Doppler multipath error in the residential house is not negligible for linear speeds above 20 cm/s.

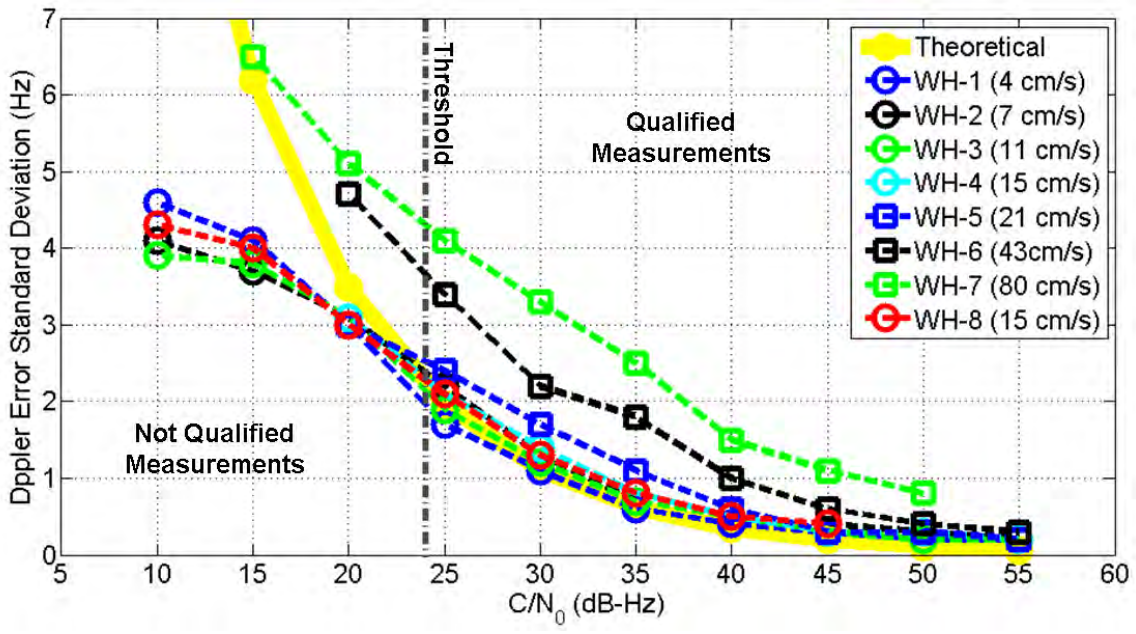

Figure 4-14: Average Standard deviation of Doppler measurements of all satellites in C/N_0 intervals of 5 dB-Hz for each test and comparing them to the theoretical standard deviation of Doppler measurements.

It was mentioned previously that for the measurements below the C/N_0 threshold the Doppler measurements are distributed on the search space. Consequently, for the Doppler measurements that are not qualified in pre-filtering, the Doppler error standard deviation is a function of the search space chosen for the GSNRx-rr™ receiver and does not match the theoretical model. In this work, for Test WH-6 and WH-7, a

search space of ± 10 Hz is chosen because of higher dynamics compared to the rest of tests that have a search space of ± 7 Hz. For signals with a C/N_0 below 25 dB-Hz, Doppler measurements are distributed among the search space. Thus, the Doppler error standard deviation is higher for Test WH-6 and WH-7 with a wider search space in the Doppler dimension.

In the next section, the velocity is estimated by the Doppler measurements using least squares. To estimate the velocity more accurately, the covariance matrix of the Doppler measurements is used for weighting. Doppler bandwidth and integration time are constant for all measurements in an individual dataset. Thus, these two parameters are part of the a priori covariance matrix and the cofactor matrix is only a function of the C/N_0. The cofactor matrix, Q_Z, is used for weighting the measurements. It is shown later that using Q_Z as a weighting matrix will make velocity measurements more accurate.

4.3.2.2 Velocity Measurements

For velocity estimation in a single point solution, clock drift should be estimated along with the three velocity components (East, North and Up), for a total of four unknowns. In contrast to the single point solution, the GSNRx-rr™ produces a Doppler difference between the static antenna and a moving antenna that does not contain clock drift, and only three unknowns (velocity components) remain in the least squares solution.

As mentioned earlier, Doppler measurements provided by the GSNRx-rr™, f_{rr}, are used for indoor Doppler characterization and for comparing the Doppler error standard deviation to the theoretical model presented in Equation 4-9. In this section, f_{rr} is used for estimating velocity and it is shown that the accuracy of velocity measurements can improve after weighting Doppler measurements with the power dependent theoretical model. However, in Section 3.2.3.3 it was discussed that a reference-rover receiver cannot be used in real applications and shows the abilities of a block processing technique in a research project. In real applications, Doppler measurements provided by a block processing technique include clock drift. In order to measure the accuracy of velocity estimation in a real application, Doppler measured at the reference antenna, f_{ref}, is added to f_{rr}. f_{ref} includes the satellite motion effect and clock drift as follows:

$$f_{rov} = f_{rr} + f_{ref} \tag{4-12}$$

$$f_{rov} = f_{rr} + U \cdot v_{sat} + cd\,, \tag{4-13}$$

where

f_{rov} is the Doppler measurement of the rover,

U is the satellite-receiver unit vector in ENU coordinate frame,

v_{sat} is the velocity vector of the satellite, and

cd is the clock drift of the receiver.

In this section both f_{rr} and f_{rov} are used for velocity measurements to fulfill the following purposes:

- Doppler measurements from the GSNRx-rr™, f_{rr}, provide the highest accuracy for velocity estimation while using a block processing technique. Also, the velocity improvement after weighting the measurements based on the power dependent theoretical method is investigated.
- The Doppler measurements of the rover antenna, f_{rov}, are used for investigating the accuracy of velocity measurements for a receiver with a block processing technique in a real application where clock drift has to be estimated as well as three velocity components.

Velocity Measurement without Clock Drift Estimation:

The relation between the Doppler measurements provided by the GSNRx-rr™ receiver, f_{rr}, and unknowns are given by

$$\begin{bmatrix} f_{rr,1} \\ f_{rr,2} \\ \vdots \\ f_{rr,k} \end{bmatrix} = \begin{bmatrix} U_{E,1} & U_{N,1} & U_{U,1} \\ U_{E,2} & U_{N,2} & U_{U,2} \\ \vdots & \vdots & \vdots \\ U_{E,k} & U_{N,k} & U_{U,k} \end{bmatrix} \begin{bmatrix} v_E \\ v_N \\ v_U \end{bmatrix} + \begin{bmatrix} \varepsilon_1 \\ \varepsilon_2 \\ \vdots \\ \varepsilon_k \end{bmatrix} \qquad 4\text{-}14$$

$$F_{rr} = HV + \varepsilon, \qquad 4\text{-}15$$

where

V is the unknown velocity vector in the ENU coordinate frame,

k is the number of observations/satellites,

H is the design matrix, and

ε is the error in the Doppler measurements.

From Equation 4-14 and 4-15 the design matrix is determined as follows:

$$H = \begin{bmatrix} U_{E,1} & U_{N,1} & U_{U,1} \\ U_{E,2} & U_{N,2} & U_{U,2} \\ \vdots & \vdots & \vdots \\ U_{E,k} & U_{N,k} & U_{U,k} \end{bmatrix}. \qquad 4\text{-}16$$

Equation 4-15, combined with the covariance matrix from Equation 4-11, leads to the following least squares solution:

$$V = \left(H^T Q_Z^{-1} H\right)^{-1} H^T Q_Z^{-1} f_{rr}. \qquad 4\text{-}17$$

Figure 4-15(a) shows the velocity measurements using least squares for Test WH-3. The black line corresponds to the true velocity. Red dots show the velocity measurements when all observations from six available satellites are used without weighting and pre-filtering. Pre-filtering based on the C/N_0 threshold is performed on the same dataset. After pre-filtering, the number of satellites and their related DOP are shown in Figure 4-15(c) and Figure 4-15(b) respectively. Blue dots in Figure 4-15(a) show the velocity measurements when the observations are weighted using the covariance matrix presented in Equation 4-11 and pre-filtering has been applied. In comparing the blue and red dots, it is evident that applying pre-filtering and weighting

measurements improves the accuracy of velocity estimates. In Test WH-3, the velocity accuracy improved from 21.8 cm/s to 12.1 cm/s. This improvement is shown in Figure 4-16 for the three velocity components.

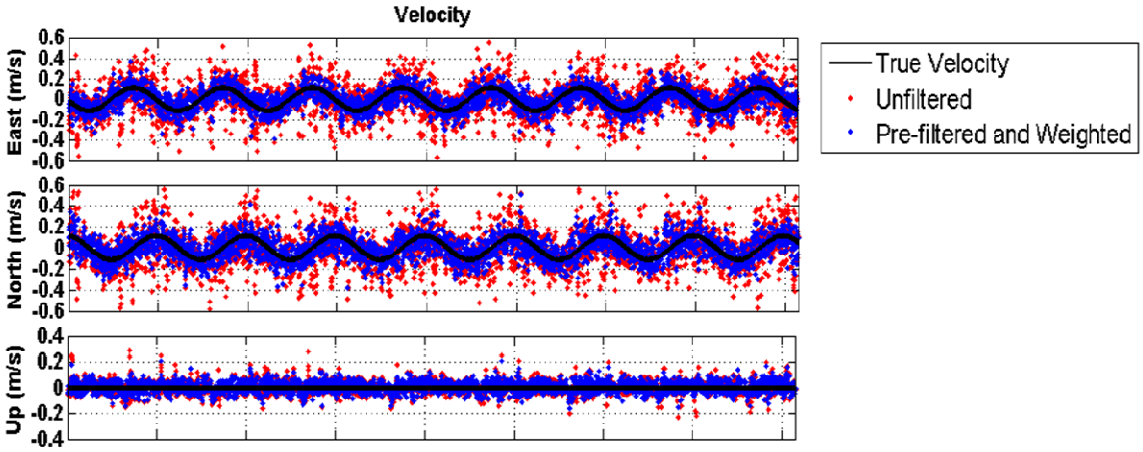

(a)

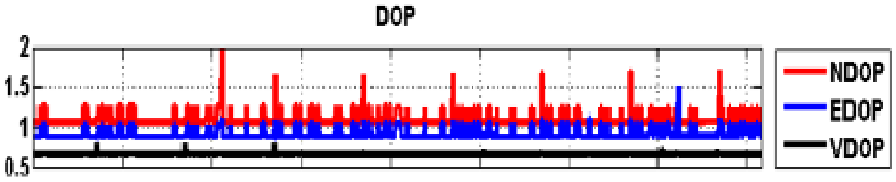

(b)

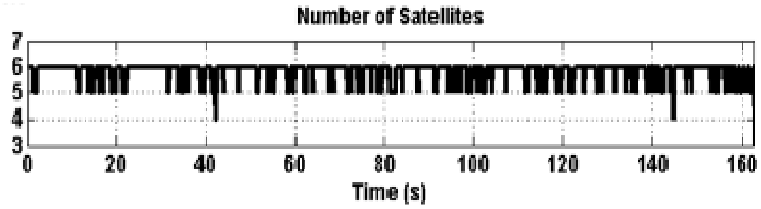

(c)

Figure 4-15: Velocity measurements without clock drift estimation (a), Dilution of precision (DOP) (b) and number of satellites (c). Weighting observations by a signal power dependent covariance matrix and pre-filtering make velocity measurements more accurate.

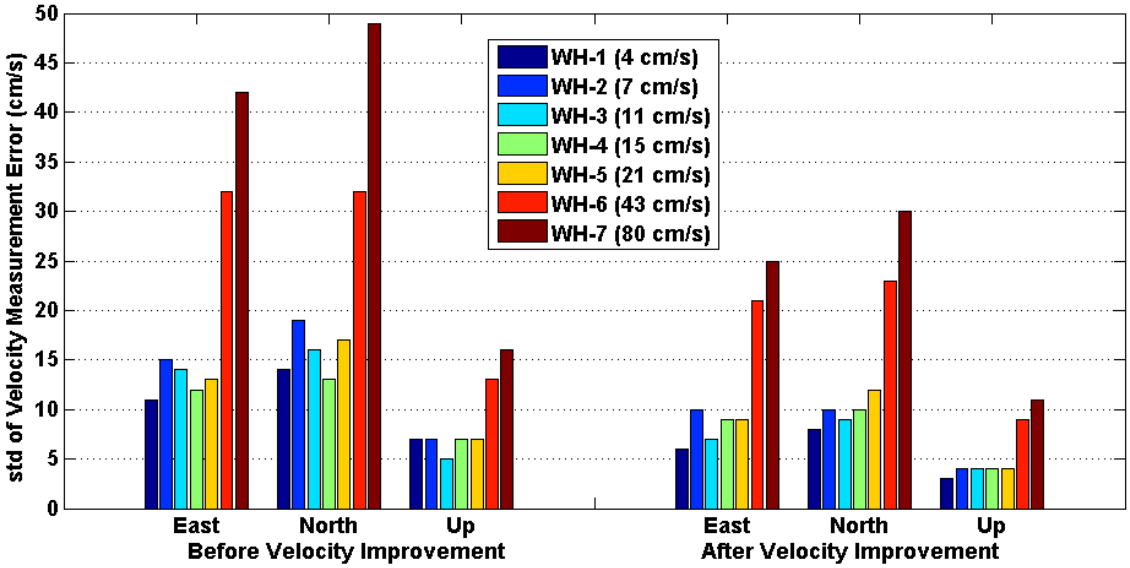

Figure 4-16: Comparing Velocity Measurements in Different Datasets Using Different Methods. Velocity improves after weighting the observations based on signal power and pre-filtering. Higher dynamics increase the velocity errors.

Velocity measurements were computed for different tests on the main floor of the house. Figure 4-16 plots the standard deviation of velocity measurement errors computed from each test. This figure shows that using the covariance matrix presented in Equation 4-11 as a weighting matrix and pre-filtering improves the estimation of velocity in all datasets. Although DOP and the number of satellites are not equal for all datasets, it is seen in this figure that the velocity error increases for datasets with higher dynamics (see also Table 4.1). This is because of the Doppler multipath error that increases for higher dynamics.

Reliability testing based on residuals is a method of blunder detection that can be used instead of pre-filtering in the navigation solutions. For velocity estimation in this work or other indoor applications where the number of satellites is insufficient for reliability testing, the navigation solution is not able to detect all the blunders. Therefore pre-filtering is utilized here for velocity estimation.

Velocity Measurement with Clock Drift Estimation:

According to Equations 4-13, 4-15 and 4-16, the relationship between the Doppler measurements provided for the rover antenna, f_{rov}, and four unknowns (velocity components and clock drift) is given by

$$\begin{bmatrix} f_{rov,1} \\ f_{rov,2} \\ \vdots \\ f_{rov,k} \end{bmatrix} = \begin{bmatrix} f_{rr,1} + cd \\ f_{rr,2} + cd \\ \vdots \\ f_{rr,k} + cd \end{bmatrix} + \begin{bmatrix} U_{E,1} & U_{N,1} & U_{U,1} \\ U_{E,2} & U_{N,2} & U_{U,2} \\ \vdots & \vdots & \vdots \\ U_{E,k} & U_{N,k} & U_{U,k} \end{bmatrix} \begin{bmatrix} v_{sat,1} & v_{sat,2} & \cdots & v_{sat,k} \end{bmatrix} \tag{4-18}$$

$$\begin{bmatrix} f_{rr,1} + cd \\ f_{rr,2} + cd \\ \vdots \\ f_{rr,k} + cd \end{bmatrix} = \begin{bmatrix} U_{E,1} & U_{N,1} & U_{U,1} & 1 \\ U_{E,2} & U_{N,2} & U_{U,2} & 1 \\ \vdots & \vdots & \vdots & \vdots \\ U_{E,k} & U_{N,k} & U_{U,k} & 1 \end{bmatrix} \begin{bmatrix} v_E \\ v_N \\ v_U \\ cd \end{bmatrix} = G \begin{bmatrix} V \\ cd \end{bmatrix} \tag{4-19}$$

$$F_{rov} = G \begin{bmatrix} V \\ cd \end{bmatrix} + HV_{sat}, \tag{4-20}$$

where

V_{sat} is the known velocity of satellites in the ENU coordinate frame,

k is the number of observations/satellites, and

G is the new design matrix when clock drift is included.

From Equation 4-19, the new design matrix when clock drift is included as an unknown is given by

$$G = \begin{bmatrix} U_{E,1} & U_{N,1} & U_{U,1} & 1 \\ U_{E,2} & U_{N,2} & U_{U,2} & 1 \\ \vdots & \vdots & \vdots & \vdots \\ U_{E,k} & U_{N,k} & U_{U,k} & 1 \end{bmatrix}. \qquad 4\text{-}21$$

Equation 4-20 leads to the following least squares solution:

$$\begin{bmatrix} V \\ cd \end{bmatrix} = \left(G^T Q_Z^{-1} G\right)^{-1} G^T Q_Z^{-1} \left(F_{rov} - HV_{sat}\right). \qquad 4\text{-}22$$

Equation 4-22 is used for Test WH-3 and the estimated velocity, DOP and number of satellites are shown in Figure 4-17. The same measurements and power dependent weighting method that were used for the velocity measurement without clock drift estimation are used here. The standard deviation of velocity increases from 12.1 cm/s to 66.5 cm/s when the clock drift is added as an unknown. This is because of the increase in DOP when clock drift is added as an unknown.

The accuracy of velocity measurements with clock drift estimation is computed for all the tests and is summarized in Figure 4-18. There are four satellites available in Test WH-6 and, after pre-filtering in this test, only three satellites remain, which is not enough for velocity estimation. Thus, the accuracy for Test WH-6 is not presented in Figure 4-18.

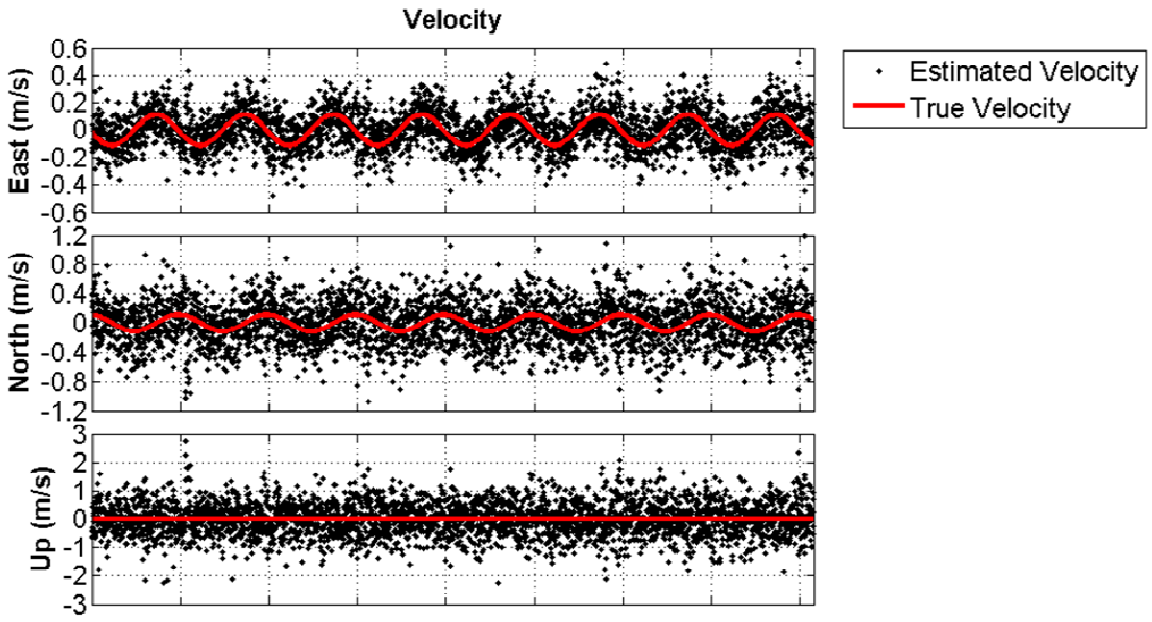

(a)

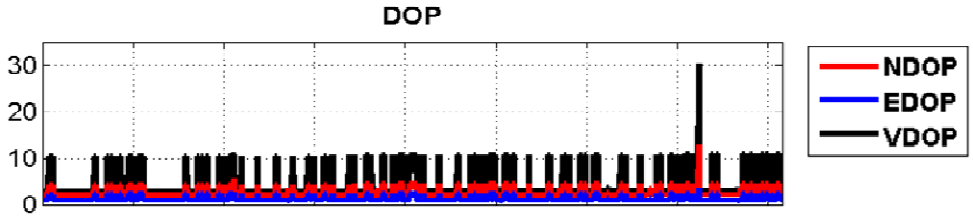

(b)

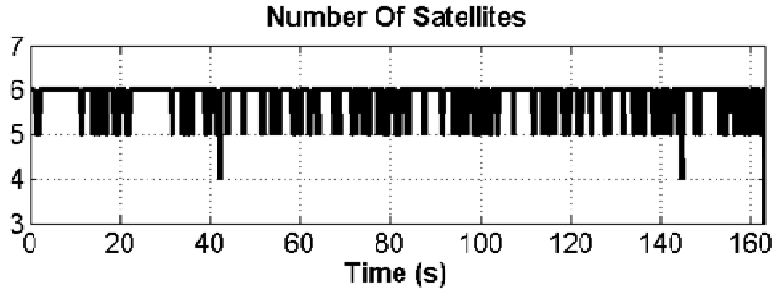

(c)

Figure 4-17: Velocity measurements with clock drift estimation (a), Dilution of precision (DOP) (b) and number of satellites (c).

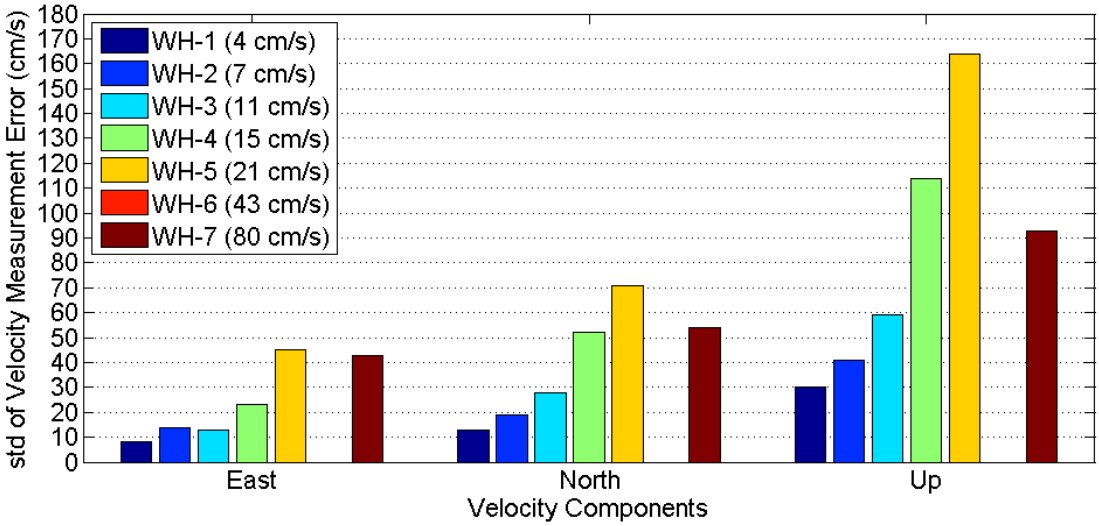

Figure 4-18: Velocity accuracy for main floor residential house tests while clock drift is unknown. The accuracy of Test WH-6 is not presented because of lack of observations.

4.3.2.3 Dead Reckoning and Trajectories Based on Velocity

The estimated velocities provided in Section 4.3.2.2 follow the true velocity (Figure 4-15 and Figure 4-17). The trajectory based on the integration of the velocity known as Dead Reckoning (DR) is provided in this section. Figure 4-19 shows the trajectory of the antenna provided by the DR method for Test WH-3 when clock drift is not considered as an unknown. This figure confirms that the trajectory follows the circular motion. Since DR provides positions based on velocity integration, velocity errors are accumulated and cause a drift in the position solution. This drift is observable in all tests.

The upward drift shown in Figure 4-19 is common in all datasets and is not the effect of velocity error accumulation. The rotation of the antenna causes carrier phase

wrap-up (Bisnath 2007) that produces a constant bias in the Doppler measurements from all the satellites. When all the Doppler measurements are biased depending on satellite geometry, the velocity solution is biased in a specific direction. Since satellites are always above the receiver, this drift usually has a vertical direction except when measurements are provided only from satellites at a corner of sky. The bias in the Doppler measurements is the same for all satellites and is equal to the rotation rate of the turntable (Tetewsky & Mullen 1997). This bias is corrected in all Doppler measurements before computing the velocity. The vertical drift in all trajectories before and after this correction is summarized for all tests in Table 4.10.

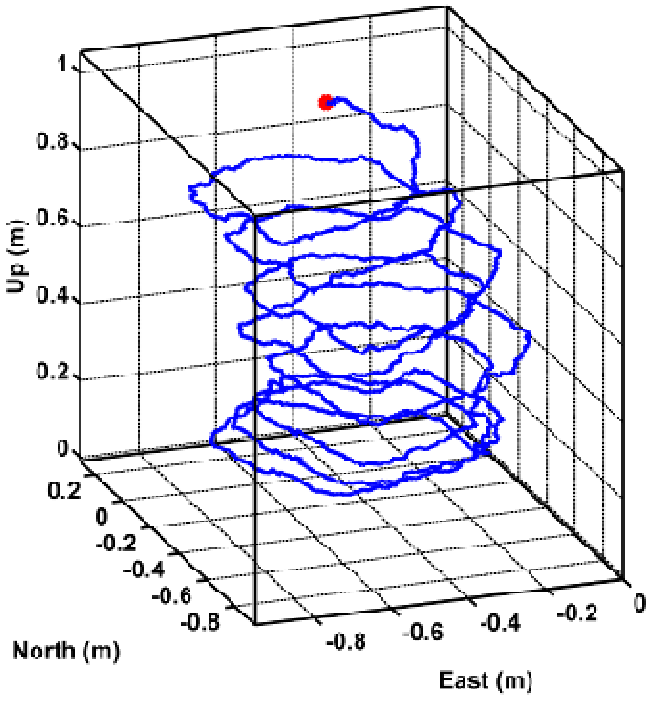

Figure 4-19: Displacement based on velocity integration for Test WH-3 when the clock drift is not considered as an unknown. Displacement follows the turntable motion.

Table 4.10: Vertical drift in trajectory provided by velocity integration before and after phase wrap-up correction.

Vertical Drift in Trajectory (m)							
Test ID	WH-1	WH-2	WH-3	WH-4	WH-5	WH-6	WH-7
Before Correction	0.5	1.5	1.1	1.5	1.2	4.2	6
After Correction	0.4	0.4	0.6	0.9	0.2	0.5	0.5
Test Duration (s)	272	265	163	174	164	173	122

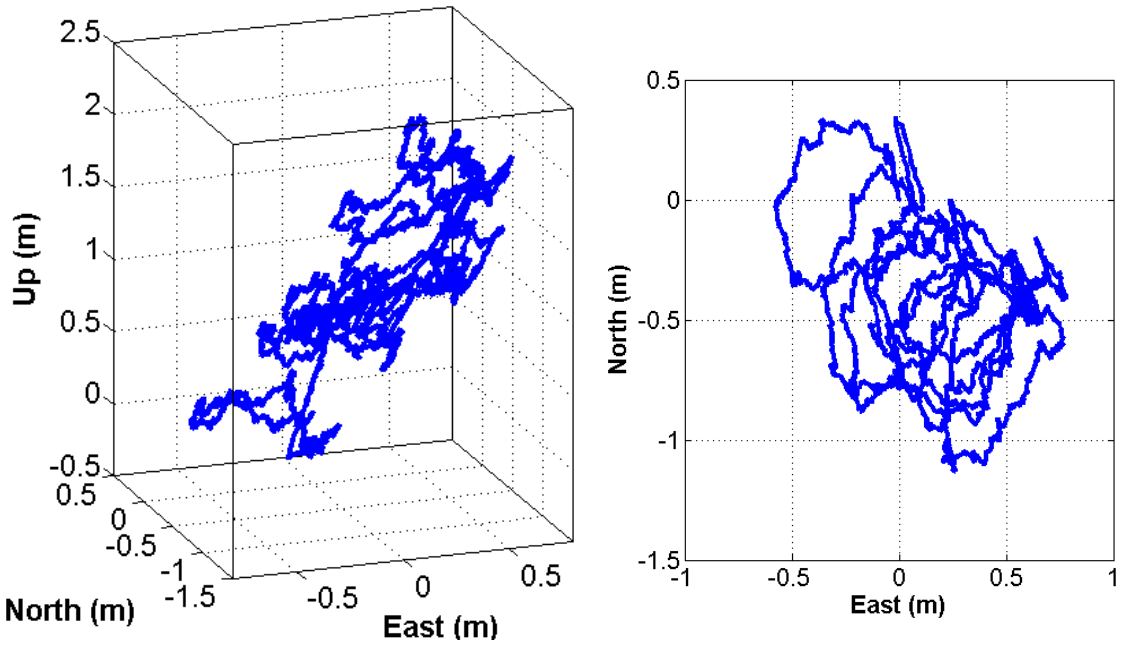

Figure 4-20: Displacement based on velocity integration for Test WH-3 when clock drift is considered as an unknown.

Figure 4-20 shows the trajectory of the antenna provided by the DR method for test WH-3 when the clock drift is considered as an unknown. Since the accuracy of velocity decreases when the clock drift is added as an unknown state, the trajectory presented in

Figure 4-20 is noisy and does not follow a pattern as circular as that of the trajectory presented in Figure 4-19.

4.4 Summary

In this chapter, the u-blox HSGPS and reference-rover receivers are used for extraction of Doppler measurements and the latter is used for indoor Doppler characterization in two different indoor environments. The quality of the measurements is thoroughly assessed using true Doppler values. From the analysis, it emerges that C/N_0 is the main factor impacting the process of Doppler estimation.

In a harsh multipath environment such as a modern concrete building, only a reference-rover is able to extract Doppler measurements. These measurements are not reliable and they do not carry enough information for indoor navigation. Only kinematic and static status of the rover can be distinguished using this information.

On the contrary, in a residential house with less attenuation, both receivers are able to provide Doppler measurements, but only measurements provided by the reference-rover receiver are reliable for indoor navigation and follow the pattern of the true Doppler values. The accuracy of Doppler measurements in such an environment follows the theoretical model introduced in Chapter Three for velocities lower than 20 cm/s and shows that the assumption of neglecting Doppler multipath errors is viable for low dynamics in a typical North American residential house, for which the estimated velocity based on Doppler measurement observations can be utilized to enhance indoor navigation. It is also observed that these estimations can be improved using pre-filtering and a power dependant weighting matrix. For pedestrian velocities higher than 20 cm/s, it

can be assumed that the power dependent model is close to Doppler measurement accuracy and velocity estimation can be improved by using this model as a weighting model.

In the residential house the accuracy of velocity measurements is assessed. While a reference-rover receiver is utilized, clock drift is not considered as a state to be estimated but in real applications this estate should be estimated. In both cases, the accuracy of velocity is measured and compared. It was shown that velocity accuracy decreases from 12.1 cm/s for measurements from a reference-rover receiver to 66.5 cm/s in real applications for a test with linear speed of 11 cm/s under signal attenuation of 10 dB.

Chapter Five: Effects of Indoor Measurement Weighting on GPS/INS Integration

This chapter presents and discusses positioning solutions obtained in the context of GPS/INS integration when GPS signals are corrupted. Specific attention is given to assessing the accuracy of the integrated system in terms of position errors.

Indoor Doppler and pseudorange observations and their accuracy were discussed in Chapter Three and Four. The main objective of this chapter focuses on the effect of indoor observation weighting on GPS/INS integration. For this purpose, different weighting models for GPS observations are utilized in an integrated navigation solution. It was mentioned in Chapter Three that in an indoor environment pseudorange and Doppler observations have different characteristics. This chapter compares and studies the effect of these observations when they are used for updating an INS. For this purpose, first both of these observations are used together for updating the INS and then each of the pseudorange and Doppler observations are separately integrated with INS (i.e. Doppler/INS versus pseudorange/INS).

In Section 5.1 the methodology and the utilized software for GPS/INS integration are discussed. Section 5.2 analyzes the results of a GPS/INS integrated system based on two sets of data collected on the main floor and in the basement of a residential house. Finally, the summary of the chapter is provided in Section 5.3.

5.1 GPS/INS Integration Methodology

In this Section the methodology and the software used for GPS/INS integration are introduced. The GSNRx-nav-ins^{TM} software was developed by the PLAN Group.

This software uses the tightly coupled integration method described in Section 2.3. GPS observations are transferred to this software from a GPS software receiver and specific forces and angular rates are provided by an IMU. This software can read observations from the GSNRx™ and GSNRx-rr™ receivers. These two receivers are used in this work for extracting GPS observations and some of their parameters are discussed in Section 5.1.1.

In order to fulfill the goals of this research, the following aspects of the GSNRx-nav-ins™ software have been modified:

- GPS weighting: GSNRx-nav-ins™ was originally only able to use the elevation dependent weighting model for GPS observations and has been modified to use the weighting models described in Section 3.4. In the context of a GPS/INS integrated navigation solution, it can be used to compare the relative performance of different weighting methods.
- Selecting GPS observations: As discussed in Chapter Three, Doppler errors have different characteristics than those of pseudorange errors in indoor environments. In order to separate and compare the effects of pseudorange and Doppler errors on an integrated system, the GSNRx-nav-ins™ software was modified to select the type of GPS observations. Here, when only Doppler measurements are selected for updating the INS, the software is referred to as Doppler/INS integrated system and when pseudorange measurements are used for this purpose, the software is referred to as a pseudorange/INS integrated system.

In the following sections the methods used to measure the GPS signal parameters and their weighting models in this work are described.

5.1.1 GPS Receivers

The performance of an integrated system and its subsequent navigation solution are related to the type of receiver used for determining GPS signal parameters. In this work, two types of receivers, namely a standard receiver and a reference-rover receiver, provide GPS observations. The software receivers introduced earlier in Section 4.2.1 are as follows:

- GSNRx™: This standard software receiver utilizes the sequential tracking loops for estimating Doppler and pseudorange measurements. The maximum integration time used in this work is equal to 20 ms. The loop filter parameters of the GSNRx software receiver utilized here are summarized in Table 5.1.

Table 5.1: Loop filter parameters adopted for the standard GSNRx™

Parameter	Value
Frequency Loop Filter Order	2
Frequency Loop Filter Bandwidth	8 Hz
Phase Loop Filter Order	3
Phase Loop Filter Bandwidth	15 Hz

- GSNRx-rr™: This reference-rover software receiver is an aided receiver that utilizes a block processing technique for extracting GPS signal parameters. The

coherent integration time and search space used in this work are summarized in Table 5.2. Search space intervals used in this table are chosen based on the maximum speed of the rover antenna and the maximum distance of the rover antenna from the reference antenna. A pedestrian carried a rover antenna inside a residential house. A frequency search space of ± 10 Hz was considered, which is sufficient for covering Doppler variations resulting from a maximum receiver speed of 2 m/s (> nominal pedestrian speed). Also, a code phase search space of ± 0.24 chips, which is equivalent to a radius of 72 m (with the reference antenna at the centre), was considered to cover any range variations within the house.

Table 5.2: Parameters adopted for the processing of the indoor data by GSNRx-rr™

Parameter	Value
Coherent Integration Time	100 ms
Doppler Interval	±10 Hz
Doppler Step	0.2 Hz
Code Interval	± 0.24 chips
Code Step	0.02 chips

It was noted in Section 3.2 that in an indoor environment, a reference-rover receiver has the following advantages over a standard receiver:

- Improved tracking robustness based on the assistance from the unobstructed reference signals from the reference antenna.
- Improved signal observability due to a longer (>20 ms) integration time and acquiring the signal instead of tracking it.

As a result, GSNRx-rr™ is expected to provide more accurate measurements compared to GSNRx™. The performance of these two receivers in terms of availability is compared in Section 5.2. Low and high boundaries on the navigation solution accuracy are also quantified based on utilizing these two receiver structures in an integrated GPS/INS system. The accuracy of navigation solutions based on the GSNRx™ and GSNRx-rr™ software receivers is compared in Section 5.2.

5.1.2 Weighting GPS Observations

In Section 3.4 practical models for weighting the GPS observations were introduced. These models are summarized here for convenience.

1- Identical variance model:

$$\mathrm{var}_{(ID)} = \sigma^2 = \sigma^2 \cdot Q_{(ID)} \qquad 5\text{-}1$$

$$Q_{(ID)} = 1, \qquad 5\text{-}2$$

where $Q_{(ID)}$ is the cofactor of the measurements for the identical variance model.

2- Elevation dependent variance model:

$$\mathrm{var}_{(ELV)} = \sigma^2 \frac{1}{\sin^2(E)} = \sigma^2 \cdot Q_{(ELV)} \qquad 5\text{-}3$$

$$Q_{(ELV)} = \frac{1}{\sin^2(E)}, \qquad 5\text{-}4$$

where $Q_{(ELV)}$ is the cofactor of the measurements for the elevation dependent variance model.

3- Power dependent variance model:

$$\mathrm{var}_{(C/N_0)} = \sigma^2 \frac{C/N_0(zenith)}{C/N_0} = \sigma^2 \cdot Q_{(C/N_0)} \qquad 5\text{-}5$$

$$Q_{(C/N_0)} = \frac{C/N_0(zenith)}{C/N_0}, \qquad 5\text{-}6$$

where $Q_{(C/N_0)}$ is the cofactor of the measurements for the power dependent variance model.

The aforementioned models are utilized for weighing Doppler and pseudorange measurements in a GPS/INS integrated navigation solution. The position accuracy of the solution related to each model is assessed to determine the performance of the different algorithms. The square root of the cofactor of the measurements for these algorithms as a function of C/N_0 is shown in Figure 5-1. In this figure it is assumed that the satellite elevation is 30 degrees.

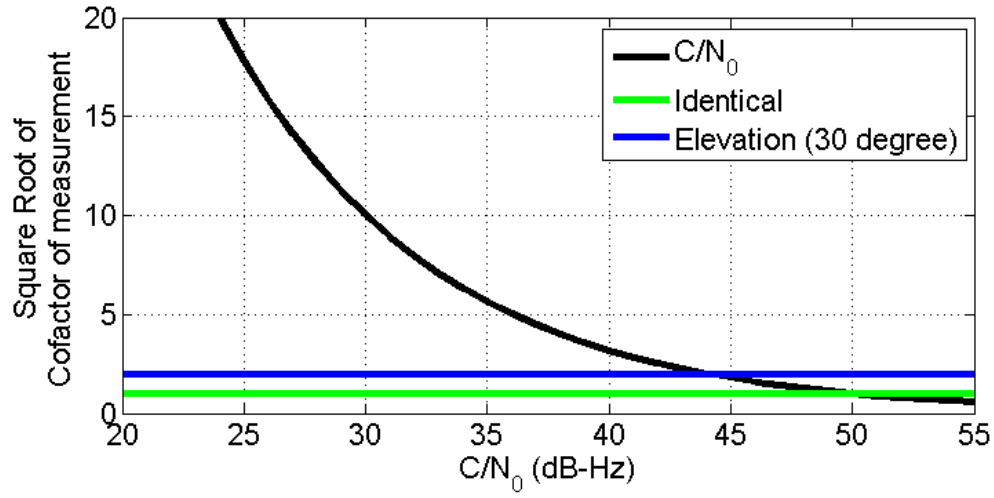

Figure 5-1: Square root of cofactor of measurements as a function of signal power. Satellite elevation is equal to 30 degrees.

Table 5.3: Default standard deviation at the zenith direction for GSNRx™ and GSNRx-rr™

GPS Observation	Default Standard Deviation of the Receivers (σ)
Doppler	0.2 Hz
Pseudorange	5 m

In these models, the standard deviation of the observations at the zenith, σ, should be determined in advance. Since in this work GSNRx™ and GSNRx-rr™ provide the measurements, their default variance values at the zenith are used for weighting the measurements in Equations 5-1, 5-3 and 5-5. Default standard deviation values for these receivers are given in Table 5.3. Moreover, the value of $C/N_0(zenith)$ is considered

equal to the average level of C/N_0 at the zenith in an open sky area, and in this work is equal to 50 dB-Hz.

5.2 Field Test Results

5.2.1 Description of Data Collection

An experiment in a typical North American residential house was conducted to evaluate the effects of GPS observation weighting on the performance of the GPS/ INS integrated system. In this experiment, a pedestrian carried the equipment using an aluminum frame. One test was performed on the main floor and one in the basement of the house. Figure 5-2 shows the inside of the house and the equipment carried by the pedestrian.

5.2.2 Equipment Used

The reference solution, required for determining the errors in the position measurements, was provided by the NovAtel's SPAN system. This system includes an L1/L2/GLONASS survey grade OEMV receiver and a tactical grade IMU (Honeywell HG1700 AG58). In order to have a more accurate reference solution, another OEMV receiver was also utilized as a base station to collect GNSS data from an antenna with a known position on the roof of the CCIT building at the University of Calgary. The Inertial Explorer (IE) software from NovAtel was then used to post-process the collected data and to provide a reference solution. In the IE software, the data was processed in forward and reverse directions, which is referred to as forward and backward processing. The forward and backward solutions are then combined for the final reference solution.

(a)

(b)

Figure 5-2: Residential house: Main floor (a) and Basement (b) data collections. The hardware for the field test is carried by the pedestrian.

In this experiment, the equipment was configured in order to collect GPS IF data from the rover antenna mounted on the aluminum frame and from the reference antenna

located outdoors. In addition to the HG1700 IMU, a lower grade IMU, namely a CPT, was placed in the aluminum frame. This IMU is comprised of Fiber Optic Gyros (FOG) and accelerometers based on Micro Electro Mechanical Systems (MEMS). The inertial sensor error model of these IMUs was discussed in Section 2.2.5.2, and the parameters of the noise and bias of the sensors in these IMUs were summarized in Table 2.1 and Table 2.2. The data collection equipment setup is shown in Figure 5-3.

The GPS IF data was collected by an NI PXI-5661 signal analyzer. This system consists of three front-ends with three channels. Each front-end includes a down-converter and a digitizer. In this experiment, two of these channels were connected to the reference and the rover antennas. The same oscillator drives both channels. The parameters used in the NI system are listed in Table 5.4.

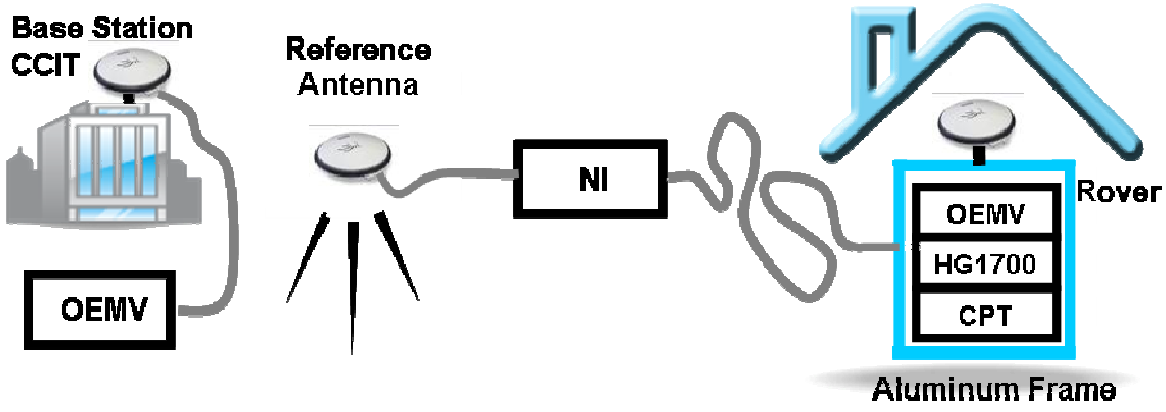

Figure 5-3: Data collection equipment setup.

Table 5.4: Parameters adopted for the data collection by the NI system.

Parameter	Value
Intermediate Frequency	0.42 MHz
Sampling Frequency	5 MHz
Sampling Type	I/Q-Complex
Quantization/Bit resolution	16 bits

5.2.3 Main Floor Test

In this section, the results of the main floor test are presented. The reference trajectory, provided by the Inertial Explorer software, is depicted in Figure 5-4. As can be seen, the rover started from an open sky area in the backyard (north of the house). This was followed by an initial alignment of INS in the presence of GNSS signals, after which the receiver was brought inside the house. The total time spent indoors was approximately five minutes. Finally, the rover was brought outside for a final alignment. The final alignment is needed for backward processing utilized in the Inertial Explorer software for improving the accuracy of the reference solution.

The estimated accuracy (standard deviation) of the reference position over time is provided by the Inertial Explorer software and is plotted in Figure 5-5. This plot shows that, when GNSS signals are available in an open sky area, the reference position solution has a high accuracy with an estimated standard deviation of better than 1 cm in each direction (East, North and Up) but, when the user enters the building and GNSS signals are blocked, the estimated position standard deviation degrades to a maximum of 20 cm ($\sqrt{14^2(height)+11^2(north)+9^2(east)}$) at t = 250 s for this test run. Since this reference is

provided by combining forward and backward processing, the lowest accuracy (20 cm) occurs in the middle of the period during which the GNSS observations are blocked (inside the house). The longer the user stays indoors, the more the reference experiences drift. Note that the use of the reference solution provided by the IE software for assessing the performance of different weighing algorithms is limited to the estimated standard deviation of the reference position solution. Hence, a comparison of the performance of scenarios with standard deviation differences smaller than the estimated standard deviation of the reference position solution would not be valid.

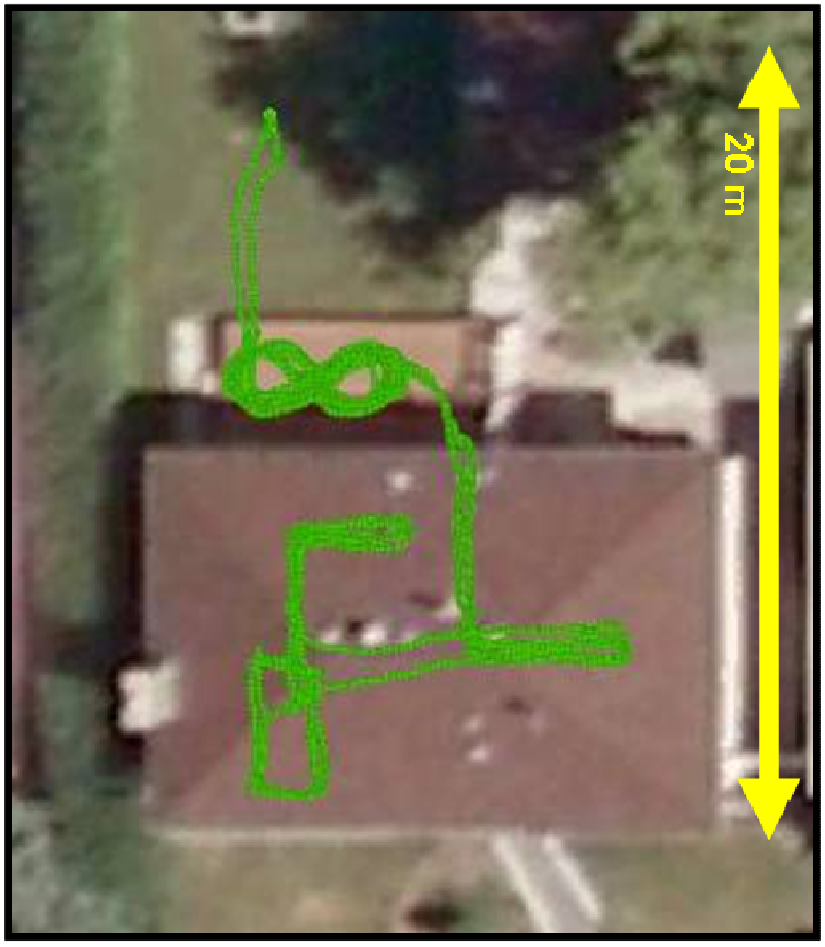

Figure 5-4: Reference trajectory of the rover for the main floor test.

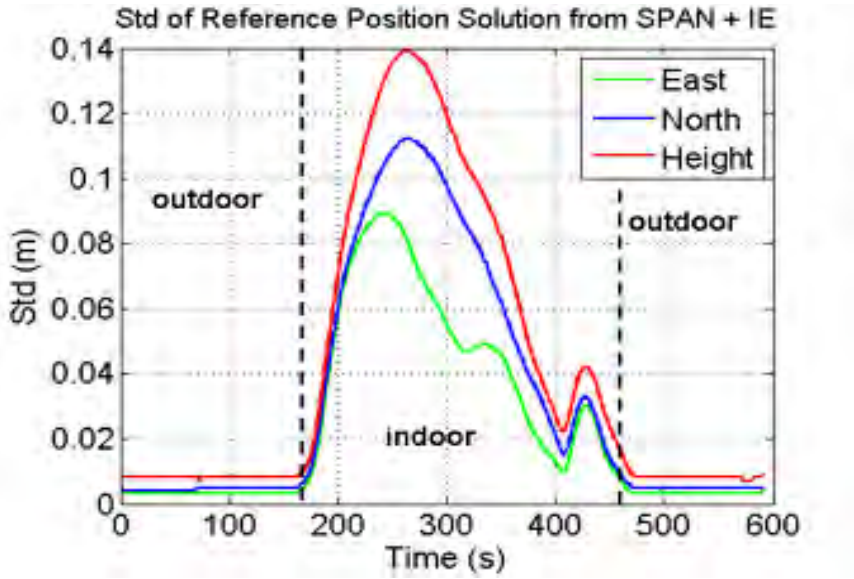

Figure 5-5: Estimated position accuracy of the reference solution for main floor test.

During the experiment, nine GPS satellites were available and the sky-plot is shown in Figure 5-6.

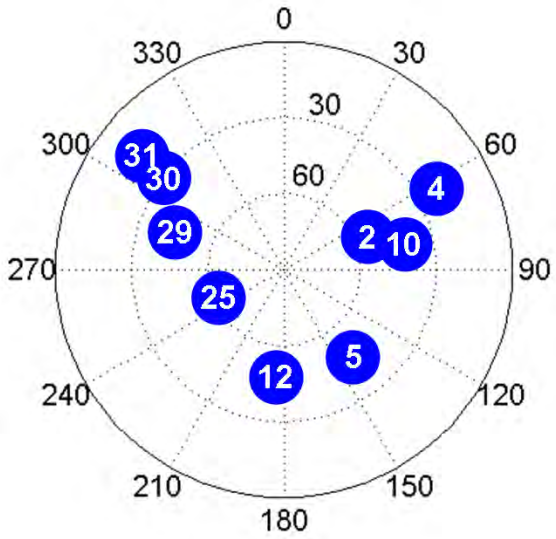

Figure 5-6: Sky-plot of GPS satellites available during the main floor test.

Below, signal availability, power, and some statistics related to available satellites are provided. Satellite 29 is chosen as an example and is discussed in detail, and the statistics of other satellites are summarized in Table 5.5.

Figure 5-7 shows the estimated C/N_0 of Satellite 29 for both the reference and rover antennas. As can be seen in this figure, for 150 s < t < 450 s where the rover antenna is inside the house, the estimated C/N_0 fluctuates due to multipath fading. This figure also shows the elevation angle of Satellite 29 as a function of time.

Based on Equations 5-2, 5-4 and 5-6, the cofactor of measurements can be calculated if the C/N_0 of the rover signal and the elevation of the satellite are known. The square root of the cofactor of measurements for Satellite 29 is calculated and shown in Figure 5-8. The cofactor of measurements is used for weighting Doppler and pseudorange measurements. As shown in Figure 5-8, the value for the identical variance model is equal to one for all satellites. For the elevation dependent variance model, it is a function of satellite elevation and is different for diverse satellites, changing slowly in time. For the power dependent variance model, the cofactor of measurements changes quickly since the C/N_0 fluctuates in time.

For Satellite 29, during the period that the rover antenna is located in the residential house, the average C/N_0 for the reference antenna is 49.5 dB-Hz and for the rover antenna it is 42.1 dB-Hz. Thus, the insertion loss in the house is approximately 7 dB for this satellite. Figure 5-7 shows the period of time that the GSNRx^{TM} is able to track the signal. This software receiver is able to track Satellite 29 94% of the time when

the rover is located in the house. During the time that GSNRx™ is not able to track the signal (6% of the measurement period), the average C/N_0 is 33.7 dB-Hz and the 95th percentile value for the C/N_0 is 40.4 dB-Hz. This shows that signals that are not tracked by GSNRx™ are attenuated below 40.4 dB-Hz.

A standard receiver starts with acquisition and, after acquiring the signal, continues with signal tracking in FLL and PLL states. Depending on the loop filter parameters and the signal power, a PLL or an FLL may lose lock, requiring the receiver to reacquire the signal. It is of interest to investigate the FLL and PLL performance of a standard receiver under multipath conditions.

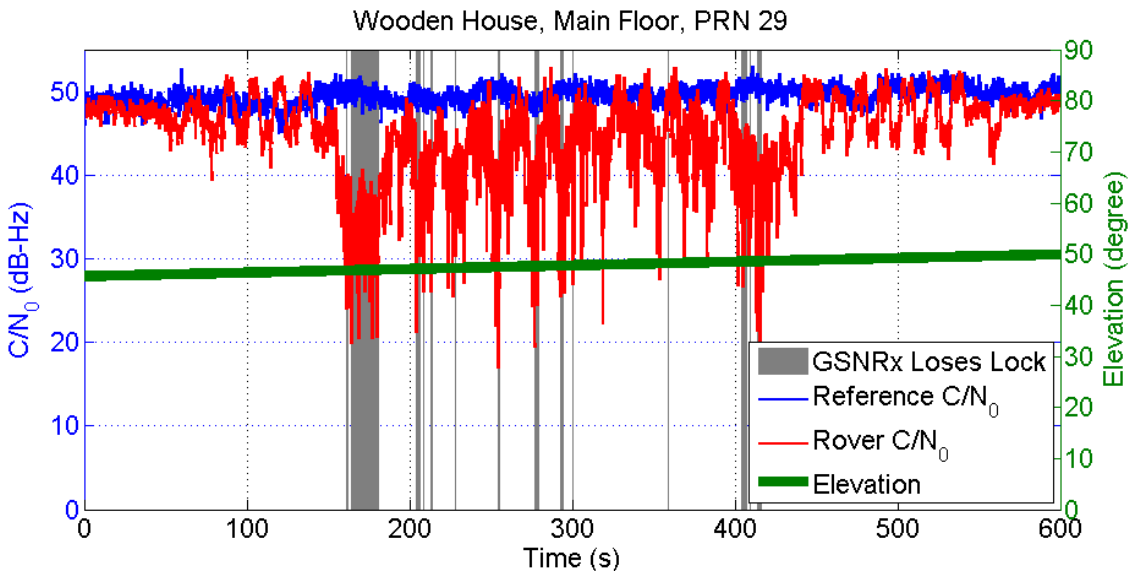

Figure 5-7: Carrier to noise ratio (C/N_0) of Satellite 29 for the reference and rover antennas and elevation angle of the satellite. In the grey areas, GSNRx™ is not able to track the signals. The rover antenna is carried on the main floor of the residential house.

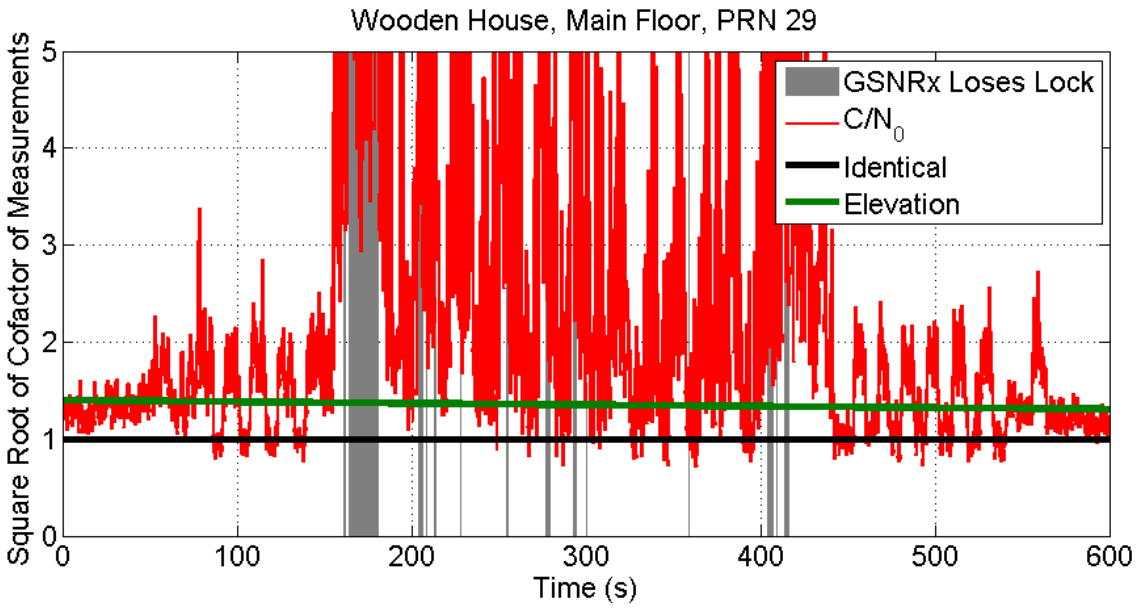

Figure 5-8: Square root of cofactor of measurements for three different variance models, namely identical, elevation dependent and power dependent. The rover antenna is carried in the main floor of the residential house.

Figure 5-9 shows the number of satellites for both GSNRx™ and GSNRx-rr™. In this figure, the number of satellites used in the navigation solution is shown. Because of the reference-rover receiver structure described in Section 3.2.3, the number of satellites tracked by the GSNRx-rr™ receiver is equal to the number of satellites tracked from the reference signal in the open sky area and is equal to nine here. On the other hand, the number of available satellites tracked by the GSNRx™ software receiver is usually less than nine and varies as the C/N_0 of different satellites varies (Figure 5-9). The GSNRx™ receiver tracks more than six satellites out of nine 99 % of the time since the loss is less than 8 dB on the main floor of the residential house.

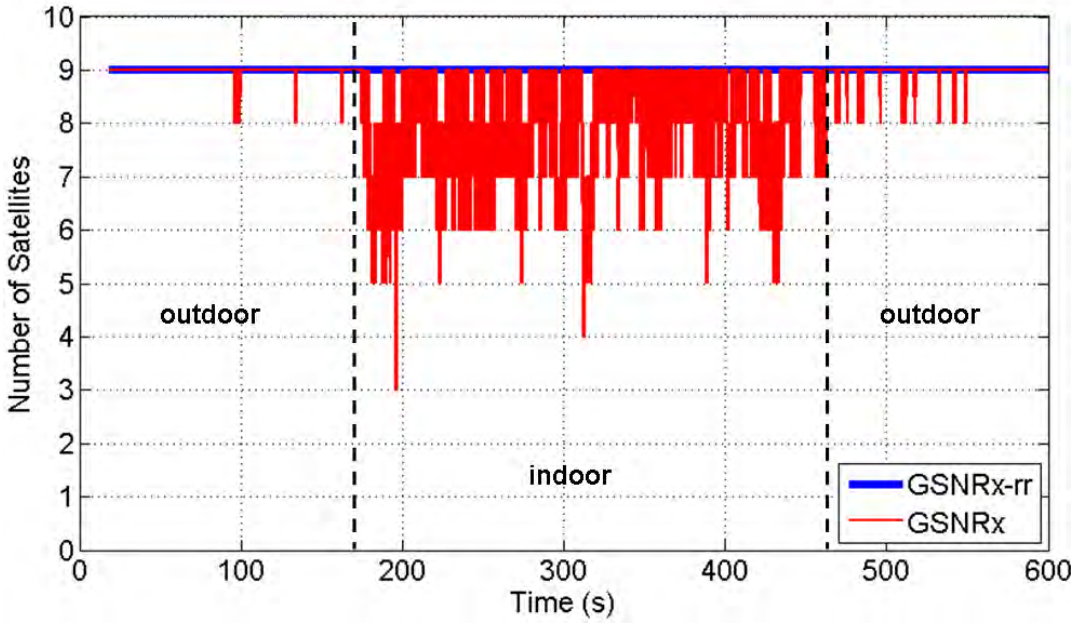

Figure 5-9: Number of satellites tracked by GSNRx™ and GSNRx-rr™ on the main floor of the residential house.

The statistics provided for Satellite 29 are given for the rest of the satellites in Table 5.5. These statistics are related to the period when the rover antenna is on the main floor of the residential house. This table shows the elevation angles of the satellites, the average signal power of the reference and rover antennas, the average and 95th percentile of signal power during periods when GSNRx™ is not able to track the signal (labeled "Lose Lock C/N_0" in Table 5.5), and the availability of the signal for GSNRx™. The average signal power for which GSNRx™ is not able to track is 34.4 dB-Hz and its 95th percentile value is 40.9 dB-Hz. This shows that signals that are not tracked by GSNRx™ are attenuated below 40.9 dB-Hz. This table also shows that the average insertion loss on the main floor of the residential house is 7 dB.

Table 5.5: Availability, elevation and power of available satellites on the main floor test of the residential house. Lose lock C/N_0 is related to the period when the standard receiver is not able to track the signal.

PRN	Elevation (degree)	Reference C/N_0 (dB-Hz)	Rover C/N_0 (dB-Hz)	Lose Lock C/N_0 (dB-Hz)		Availability for GSNRx
				Average	95th Percentile	
2	51	50.2	43.7	38.0	44.6	97%
4	16	41.5	33.7	31.6	37.4	59%
5	46	48.6	42.6	35.5	42.5	96%
10	42	47.8	41.4	36.0	41.5	95%
12	39	47.7	41.2	35.6	44.3	91%
25	59	52.3	45.5	36.7	42.3	99%
29	47	49.5	42.1	33.7	40.4	94%
30	29	45.9	37.9	32.1	38.6	82%
31	16	41.0	34.1	30.9	36.8	63%

The position solution obtained for the main floor experiment using the GSNRx-nav-ins™ software is reported in the following sections. In these solutions, the CPT IMU provides the raw IMU data.

5.2.3.1 Standard Tracking

GPS observations provided by the GSNRx™ software are integrated with INS using the GSNRx-nav-ins™ software. The different variance models are used for weighting GPS observations and the corresponding results are compared in this section.

The reference trajectory provided by the Inertial Explorer software and the estimated trajectories of the rover antenna for different weighting methods are shown in Figure 5-10. As can be seen in this figure, the position solutions provided by the GSNRx-nav-ins™ software closely follow the reference trajectory.

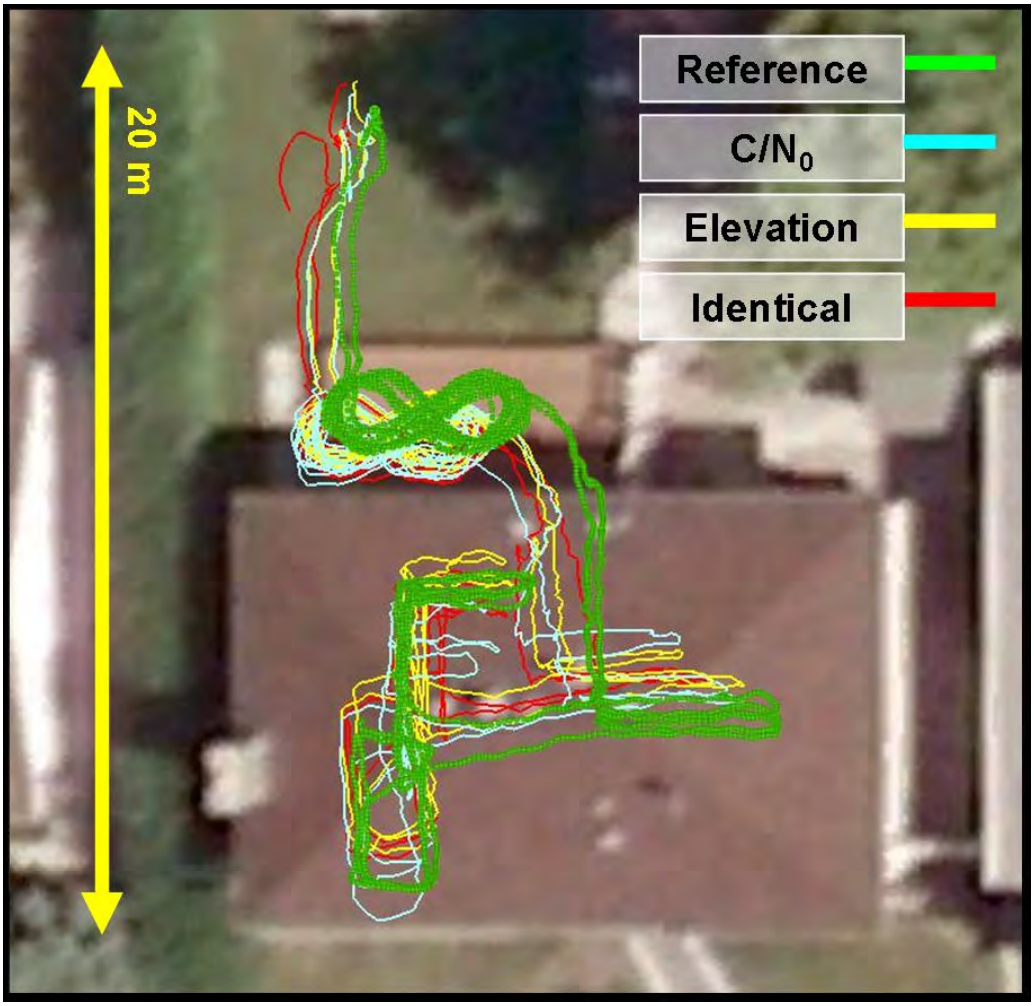

Figure 5-10: Trajectory obtained from GSNRx-nav-ins™. The CPT provides raw IMU data and GSNRx™ provides GPS observations. Three different weighting methods for the GPS observations, namely elevation dependent, power dependent and identical variance, were used for GPS/INS integration.

The trajectories shown in Figure 5-10 are compared with the reference solution in Figure 5-11 and the Root Mean Square (RMS) position errors are given in Table 5.6 It can be seen from Table 5.6 that the RMS position errors in the East and North directions

(horizontal plane) for three weighting methods are quite similar. In contrast, the RMS position errors in height for the identical and power weighting methods are about 50% lower than the elevation weighting. This table shows that the RMS of the position errors in the North and East directions for these three weighting methods differ by 13 cm, at most. This difference is not larger than the estimated accuracy of the reference position solution provided in Figure 5-4. As a result, it is not possible to confidently say which solution is better in the horizontal plane. The RMS height errors for three different weighting methods differ by more than 1 m, which is bigger than the estimated accuracy of the height reference. Thus, it is valid to compare the solutions of different weighting algorithms based on the RMS of height errors or three-dimensional RMS errors. This comparison is provided below.

Table 5.6: Accuracy of the integrated navigation solution of the main floor test while using the standard tracking receiver and the CPT IMU.

Direction	RMSE (m) for Different Weightings		
	C/N_0	Elevation	Identical
East	0.80	0.72	0.85
North	0.78	0.67	0.72
Height	3.28	5.57	2.30
3D	3.46	5.65	2.55

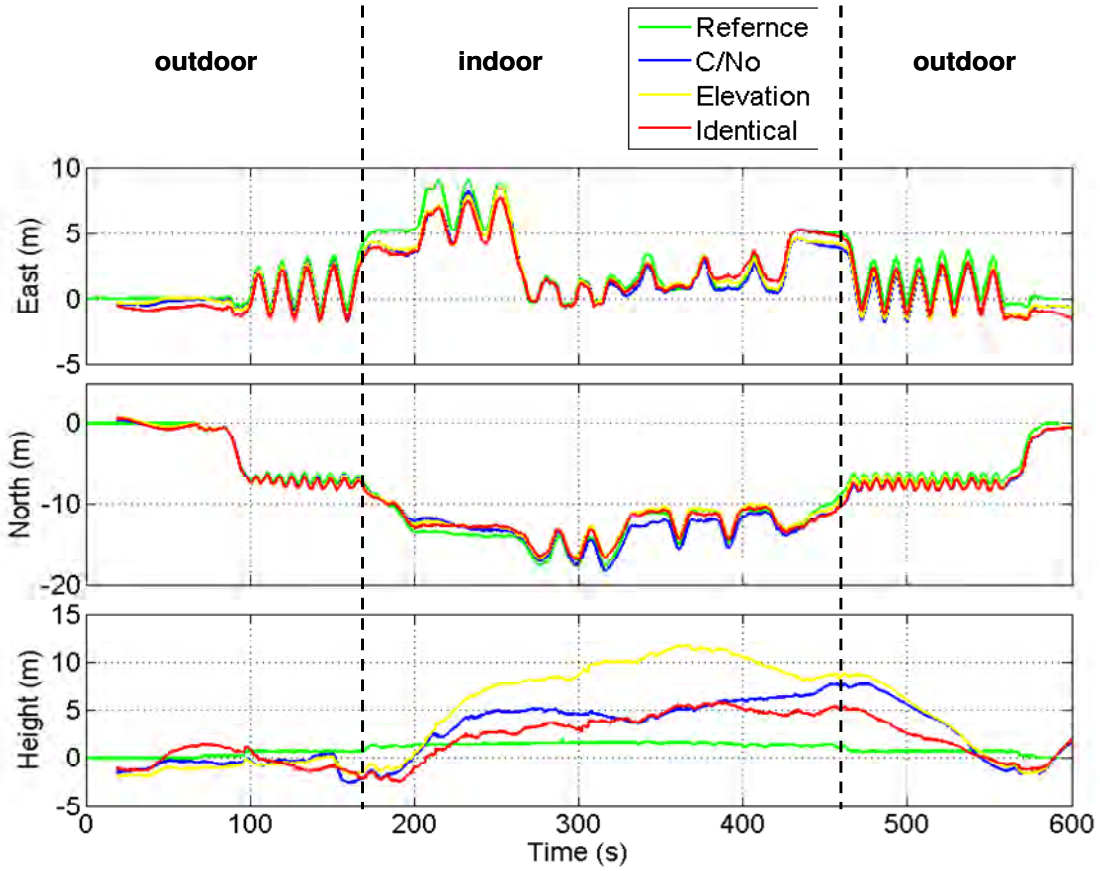

Figure 5-11: Position components of the main floor test obtained from GSNRx-nav-ins™ using the GSNRx™ for GPS and the CPT IMU using different measurement weighting schemes.

Elevation weighting in an indoor environment is not a perfect model since the insertion loss and fading affect the quality of the impinging signals, such that those signals arriving from the zenith do not necessarily carry more information than those arriving from the horizon. This explains why the elevation weighting method has the lowest accuracy with an RMS error of 5.6 m.

Table 5.5 showed that for all satellites the insertion loss on the main floor of the residential house is 7 dB on average. Also, the average C/N_0 of signals that GSNRx™

is not able to track is 34 dB-Hz, and measurements provided by this software are related to signals with C/N_0 values higher than 40 dB-Hz. Note that for signals with a C/N_0 higher than 40 dB-Hz, the multipath errors dominates over the signal attenuation errors and the C/N_0 does not completely describe the accuracy of the measurements. As an example, the C/N_0 of the reference signal in Figure 5-7 at t = 394 s is 48 dB-Hz, while the C/N_0 of the rover signal is 52 dB-Hz. This arises from the fact that the superposition of all secondary paths at the rover antenna is constructive, therefore making the multipath error the dominant source of measurement error. Since the receiver has no information regarding multipath geometry and multipath error, an identical weighting method with no information about the accuracy of measurements is the best model to use. Table 5.6 demonstrates this by comparing the RMS of the three-dimensional position errors. The RMS of the three-dimensional error for the identical weighting method is equal to 2.6 m.

Table 5.5 shows that the average C/N_0 of the signals tracked by GSNRx^{TM} is higher than 40 dB-Hz. Also, Figure 5-1 shows that for signals with a high C/N_0 (> 40 dB-Hz), the cofactor of measurements for the power dependent model is close to that of the identical model. As a result, these two weighting models are similar for the signals provided by GSNRx^{TM}, and the RMS of the position errors related to these weighting models differ by less than 1 m.

5.2.3.2 Reference-Rover

A similar data processing to that conducted in Section 5.2.3.1, was repeated with GPS observations provided by the GSNRx-rr™ and IMU data from the CPT. Trajectory results for different weighting models are plotted in Figure 5-12. The location of the reference antenna is also shown in this figure.

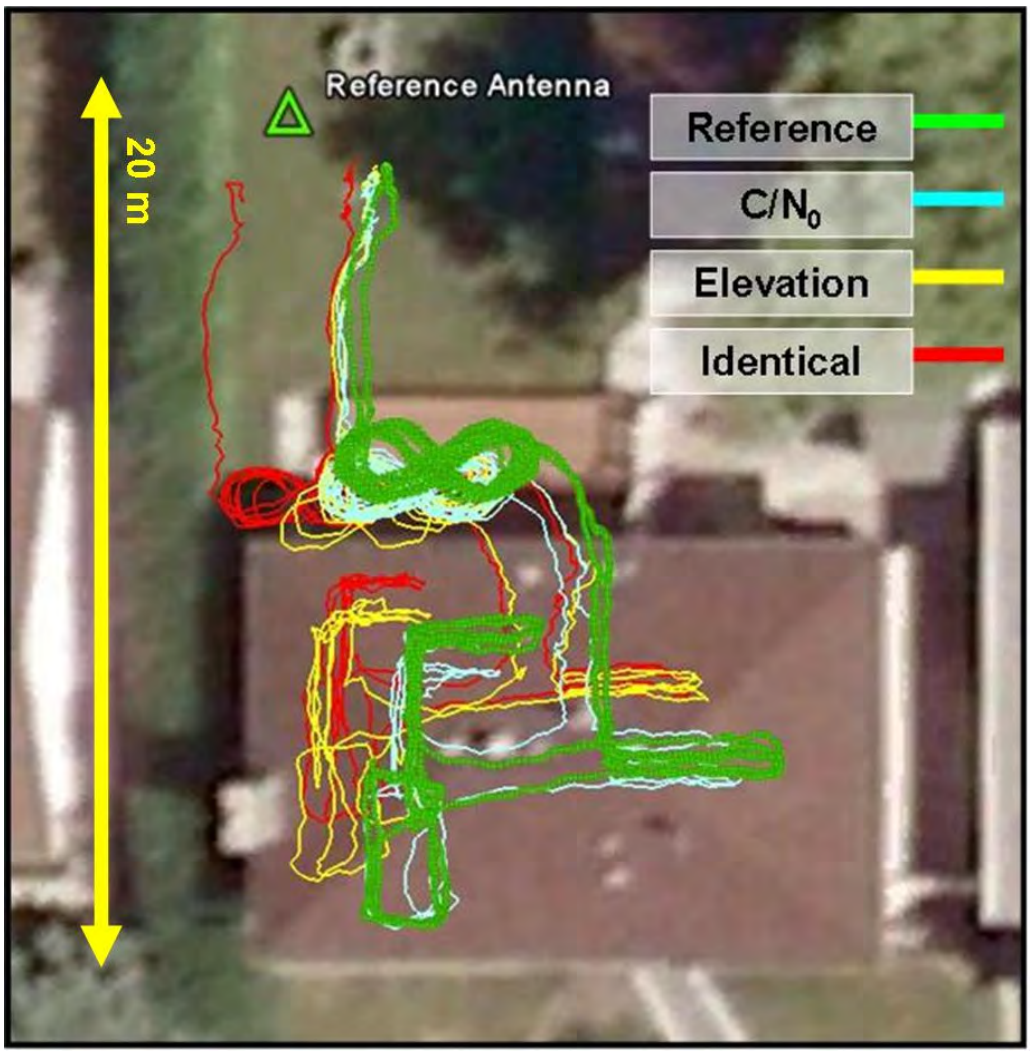

Figure 5-12: Trajectory obtained using GSNRx-nav-ins™. The CPT provides raw IMU data and the GSNRx-rr™ provides GPS observations. Three different weighting methods for the GPS observations, namelyelevation dependent, power dependent and identical variance, were used in the GPS/INS integration.

The trajectories shown in Figure 5-12 are compared with the reference solution in Figure 5-13 and the RMS of position errors are given in Table 5.7.

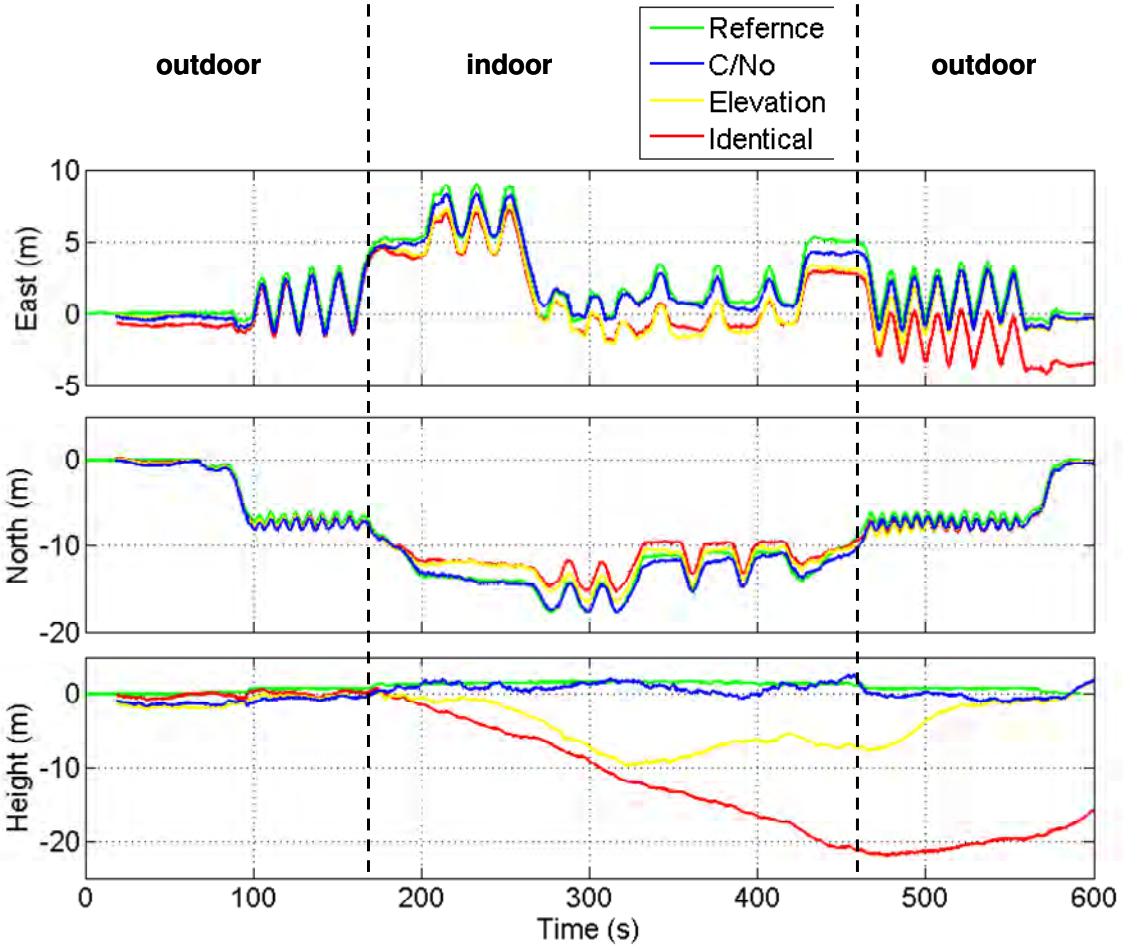

Figure 5-13: Position components of the main floor test obtained from GSNRx-nav-ins™ using GSNRx-rr™ for GPS observations and CPT IMU.

Table 5.7 shows that the power dependent weighting method with a three-dimensional RMS error of 1.5 m is the most efficient method when GSNRx-rr™ provides GPS measurements. It was mentioned before that GSNRx™ cannot provide GPS

observations on the main floor when the signal is attenuated below 40 dB-Hz. As a result, the additional measurements provided by the GSNRx-rr™ belong to signals with C/N_0 values lower than 40 dB-Hz. The average power of these signals for different satellites is summarized in Table 5.5. The Doppler and pseudorange measurements of these signals are less accurate due to the signal attenuation errors. These measurements can improve the performance of the GPS/INS integrated system only if their accuracy is correctly modeled in a weighting method. The identical and elevation dependent methods do not consider signal attenuation errors in their weightings and result in increased RMS position errors of 7.5 m and 15.6 m for the elevation and the identical weighting algorithms, respectively. In contrast, the power dependent weighting method considers the signal attenuation error for weak signals and the RMS of position error is 1.5 m.

Table 5.7: Accuracy of the integrated navigation solution of the main floor test while using a reference-rover receiver and CPT IMU.

Direction	RMSE (m) for Different Weightings		
	C/N_0	Elevation	Identical
East	0.50	1.34	2.00
North	0.56	0.98	1.32
Height	1.3	7.40	15.49
3D	1.5	7.58	15.67

5.2.3.3 Doppler/INS versus Pseudorange/INS

In the previous navigation solutions both Doppler and pseudorange measurements were used for GPS/INS integrations. In this section each of them is separately integrated

with the INS using the modified version of the GSNRx-nav-ins™ software and their performance is compared. In both cases the observations were provided by the GSNRx-rr™, weighted by C/N_0, and the CPT was used as an IMU since this configuration provided the best overall performance. The trajectories depicted in Figure 5-14 show that the Doppler/INS integration has short-term accuracy in position, but drifts when time passes. In contrast, the pseudorange/INS integrated solution is noisier but does not drift in time.

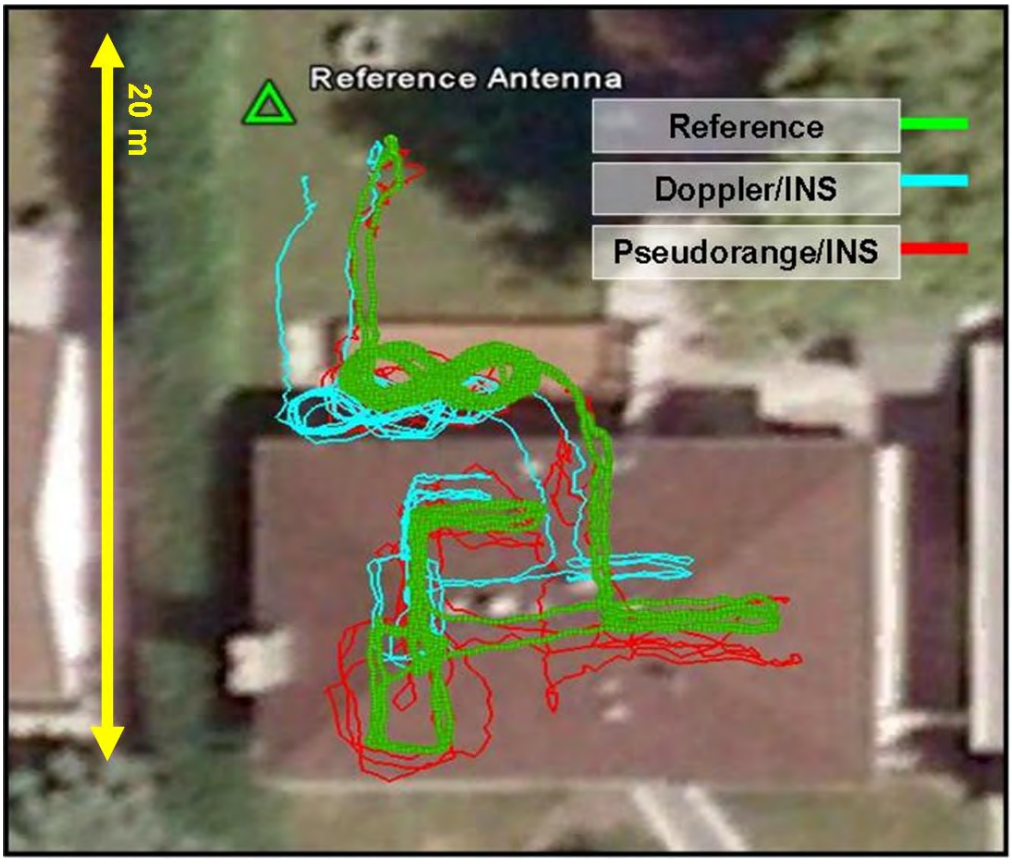

Figure 5-14: Trajectory obtained from the GSNRx-nav-ins™. The CPT provides raw IMU data and GSNRx-rr™ provides GPS observations. Doppler and pseudorange were used separately for updating the INS.

Since initial alignment is necessary before entering the residential house, both Doppler and pseudorange observations were used in the integrated solution and, afterwards, only one of them continued to update the INS. In so doing, the benefit of including the pseudorange and the Doppler measurements towards position estimation in indoor environments can be assessed.

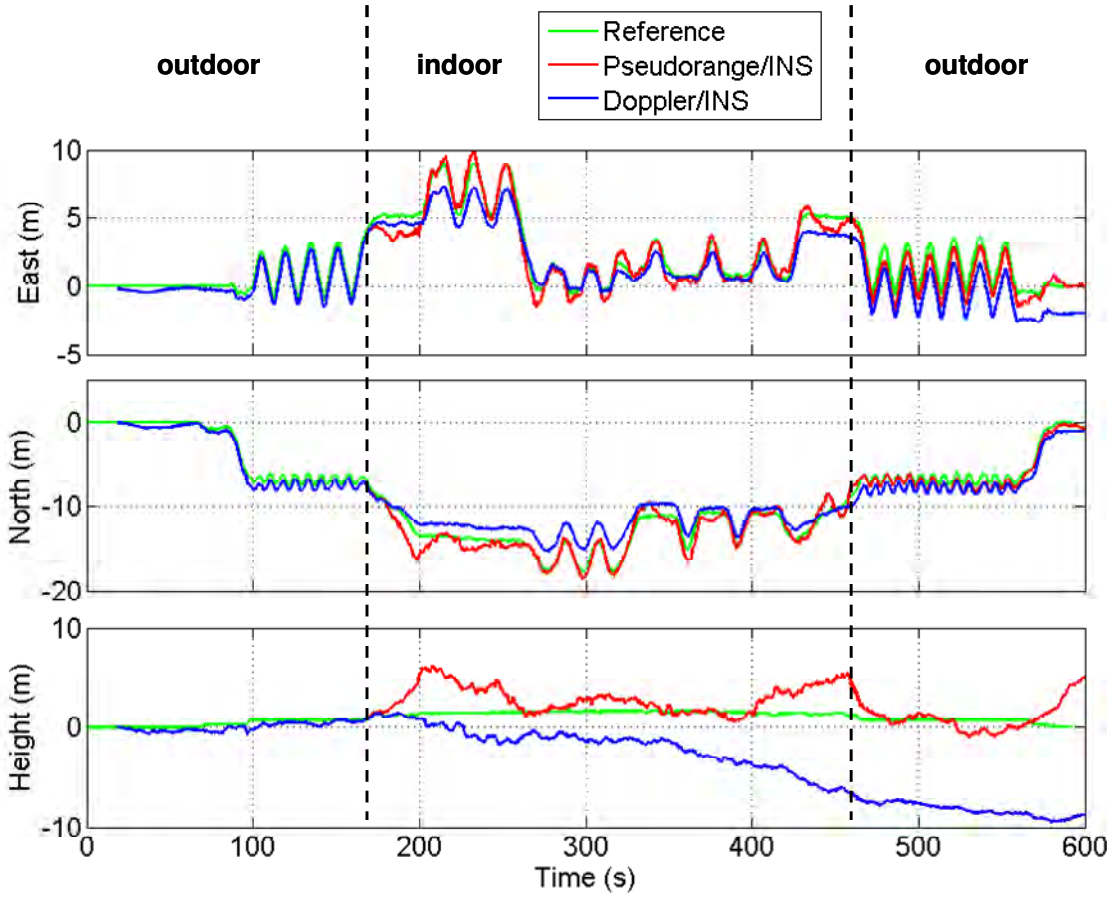

Figure 5-15: Position components of the main floor test obtained from GSNRx-nav-ins™ using the GSNRx-rr™ for GPS observations. Doppler and pseudorange were used separately for updating the INS.

The RMS of position errors of these two cases are compared in Figure 5-15 and Table 5.8. It is obvious that using both Doppler and pseudorange measurements provides a more accurate solution than using only one of these observations does. This is seen through a comparison of Table 5.7 and Table 5.8.

Table 5.8: Accuracy of the integrated navigation solution of the main floor test while Doppler and pseudorange measurements are used separately for updating the INS

Direction	RMSE (m) for Different Methods	
	Pseudorange/INS	Doppler/INS
East	0.70	1.09
North	0.86	1.22
Height	1.69	5.09
3D	2.02	5.34

In order to make the comparison easier, the RMS of three-dimensional position errors for different methods and receivers on the main floor of the residential house are summarized in Figure 5-16.

This figure shows that the position solution provided by the GPS/INS integrated system has the highest accuracy when the power dependent variance model is used for weighting the GPS measurements from the reference-rover receiver. For the power dependent weighting method, the RMS of position error is 1.5 m when a reference-rover receiver is used. On the other hand, the RMS of position error is 2.3 m for the highest performance of a GPS/INS integrated system when a standard receiver provides

measurements. This shows a 35% improvement in RMS position error when a reference-rover receiver provides GPS measurements instead of a standard receiver. The two advantages of a reference-rover receiver are higher observability and tracking robustness, which are the reasons for improved position solution. The number of satellites for both receivers is compared in Figure 5-9. All satellites are always available to the reference-rover receiver and the availability of each of them for the standard receiver is given in Table 5.5.

Figure 5-16 also shows that, for the data processed, Pseudorange/INS is better than Doppler/INS since Doppler/INS without position update drifts in time.

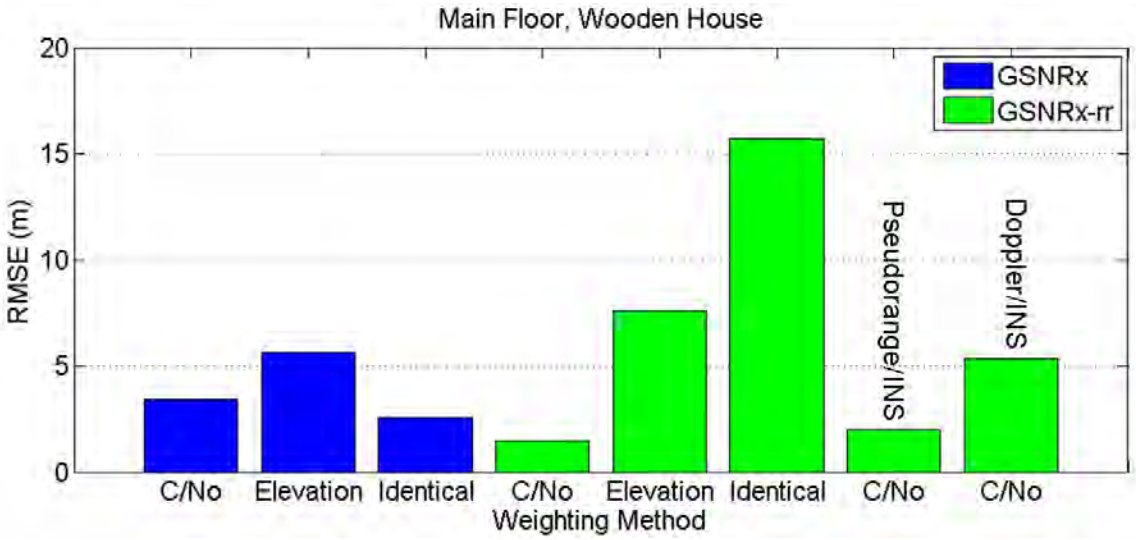

Figure 5-16: RMS of three-dimensional position errors for different methods and receivers on the main floor of residential house.

5.2.4 Basement Test

During this experiment, the pedestrian carried the equipment to the basement of the house described in the previous section. The reference solution provided by the SPAN

system and the IE software is shown in Figure 5-17. Just as for the main floor test, the rover started with an initial alignment in the open sky area in the backyard. Then the rover entered the house and used the stairs to enter the basement. Afterwards, the rover was taken outside from the front door through an area with foliage, and brought to the backyard again. The total time spent in the basement was approximately three minutes (from t = 220 s to t = 400 s).

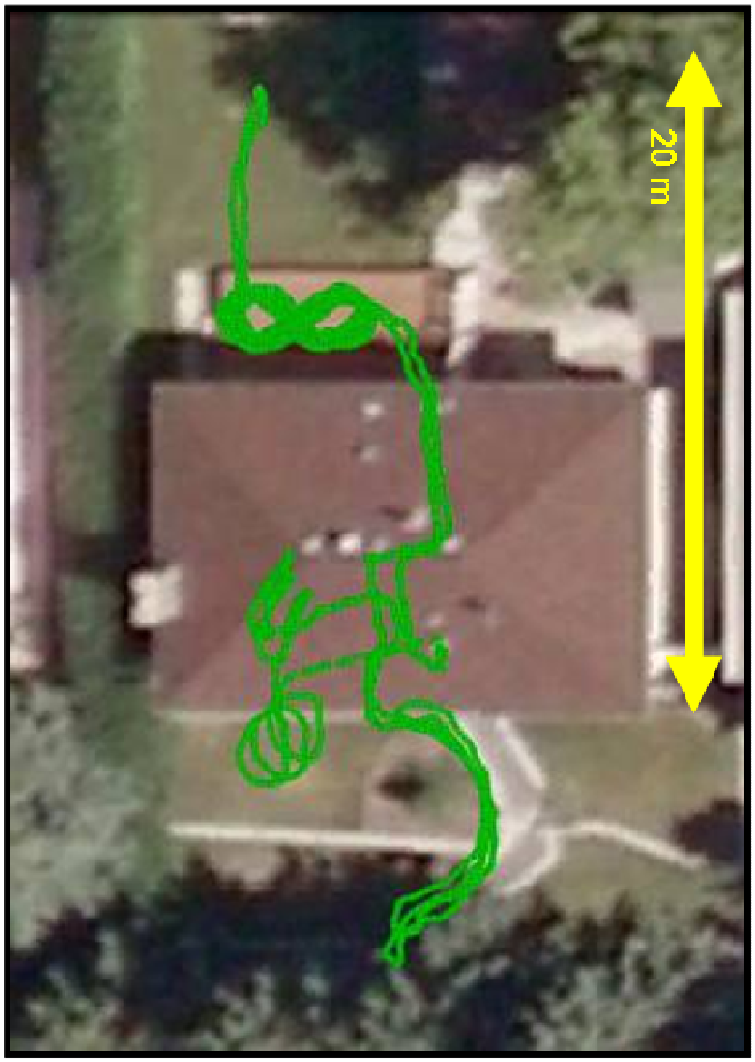

Figure 5-17: Reference trajectory of the rover for the basement test

The estimated accuracy (standard deviations) of the reference position over time provided by the SPAN (HG1700 and OEMV receiver) system and IE software are plotted in Figure 5-18. In the basement, the estimated standard deviation of this solution as a reference position is a maximum of 63 cm ($\sqrt{33^2(height)+37^2(north)+39^2(east)}$) at t = 330 s. This accuracy is lower than the accuracy of the reference solution in the main floor test where the maximum estimated standard deviation was 20 cm. Nevertheless, this accuracy is good enough for comparing the solutions, given that their error standard deviations differ more than the estimated standard deviation of the reference position shown in Figure 5-18.

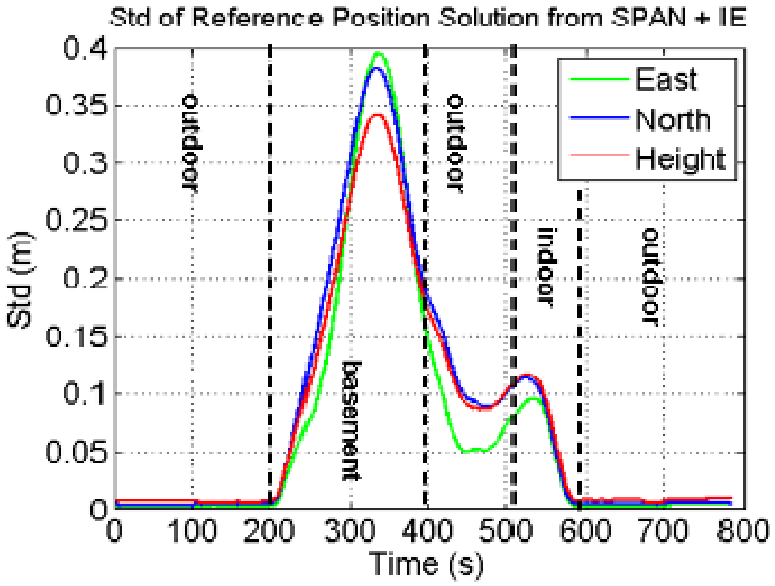

Figure 5-18: Estimated position accuracy of the reference solution for the basement test.

During the experiment, eight GPS satellites were available and the sky-plot is shown in Figure 5-19. Signal availability, power, and other statistics related to available satellites are provided below. Satellite 21 is chosen as an example and is discussed in detail, and the statistics of the other satellites are summarized in Table 5.9.

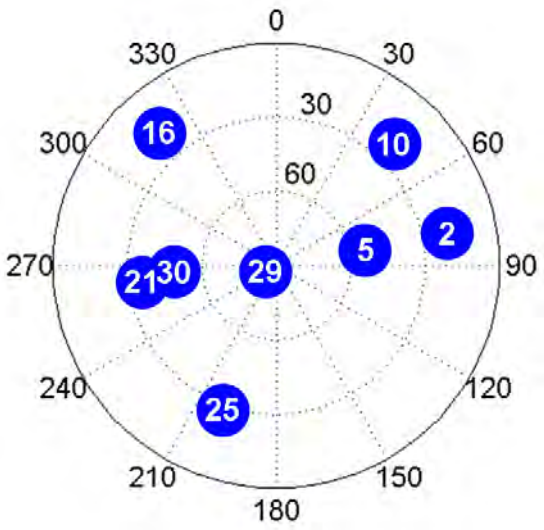

Figure 5-19: Satellite sky-plot during the basement test

Figure 5-20 shows the C/N_0 of Satellite 21 for the reference and rover antennas. This figure also shows the elevation angle of the same satellite as a function of time. The signals collected in the basement are more attenuated than the signals collected on the main floor. The average C/N_0 while the antenna is located in the basement was measured for the reference and rover antennas and is equal to 47.1 and 32 dB-Hz, respectively. This shows 15 dB of loss in the basement for Satellite 21. This additional attenuation, when compared to the main floor, further degrades the quality of the measurements and their availability. GPS measurements are only available to GSNRx™

47% of the time when the rover is in the basement, and the average C/N_0 when this receiver is not able to track the signal in the basement is 30.2 dB-Hz and its 95th percentile value is 36.8 dB-Hz.

The grey area in Figure 5-20 shows the period that GSNRx^{TM} is not able to track the signals. By looking at this figure and the 95th percentile value of the C/N_0, it can be said that GSNRx^{TM} is not able to track signals when the signal strength is lower than 36.8 dB-Hz.

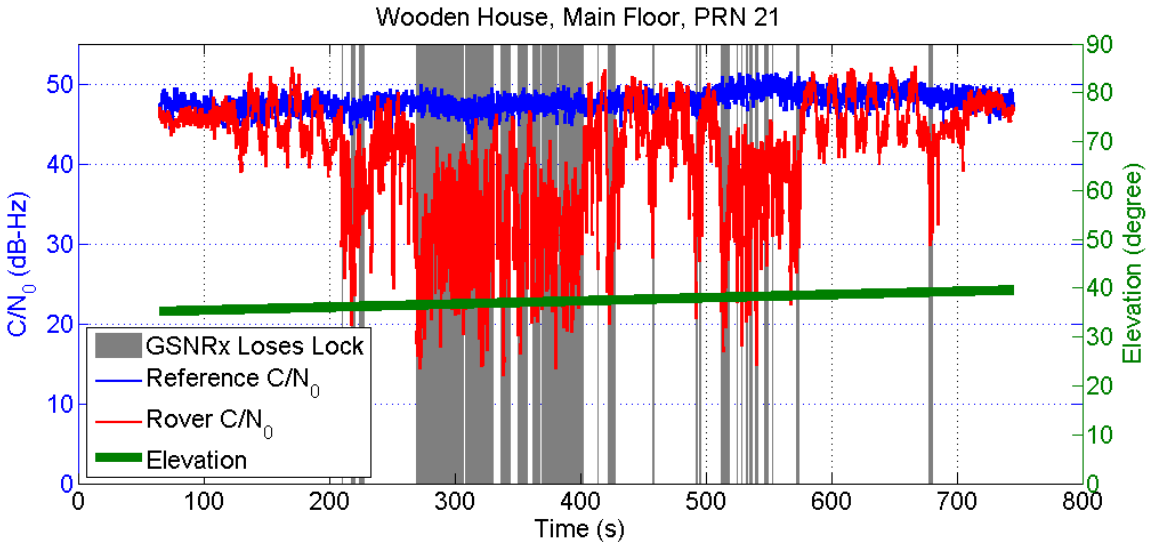

Figure 5-20: Carrier to noise ratio (C/N_0) of Satellite 21 for the reference and rover antennas and elevation angle of the satellite. During the grey area periods, GSNRx^{TM} is not able to track signals. The rover antenna is carried in the basement of the residential house.

The number of satellites that GSNRx™ and GSNRx-rr™ track and pass to the navigation solution in the basement test is shown in Figure 5-21. GSNRx-rr™ tracks eight satellites during the test. Because of the additional insertion loss in the basement that was described earlier, GSNRx™ loses lock frequently in the basement and less than five satellites are available there. Also, for a period of time only one satellite is tracked.

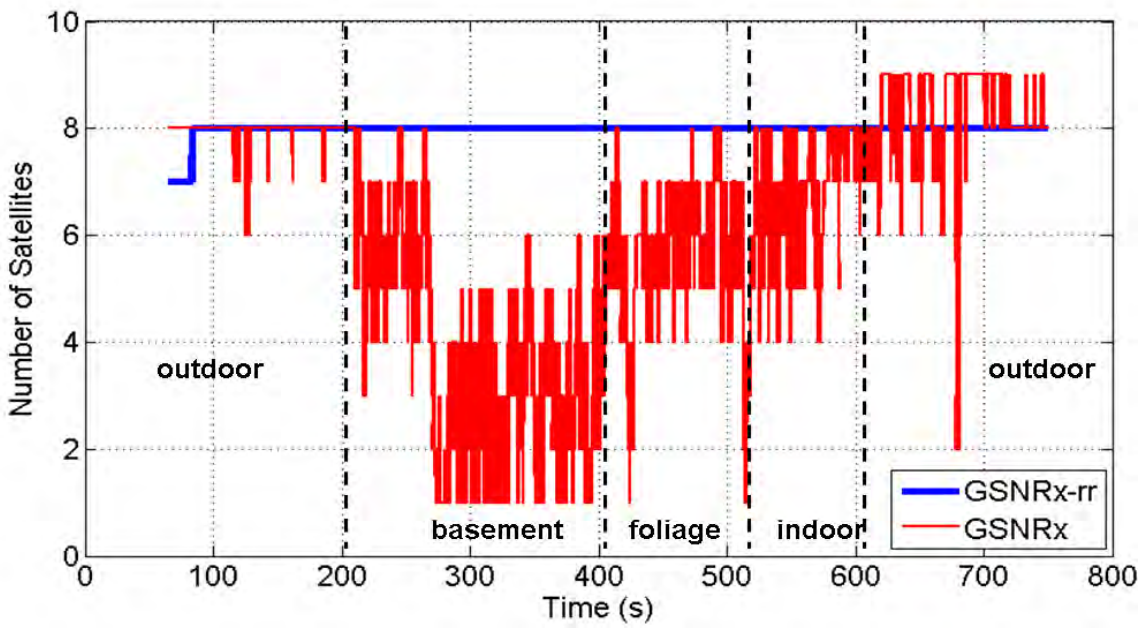

Figure 5-21: Number of satellites tracked by GSNRx™ and GSNRx-rr™ receivers in the basement of the residential house.

The statistics presented for Satellite 21 are also provided for the rest of the satellites in Table 5.9 for the period that the rover antenna is in the basement. This table shows the elevation angle of the satellites, the average signal power of the reference and rover antennas, and the average and 95th percentile of the signal power during the period

that GSNRx™ is not able to track the signals and availability of the signals for GSNRx™. The average signal power for which GSNRx™ is not able to track is 28.1 dB-Hz and its 95th percentile value is 34.8 dB-Hz. This shows that signals that are not tracked by GSNRx™ are attenuated below 34.8 dB-Hz. This table also shows that the average loss in the basement of the house is 16 dB.

Table 5.9: Availability, elevation and power of available satellites in the basement test of the residential house. Lose lock C/N_0 is the average of C/N_0 when the standard receiver is not able to track the signals.

PRN	Elevation (degree)	Reference C/N_0 (dB-Hz)	Rover C/N_0 (dB-Hz)	Lose Lock C/N_0 (dB-Hz)		Availability for GSNRx
				Average	95th Percentile	
2	16	41.9	25.3	25.2	30.9	30%
5	56	50.3	33.7	30.8	39.7	61%
10	16	39.5	23.9	23.8	29.5	29%
16	14	39.2	24.8	24.5	31.0	29%
21	36	47.1	32.0	30.2	36.8	47%
25	27	44.7	29.7	28.8	34.6	39%
29	83	52.7	38.2	30.7	38.7	89%
30	42	48.6	33.9	31.3	37.3	61%

The navigation solution obtained for the basement experiment using GSNRx-nav-ins™ is reported in the following. In all these solutions, the CPT IMU provides raw IMU data.

5.2.4.1 Standard Tracking

The GPS signals collected in the basement suffer an additional attenuation with respect to the main floor. Consequently, the standard receiver cannot track the signal most of the time. The percentage of signal availability for each satellite is presented in

Table 5.9 and it is shown that for five satellites out of eight, the standard receiver is only able to track the signal less than 50% of the time that the rover is in the basement. This table also shows that the average signal power of the rover is 30.2 dB-Hz for all the satellites.

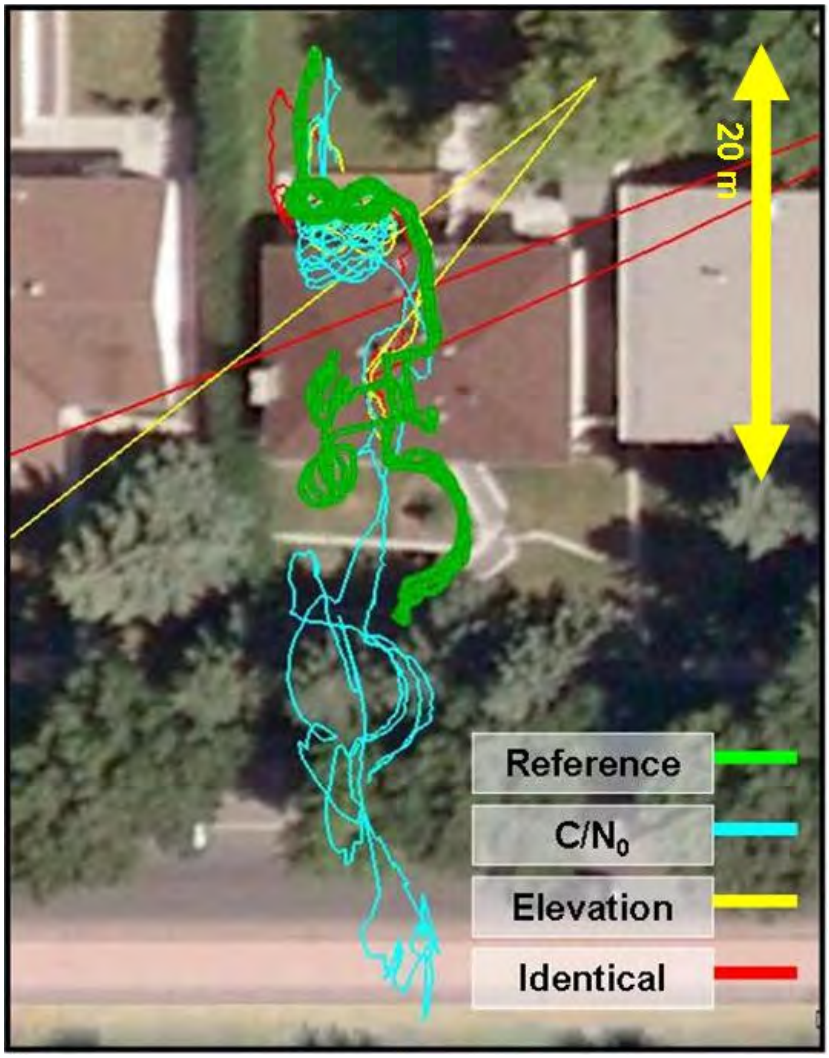

Figure 5-22: Basement trajectory obtained from GSNRx-nav-ins™. The CPT provides raw IMU data and GSNRx™ provides GPS observations. Elevation dependent and identical variance models made the navigation solution diverge when the rover entered the basement.

A low number of observations and their low signal strength cause the navigation solution to diverge when they are weighted by the identical and elevation dependent models. This is shown in Figure 5-22. In contrast, the power dependent weighting model considers the quality of the measurements based on their signal strength. Although the trajectory does not follow the reference solution in the basement, it does not diverge and follows the trajectory when the rover returns to the open sky. Thus, for the basement where the C/N_0 is very low, the power dependent weighting method is significantly better than the elevation and identical weighting methods.

5.2.4.2 Reference-Rover

Compared to standard tracking, the GPS observations obtained from the GSNRx-rr™ are more accurate because of a longer coherent integration time (100 ms versus 20 ms) and all eight satellites are available to this receiver. As before, GPS measurements are utilized for updating the integrated navigation solutions using different weighting models and the corresponding trajectories are depicted in Figure 5-23.

Similar to the previous cases presented in the main floor test, for attenuated signals the main factor impacting the quality of the measurements is the C/N_0. As shown in Figure 5-24 and Table 5.10, the power dependent weighting model can provide the best accuracy as opposed to other methods. The insertion loss in the basement is approximately 16 dB, which is 9 dB more than the average insertion loss on the main floor. For these signals, attenuation errors are more dominant than multipath errors. As a result, the power dependent method is better than the elevation and identical methods.

The RMS of the three-dimensional position errors for the power dependent weighting model is 2.3 m and for the elevation dependent and identical models is equal to 5.0 and 15.3 m, respectively.

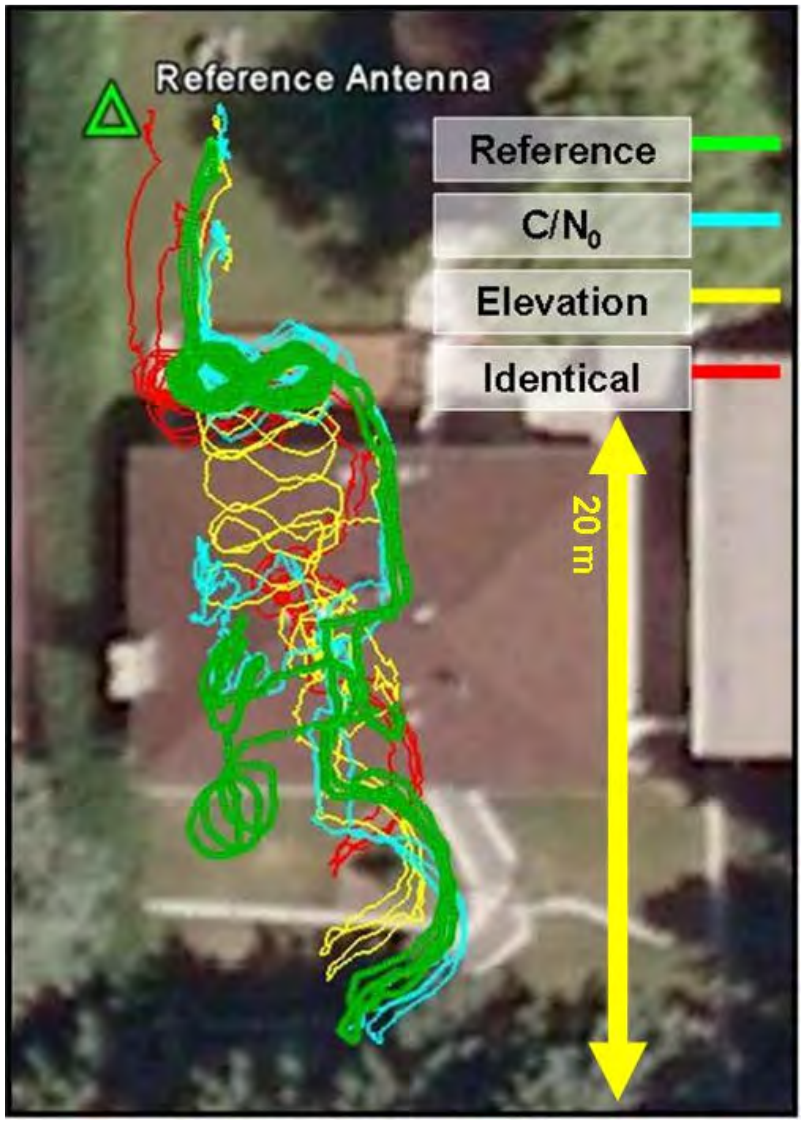

Figure 5-23: Trajectory obtained from GSNRx-nav-ins™ in the basement. The CPT provides raw IMU data and GSNRx-rr™ provides GPS observations. Three different weighting methods for the GPS observations, namely, elevation dependent, power dependent and identical variance, were used in the GPS/INS integration.

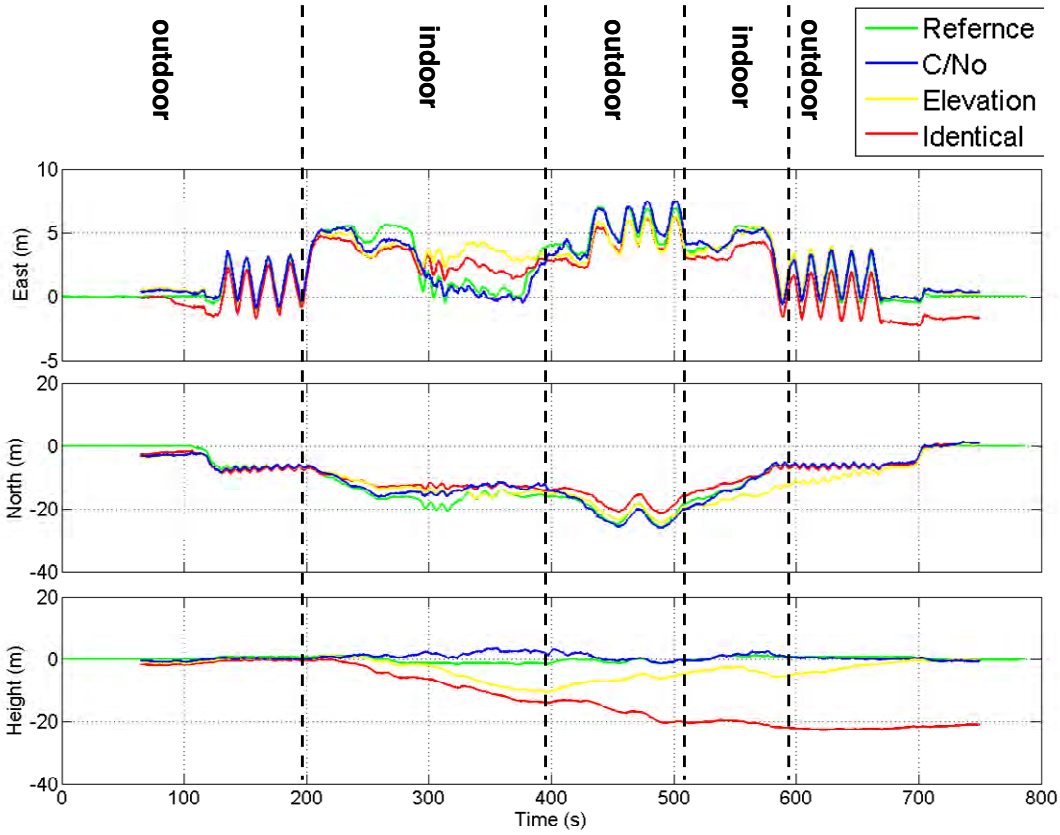

Figure 5-24: Position components of the basement test obtained from GSNRx-nav-ins^{TM} software using GSNRx-rr^{TM} for GPS observations and CPT IMU.

Table 5.10: Accuracy of the basement integrated navigation solution while using a reference-rover receiver and CPT IMU

Direction	RMSE (m) for Different Weightings		
	C/N_0	Elevation	Identical
East	0.47	1.15	1.21
North	1.67	2.61	2.58
Height	1.67	4.16	15.05
3D	2.36	5.04	15.31

5.2.4.3 Doppler/INS versus Pseudorange/INS

In this section, each of the Doppler and pseudorange observations provided by the GSNRx-rr™ were integrated with the INS separately to compare their performance on the navigation solution and assess the advantages of each for updating the INS.

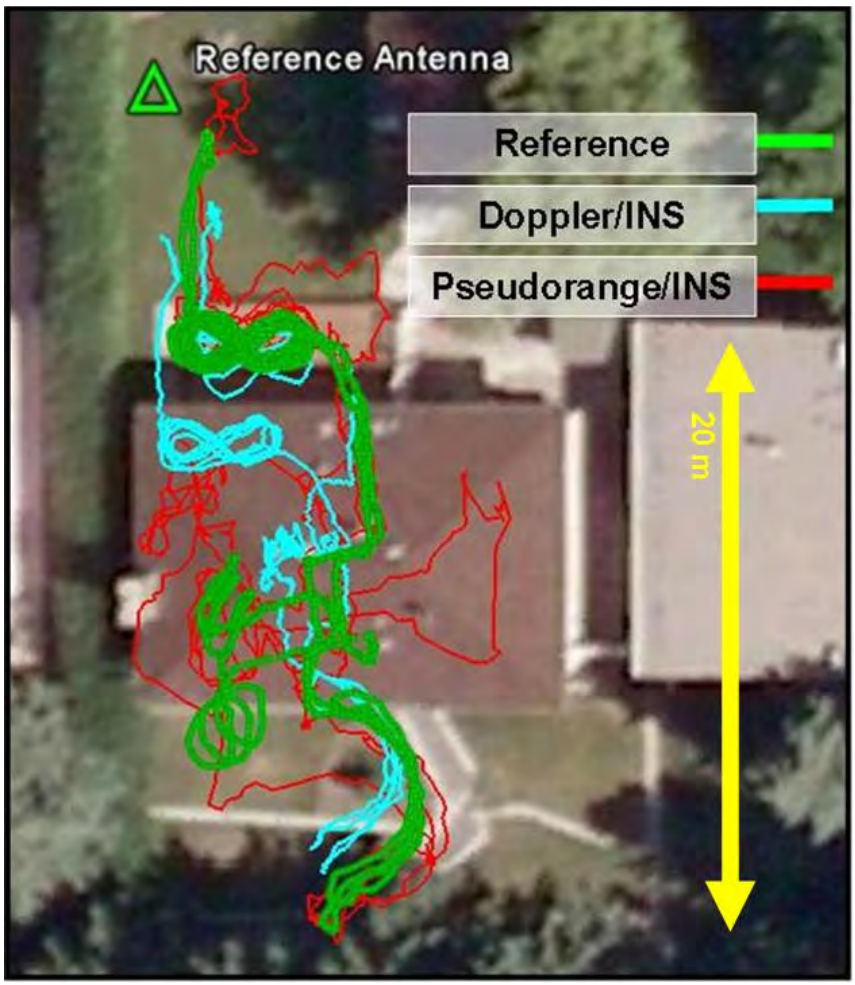

Figure 5-25: Trajectory obtained from GSNRx-nav-ins™. The CPT provides raw IMU data and GSNRx-rr™ provides GPS observations. Doppler and pseudorange measurements were used separately for updating the INS.

In both cases, when using Doppler or pseudorange measurements, the observations were weighted by the C/N_0 and the CPT was used as the IMU. Similar to Section 5.2.3.3, the trajectories depicted in Figure 5-25 show that the Doppler/INS integration has a good short-term accuracy in position, but drifts with time since the position is not updated. In contrast, the pseudorange/INS integrated solution is noisier (since the pseudorange multipath is unlimited) but does not drift in time since the position is updated directly. As shown in Chapter Three, the Doppler multipath is limited by the receiver velocity. Given the fact that the Doppler/INS position solution drift over a short period of time is negligible, the Doppler/INS has better short-term accuracy in comparison to the pseudorange/INS. The accuracy of these two cases is compared in Figure 5-26 and Table 5.11.

Table 5.11: Accuracy of the basement integrated navigation solution when Doppler and pseudorange measurements are used separately for updating the INS

Direction	RMSE (m) for Different Methods	
	Pseudorange/INS	Doppler/INS
East	1.32	1.00
North	1.94	2.72
Height	3.66	11.46
3D	4.34	11.82

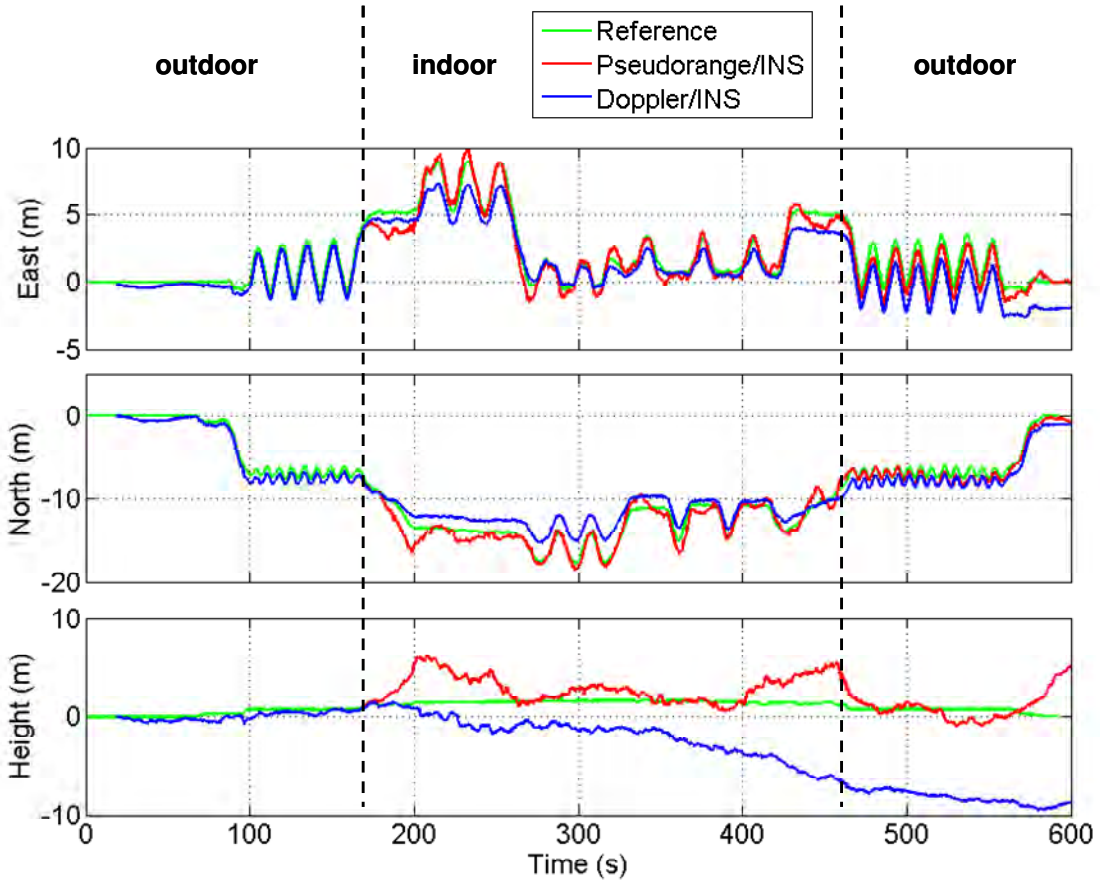

Figure 5-26: Position components of the basement test obtained from the GSNRx-nav-ins™ software using GSNRx-rr™ for GPS observations. Doppler and pseudorange measurements were used separately for updating the INS.

In order to make the comparison easier, the RMS of three-dimensional position errors for different methods and GSNRx-rr™ in the basement are summarized in Figure 5-27. This figure shows that the position solution provided by the GPS/INS integrated system has the highest accuracy when the power dependent variance model is used.

Doppler/INS and Pseudorange/INS solutions are less accurate than GPS/INS solutions since more information can be inferred from combined Doppler and

pseudorange measurements. Also, the Pseudorange/INS solution is better than the Doppler/INS solution since Doppler/INS without position update drifts in time.

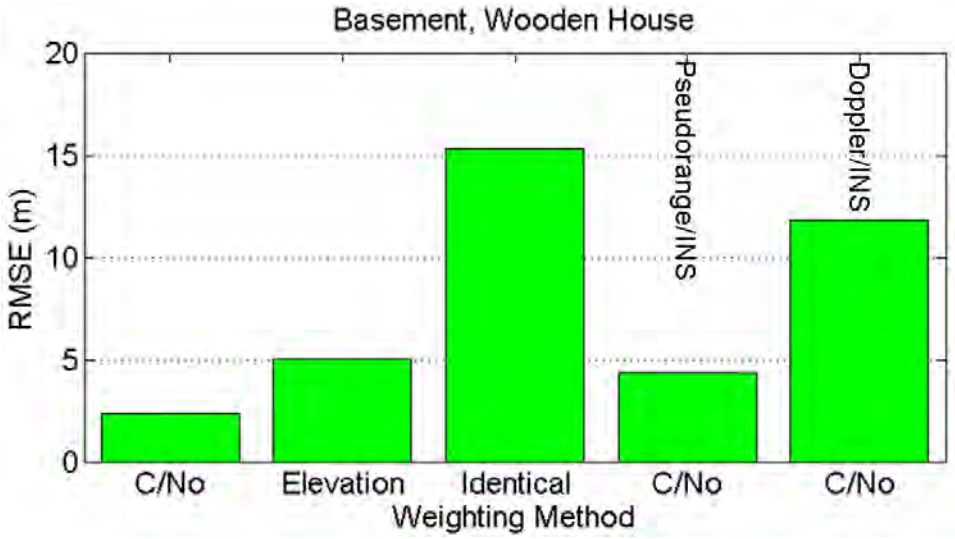

Figure 5-27: RMS of three-dimensional position errors for different methods and GSNRx-rr™ in the basement of the residential house. The position solutions provided by GSNRx™ observations do not follow the trajectory.

5.3 Summary

In this chapter, two different types of GPS receivers were utilized in two different indoor environments and three variance models were tested for weighting GPS measurements in a GPS/INS integrated system. The accuracy of the position solutions was assessed through a comparison with the reference solution provided by the Inertial Explorer software. The RMS position errors for different scenarios are summarized in Table 5.12.

Table 5.12: RMS position errors for different types of receivers, different environments and different weighting methods.

RMSE (m) of Integrated System for Different Methods, Locations, Receivers and Observations									
Location		Main Floor				Basement			
Receiver		GSNRx	GSNRx-rr			GSNRx	GSNRx-rr		
Observations: Pseudorange (P) Doppler (D)		P, D	P, D	P	D	P, D	P, D	P	D
Weighting Method	C/No	3.46	1.5			Does not follow Reference	2.36		
	Elevation	5.65	7.58			Diverges	5.04		
	Identical	2.55	15.67	2.02	5.34	Diverges	15.31	4.34	11.82

From the analysis, it emerges that the main factor impacting the quality of GPS observations is the C/N_0 and a power dependent variance model was introduced and shown to be the most effective way of weighting the observations indoors. When the GSNRx™ observations are used on the main floor, an identical method is more efficient than a power dependent method. On the main floor, the signal strength loss is only 7 dB and the GSNRx™ provides measurements for signals with a C/N_0 that is higher than 40 dB-Hz. For these measurements, multipath errors dominate over signal attenuation errors. Since there is no information for multipath errors and they are not a function of C/N_0, the power dependent model does not describe the accuracy of these measurements.

Doppler/INS and pseudorange/INS integrated systems were compared and it was shown that Doppler measurements improve the short-term accuracy of the position

solution and pseudorange measurements improve its long-term accuracy. As a result, a combination of both measurements is useful in an integrated system.

Due to limited indoor Doppler multipath errors, Doppler measurements should be used in an integrated system whenever available to the receiver. In contrast, indoor pseudorange multipath errors are unlimited. These measurements can decrease the short-term accuracy of the solution but they are necessary for updating the position. Therefore, for future work, Doppler/INS solutions should be studied when their positions are updated by only reliable information. This information could be provided by pseudorange measurements when they are somehow validated or by knowing the coordinates of the receiver from sources other than GPS satellites (coordinate updates). Also, investigation of how frequently the position of the Doppler/INS integrated system should be updated to achieve an acceptable accuracy for indoor applications should be conducted.

Chapter Six: Conclusions and Recommendations

This chapter provides conclusions pertaining to the characteristics of indoor GPS observations and the variance models utilized for weighting these observations in a GPS/INS integrated system. The conclusions of this work are presented in Section 6.1 and possible future work in this field of research is recommended in Section 6.2.

6.1 Conclusions

The following conclusions have been made from the research presented throughout this thesis:

1. Indoor GPS observations suffer from two main sources of error: attenuation errors and multipath errors. For indoor measurements provided from strong signals, multipath errors are dominant. In contrast, for weak signals for which attenuation errors grow exponentially, multipath errors are usually negligible in comparison and the power dependent variance model can be used for weighting measurements in navigation solutions such as least-squares estimation or Kalman filtering. In many indoor environments where the signal loss is 15 dB or higher, the power dependent model enhances the navigation solution.

2. In an indoor environment, a reference-rover receiver has two advantages over other receivers such as standard and HS GPS receivers. First, improved tracking robustness based on assistance from the unobstructed reference signals from the reference antenna (A-GPS) and second, improved signal observability due to a longer (>20 ms) integration time and signal acquisition rather than signal tracking

(block processing). These advantages were investigated for indoor observations and, compared to standard (GSNRx^{TM}) and commercial HS (u-blox) receivers, better performance in terms of accuracy and availability of observations was provided by the reference-rover receiver (GSNRx-rr^{TM}).

3. In a harsh multipath environment such as a modern concrete building where signal power loss is 20 dB or higher, attenuation is responsible for the dominant Doppler error (i.e., noise). This error can be compensated for by a long (200 ms) integration time but, unfortunately, higher user dynamics disable the effectiveness of a long integration time and increase multipath errors. For these reasons, the quality of Doppler measurements is lower when the receiver is in motion. In contrast, for a static receiver, signal acquisition is successful with a long integration time and the Doppler multipath error is largely reduced or eliminated. As a result, in such an environment only when the receiver is static, its velocity can be determined accurately using Doppler measurements.

4. In a residential house with less attenuation, Doppler measurements provided by the reference-rover receiver are reliable for indoor navigation and follow the pattern of the true Doppler. The accuracy of Doppler measurements in such an environment follows the theoretical model introduced in Chapter Three for velocities lower than 20 cm/s and shows that the assumption of neglecting the Doppler multipath error is viable for low dynamics in such a building, for which the estimated velocity based on Doppler measurement observations can be utilized to enhance indoor navigation. It is also observed that these estimations

can be improved using pre-filtering and a power dependant weighting matrix. For pedestrian velocities higher than 20 cm/s it can be assumed that the power dependent model is close to Doppler measurement accuracy and improves velocity estimation by using this model as a weighting model.

5. Since additional unknowns increase DOP (for a given set of observations), the accuracy of velocity components decreases when the clock drift is unknown. While a reference-rover receiver is utilized for Doppler measurements, the clock drift is not considered as a state to be estimated but in real applications this state should be estimated. In a residential house it was shown that velocity accuracy decreases from 12.1 cm/s for measurements from a reference-rover receiver to 66.5 cm/s in real applications for a test with a linear speed of 11 cm/s.

6. For a GPS/INS integration system, it emerges that the most effective way of weighting the observations indoors is the power dependent variance model. This model has a better performance than the elevation dependent variance model. Only when a standard receiver provides observations and signal attenuation is low (< 10 dB), the identical weighting method is more efficient than the power dependent method. For these indoor GPS observations, multipath errors are more dominant than signal attenuation errors. Since there is no information for multipath errors and they vary based on multipath geometry, the power dependent model does not describe the accuracy of these observations.

7. In an indoor GPS/INS integration system, Doppler measurements improve the short-term accuracy of the position solution and pseudorange measurements improve its long-term accuracy. As a result, a combination of both measurements leads to better results.

6.2 Recommendations

Based on the results and conclusions of this research the following are some of the recommendations for future work:

1. Although a reference-rover receiver overcomes indoor limitations, this receiver cannot be used for real applications. A cable is required between the reference and rover antennas to synchronize collected datasets from the reference and rover antennas. In order to synchronize these datasets without running a cable some research should be conducted. As an example, mobile networks can be utilized for time synchronization between the base station and the mobile handheld. Then the reference antenna can be located at the base station and the handheld can be considered as the rover antenna.

2. Indoor Doppler measurements were characterized and it was shown that the variance of Doppler errors is a function of both C/N_0 and receiver velocity. But in navigation solutions such as velocity estimation and GPS/INS integration, Doppler measurements were only weighted according to their signal power. It is worthwhile to investigate the performance of these navigation solutions when these measurements are weighted as a function of both receiver velocity

and C / N_0. In so doing, Doppler measurements related to static periods are more weighted and this might increase the performance of the navigation solution.

3. The theoretical variance model was provided and tested for Doppler measurements when signals were attenuated. Further studies are required to provide a similar variance model for pseudorange measurements when signals are attenuated. Also, some data collections should be conducted to verify whether the variance of pseudorange measurements matches the proposed theoretical model.

4. Due to limited indoor Doppler multipath errors, Doppler measurements should be used in an integrated system whenever it is available to the receiver. In contrast, indoor pseudorange multipath errors are unlimited. These measurements can decrease the short-term accuracy of the solution but they are necessary for updating the position. Therefore, for future work, Doppler/INS solutions should be investigated and updated with only reliable measurements. This information could be provided by pseudorange measurements when these are somehow validated or by knowing the coordinates of the receiver from sources other than GPS satellites (coordinate update). Investigations should also be conducted into how frequently the position of the Doppler/INS integrated system should be updated to achieve an acceptable accuracy for various classes of indoor applications.

References

Afzal, H. (2011) *Use of Earth's Magnetic Field for Pedestrian Navigation*, PhD Thesis, Report No. 20330, Department of Geomatics Engineering, The University of Calgary, Canada.

Aminian, B., V. Renaudin, D. Borio, and G. Lachapelle (2010), "Indoor Doppler Measurements and Velocity Characterization Using a Reference-Rover Software Receiver," in *Proceedings of GNSS10, The Institute of Navigation,* September 2010, Portland, OR

Anyaegbu, E. (2006) "A Frequency Domain Quasi-Open Loop Tracking Loop for GNSS Receivers," in Proceedings of the ION GNSS, 26 - 29 Sept, Fort Worth, TX, pp. 790 - 798

Bancroft, J. (2010) *Multiple Inertial Measurement Unit Fusion for Pedestrian Navigation*, PhD Thesis, published as Report No. 20320, Department of Geomatics Engineering, University of Calgary, Canada

Bensky, A. (2008) *Wireless Positioning Technologies and Applications*, Artech House

Bisnath, S. (2007) "What is carrier phase wind-up? What is its effect on GNSS performance/operation?" *GNSS Solutions Column, Inside GNSS*, July-August Issue, pp. 32-35.

Borio, D. and C. O'Driscoll (2009) *GNSS Receiver design*, ENGO 638 lecture notes, Department of Geomatics Engineering, University of Calgary

Borio D., N. Sokolova and G. Lachepelle (2010) "Doppler Measurement Accuracy in Standard and High-Sensitivity GNSS Receivers," *IET Radar, Sonar & Navigation. Accepted for publication,* Nov. 2010

Borio, D., N. Sokolova, and G. Lachapelle (2009) "Doppler Measurements and Velocity Estimation: a Theoretical Framework with Software Receiver Implementation," *in Proceedings of GNSS09, The Institute of Navigation*, September 2009, Savannah, GA

Brown, A. K. and P. Olson (2005) "Urban/Indoor Navigation Using Network Assisted GPS," in *Proceedings of the Proceedings of the 61st Annual Meeting of The Institute of Navigation*, , Cambridge, MA, pp. 1131 – 1136

Cheung, K.W., H. C. So, W.-K. Ma, and Y. T. Chan (2004), "Least Squares Algorithms for Time-of-Arrival-Based Mobile Location," *IEEE Transactions on Signal Processing,* Vol. 52, No. 4, April 2004.

El-Sheimy, N. (2007) *Inertial Techniques and INS/DGPS integration*, ENGO 623 Lecture Notes, Department of Geomatics Engineering, University of Calgary, Canada

Feng, G. and F. van Graas (1999) "GPS Receiver Block Processing," in *Proceedings of the 12th International Technical Meeting of the Satellite Division of The Institute of Navigation (ION GPS 1999)*, September 1999, pp. 307-316, Nashville, TN

Godha, S. (2006) *Performance Evaluation of Low Cost MEMS-Based IMU Integrated With GPS for Land Vehicle Navigation Application*, MSc Thesis, published as UCGE Report No. 20239, Department of Geomatics Engineering, University of Calgary, Canada

Godha, S., G. Lachapelle, and M.E. Cannon (2006) "Integrated GPS/INS System for Pedestrian Navigation in a Signal Degraded Environment," in *Proceedings of the 19th International Technical Meeting of the Satellite Division of The Institute of Navigation (ION GNSS 2006)*, September 2006, pp. 2151-2164, Fort Worth, TX

Groves, P.D. (2008) *Principles of GNSS, Inertial, and Multisensor Integrated,* Artech House

Hu, C., W. Chen, J. Miao, Z. Guo, B. Wei, and Z. Yuan (2009) "Assisted GPS Positioning under Weak Signal Environments," in *Proceedings of the 22nd International Technical Meeting of The Satellite Division of the Institute of Navigation (ION GNSS 2009)*, September 2009, pp. 2602-2609, Savannah, GA

Jekeli, C. (2000) *Inertial Navigation Systems with Geodetic Applications,* Walter de Gruyter, New York

Kao, W.W. and C-L. Tsai (2003) "Carrier Phase Indoor Positioning Using Pseudolites and INS," in *Proceedings of the 16th International Technical Meeting of the Satellite Division of The Institute of Navigation*, September 2003, pp. 2593-2598, Portland OR

Kaplan, E.D. (1996) *Understanding GPS Principles and Applications,* ArtechHouse

Karunanayake, D., M.E. Cannon, G. Lachapelle, G. Cox (2004) "Evaluation of AGPS in Weak Signal Environments Using a Hardware Simulator" in *Proceedings of ION GPS/GNSS of The Institute of Navigation*, 21-24 September 2004, pp. 416-2426, Long Beach CA

Kwakkel, S. (2008) *Human Lower Limb Kinematics Using GPS/INS*, MSc Thesis, published as UCGE Report No. 20279, Department of Geomatics Engineering, University of Calgary, Canada

Lachapelle, G. (2009) *Advanced GNSS Theory and Applications*, ENGO 625 Lecture Notes, Department of Geomatics Engineering, University of Calgary, Canada

Lau, L., and E. Mok (1999), "Improvement of GPS Relative Postioning Accuracy by Using SNR," *Journal of Surveying Engineering,* November 1999.

Lee, W.C.Y. (1997) *Mobile Communications Engineering: Theory and Applications* McGraw-Hill Professional Book Group, 2nd Edition

Leva, J. L., M. U. de Haag, and K. V. Dyke (1996) "Performance of Standalone GPS," E. D. Kaplan, ed., *Understanding GPS Principles and Applications*, chapter seven. Artech House

Mezentsev, O. (2005) *Sensor Aiding of HSGPS Pedestrian Navigation*, PhD Thesis, published as UCGE Report No. 20212, Department of Geomatics Engineering, University of Calgary, Canada

Mezentsev, O., J. Collin and G. Lachapelle (2005) "Pedestrian Dead Reckoning n A Solution to Navigation in GPS Signal Degraded Areas?" *Geomatica*, 59, 2, 175-182.

Misra, P. and P. Enge (2006) *Global Positioning System – Signals, Measurements, and Performance*, Ganga - Jamuna Press, second edition

O'Driscoll, C., D. Borio, M.G. Petovello, T. Williams and G. Lachapelle (2009) "The Soft Approach: A Recipe for a Multi-System, Multi-Frequency GNSS Receiver," *Inside GNSS Magazine*, Volume 4, Number 5, pp. 46-51. (http://www.insidegnss.com/node/1635)

Olynik, M., M.G. Petovello, M.E. Cannon, and G. Lachapelle (2002) "Temporal Variability of GPS Error Sources and Their Effect on Relative Positioning Accuracy," *Proceedings of the ION* NTM-2002, January 28-30, San Diego, CA pp.877-888.

Pahlavan K., F. Akgul, F. Dovis, Y. Ye, T. Morgan, F. Alizadeh-Shabdiz ,M. Heidari and C. Steger (2010) "Taking Positioning Indoors Wi-Fi Localization and GNSS" *Inside GNSS*, May , pp. 40-47

Petovello, M.G. (2009) *Estimation for Navigation*, ENGO 699 Lecture Notes, Department of Geomatics Engineering, University of Calgary, Canada

Petovello, M.G. (2003) *Real-time Integration of a Tactical-Grade IMU and GPS for High-Accuracy Positioning and Navigation*, PhD Thesis, published as UCGE Report No. 20173, Department of Geomatics Engineering, University of Calgary, Canada

Petovello M.G. and C. O'Driscoll (2007) "GSNRx^{TM} Algorithm Design Document", *Position, Location And Navigation (PLAN) Group*, November, 77 pp.

Petovello, M. G., O. Mezentsev, G. Lachapelle, and M. Cannon (2003) "High sensitivity GPS velocity updates for personal indoor navigation using inertial navigation systems," in *Proceeding of ION/GPS*, Sept. 2003, pp. 2886–2896, Portland, OR

Rappaport, T. S. (2002) *Wireless Communications: Principles and Practice*, Prentice Hall PTR, 2nd Edition

Reed, J.H., K.J. Krizman, B.D. Woerner, and T.Z. Rappaport (1998), "An overview of the challenges and progress in meeting the E-911 requirement for location service," *IEEE Communication Magazine*, Vol. 36, April 1998, pp. 30-37

Satyanarayana, S., D. Borio and G. Lachapelle (2010) "Power Levels and Second Order Statistics for Indoor Fading Using a Calibrated A-GPS Software Receiver.," in *Proceedings of GNSS10, The Institute of Navigation*, 21-24 Sep, Session E1, Portland, OR

Satyanarayana, S., D. Borio, and G. Lachapelle (2009) "GPS L1 Indoor Fading Characterization Using Block Processing Techniques," in *Proceedings of the 22nd International Technical Meeting of The Satellite Division of the Institute of Navigation (ION GNSS 2009)*, September 2009, pp. 1742-1755, Savannah, GA

Sokolova, N. (2009) *Doppler Measurements and Velocity Estimation: Comparison of Standard and High Sensitivity Receivers*, MSc Thesis, published as Report No. 20299, Department of Geomatics Engineering, University of Calgary, Canada

Szarmes, M., S. Ryan, G. Lachapelle and P. Fenton (1997) DGPS "High Accuracy Aircraft Velocity Determination Using Doppler Measurements," in *Proceedings of International Symposium on Kinematic Systems in Geodesy*, Geomatics and Navigation - KIS97 (Banff, June 3-6), Dept of Geomatics Engineering, The University of Calgary, 167-174

Tarrio, P., A.M. Bernardos and J.R. Casar (2011), "Weighted Least Squares Techniques for Improved Received Signal Strength Based Localization," *Sensors 2011,* 11(9), 8569-8592.

Tetewsky, A. K., and F. E. Mullen (1997), "Carrier phase wrap-up induced by rotating GPS antennas," *GPS World*, 8 (2), 51-57

Uijt de Haag, M. (1999) *An investigation into the application of block processing techniques for the Global Positioning System,* PhD Thesis, Ohio University, United States

van Graas, F. and A. Soloviev (2004), "Precise Velocity Estimation Using a Stand-Alone GPS Receiver," *Navigation, Journal of the Institute of Navigation*, Vol. 51 No. 4, pp. 283–292

van Graas, F., A. Soloviev, M. Uijt de Haag, S. Gunawardena, M.S. Braasch (2005) "Comparison of Two Approaches for GNSS Receiver Algorithms: Batch Processing and Sequential Processing Considerations," *Proceedings of the 18th International Technical Meeting of the Satellite Division of The Institute of Navigation (ION GNSS 2005)*, September 2005, pp. 200-211, Long Beach, CA

van Diggelen, F. (2009) *A-GPS: Assisted GPS, GNSS, and SBAS*, Artech House

Ward, P. W., J. W. Betz, and C. J. Hegarty (1996) "Satellite Signal Acquisition, Tracking, and Data Modulation," E. D. Kaplan, ed., *Understanding GPS Principles and Applications*, chapter five. Artech House

Watson, R., G. Lachapelle, R. Klukas, S. Turunen, S. Pietil and I. Halivaara (2006) "Investigating GPS Signals Indoors with Extreme High-Sensitivity Detection Techniques," *Navigation*, *Journal of the Institute of Navigation*, Vol. 52 No. 4, pp. 199-213, Alexandria VA

Wieser, A. (2007) "How important is GNSS observation weighting?" *GNSS Solutions Column, Inside GNSS*, January-February Issue, pp. 26-28.

Wieser, A., M. Gaggl Geodesy, and H. Hartinger (2005), "Improved Positioning Accuracy with High-Sensitivity GNSS Receivers and SNR Aided Integrity Monitoring of Pseudo-Range Observations," *ION GNSS 18th International Technical Meeting of the Satellite Division*, 13-16 September 2005, Long Beach, CA.

Xiang, Z., S. Song, J. Chen, H. Wang, J. Juang, and X. Gao (2004), "A Wireless LAN-based Indoor Positioning Technology'', *IBM Journal of Research and Developmen*t, Vol. 48, No.5/6

Yang, C. and S. Han (2007) "Tracking of Weak GPS Signal with BACIX," in *Proceedings of the ION GNSS*, 25 - 28 Sept, Fort Worth, TX, pp. 2797 - 2807

Zhao, X., C. Goodall, Z. Syed, B. Wright, and N. El-Sheimy (2010) "Wi-Fi Assisted Multi-sensor Personal Navigation System for Indoor Environments," in *Proceedings of the 2010 International Technical Meeting of The Institute of Navigation*, January 2010, pp. 236-243, San Diego CA

APPENDIX A: INS/GNSS INTEGRATED SYSTEM AS AN INDOOR VELOCITY REFERENCE AND ITS ACCURACY

In this appendix, a commercial NovAtel SPAN system equipped with a Honeywell HG1700 inertial measurement unit is introduced as a reliable velocity reference for indoor applications. Also, the accuracy of this reference is investigated and several ways through which to improve this accuracy are introduced.

A.1. Experimental Data collection

In this data collection the performance of the NovAtel SPAN system is evaluated as an indoor velocity reference. The SPAN system collects both GNSS and INS data. Only INS data is available indoors and as such might be used to produce a velocity reference for indoor applications. In order to find the accuracy of the INS-only solution, INS and GNSS data have been collected outdoors and the integrated solution served as a reference for accuracy analyses.

The instruments used for this data collection are shown in Figure A 1. Since accurate analysis is necessary for reference accuracy measurement, a base antenna was used on the rooftop of the CCIT building to provide differential GPS processing capability.

Figure A 2 shows the environment where the data was collected. This data was collected in an open area in order to have enough satellites in view and to provide a good reference for analyzing the results.

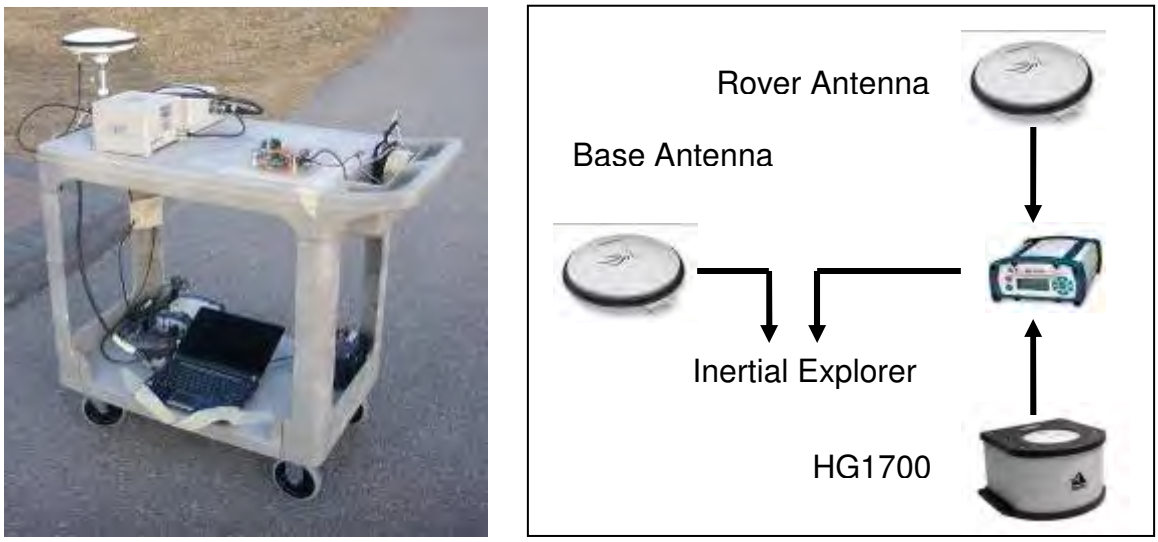

Figure A 1: Instrumentation used during the data collection (GNSS/INS)

Figure A 2: Data collection environment and base antenna

A.2. Methodology During Data Collection

Initial and final alignments were applied before and after data collection. These alignments include static and dynamic (figure eight) techniques. Zero velocity update (ZUPT) is another method applied during this data collection. The INS solution is affected by errors that drift the velocity estimation. This drift increases with time. The post-processing algorithm can recognize zero velocity in the INS data and use the corresponding information to correct for the accumulated errors. This method is called ZUPT. Therefore, data was collected with 20 seconds of walking and 10 seconds of stopping to take advantage of ZUPT. This is the same type of motion used for indoor tests.

A.3. Analysis

The analysis is done by the Inertial Explorer software which is commercial software from NovAtel. Inertial Explorer processes the collected data from the SPAN system and provides the velocity measurements.

Data was collected outdoors so both INS and GNSS data were collected. Inertial explorer integrates GNSS and INS data using a tightly coupled method. Therefore, a very accurate velocity solution with estimated accuracy is provided.

Also, this software can remove the GNSS data and process the INS only data. It can remove part or all of the GNSS data. This feature is used to simulate the condition when the system enters an indoor area. In this work, the GNSS data is removed completely and only the part related to the INS alignment is kept. The simulated indoor

solution can be compared with the accurate GNSS/INS integrated solution and the accuracy of INS only data with GNSS outage can be measured.

Figure A 3 shows the accurate velocity using Inertial Explorer (tightly coupled method) for an INS/GNSS integrated solution with both forward and backward processing.

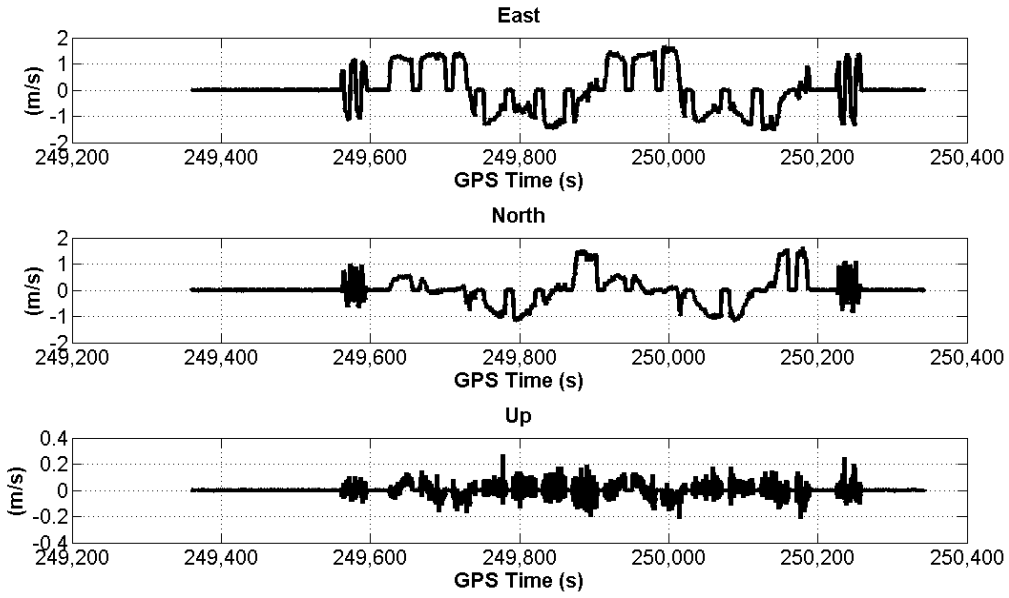

Figure A 3: Tightly coupled method as a reference (GNSS/INS integrated solution)

Afterwards, GNSS data is excluded for the period of time that indoor conditions are simulated. This period is about 10 minutes and is presented in Table A 1.

Table A 1: GNSS outage (GPS time(s))

From	To
249610	250200

Figure A 4 depicts the differences between the velocity provided by a GNSS/INS integrated system and the indoor simulated solution after a GNSS outage.

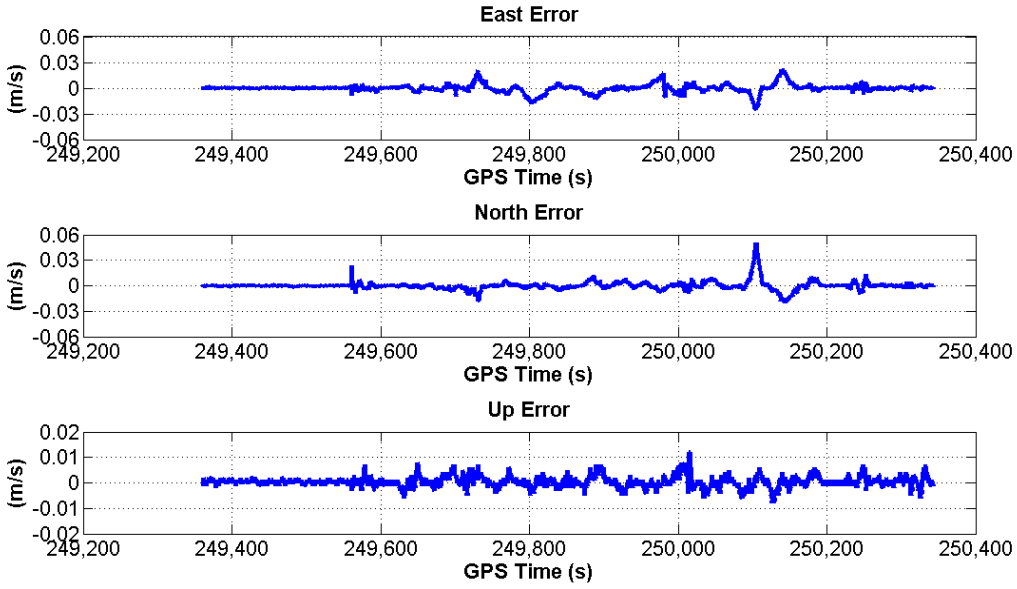

Figure A 4: Error of the simulated indoor solution compared to GNSS/INS integrated solution

In the following, the accuracy of the simulated indoor velocity solution is evaluated. To assess this accuracy two error sources must be cumulated:

- Error of the GNSS/INS integrated velocity solution.
- The differences between the GNSS/INS integrated solution and the indoor simulated velocity estimation shown in Figure A 4.

Figure A 5 shows the estimated errors related to the GNSS/INS integrated velocity solution derived by the Inertial Explorer software.

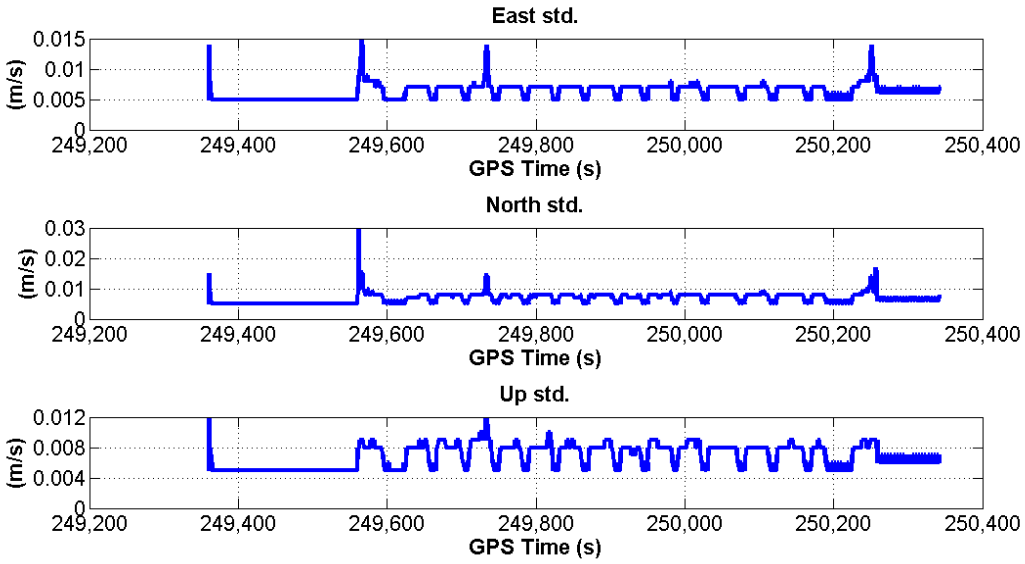

Figure A 5: Estimated standard deviation of velocity for GNSS/INS integrated velocity solution

The difference of the GNSS/INS integrated solution and the indoor simulated velocity solution was shown in Figure A 4 . In the worst case scenario these two error sources have the same sign and their absolute values are added together. By adding the absolute values of these errors together in Figure A 6, the estimated errors of the indoor velocity reference are achieved.

Table A 2 shows the Root Mean Square (RMS) of the errors, as well as the maximum errors. In other words, it is showing the accuracy of the indoor velocity

reference and the maximum velocity errors which can happen when the SPAN system is used indoors as a velocity reference.

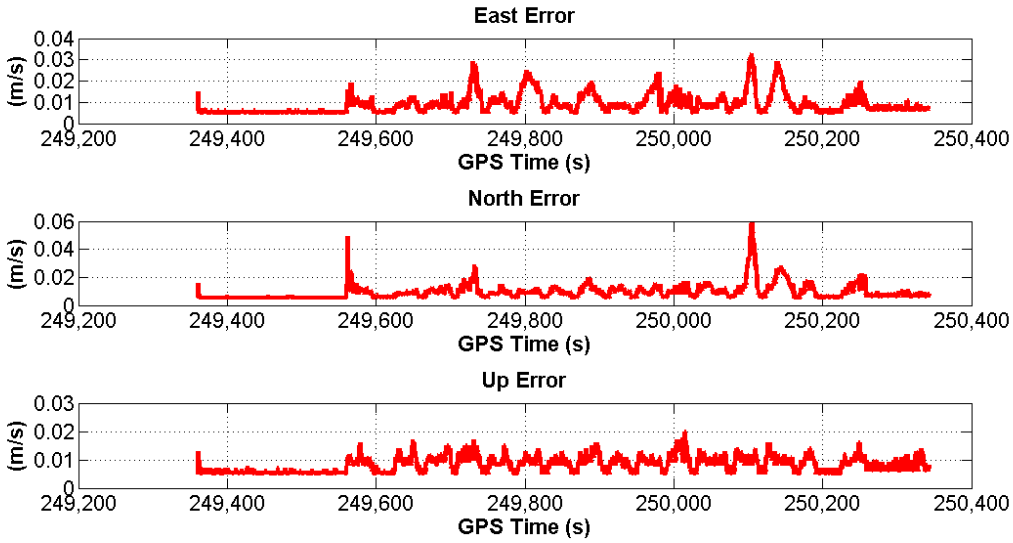

Figure A 6: Cumulated velocity errors related to simulated indoor data

Table A 2: Statistics for the velocity accuracy of HG-1700 indoors

(cm/s)	RMS East	RMS North	RMS Up	Max East	Max North	Max Up
	1.0	1.1	0.9	3.3	6.0	2.0

According to measurements provided in Table A 2, the accuracy of the velocity reference solution with ZUPT for indoor application is 1.7 cm/s ($\sqrt{(1.0)^2+(1.1)^2+(0.9)^2}=1.7$).